

Synthesis of Nanomaterials and Macromolecular Architectures for Dual Drug Delivery Systems,  
Biosensors, and Antimicrobial Films

By

Jacob Nathaniel Lockhart

Dissertation

Submitted to the Faculty of the  
Graduate School of Vanderbilt University  
in partial fulfillment of the requirements

for the degree of

DOCTOR OF PHILOSOPHY

in

Chemistry

December 16, 2017

Nashville, Tennessee

Approved:

Eva M. Harth, Ph.D.

John A. McLean, Ph.D.

Steven D. Townsend, Ph.D.

Scott A. Guelcher, Ph.D.

To an amazing group of family, friends, and advisers;  
without you this work would not be possible.

*In loving memory of grandmother Margueritte.*

## ACKNOWLEDGEMENTS

This work was made possible thanks to financial support in part by the Juvenile Diabetes Research Foundation and funding from the Vanderbilt University Department of Chemistry.

First, I would like to express my most sincere thanks to Dr. Eva Harth for her scientific guidance, wise counsel, and indefatigable enthusiasm. She welcomed me into her group as an analytical chemist, offered invaluable knowledge and training over the years, and enabled incredible learning opportunities which made me into a highly skilled and well-rounded scientist. I am forever grateful for her support, kindness and mentorship.

I would also like to thank my outstanding committee for their extremely helpful professional and technical discussions over the years, encouraging me to dig deep and push myself farther than I ever thought was possible. To Dr. McLean, who stimulated my interest in pursuing graduate studies and offering his sage advice. To Dr. Townsend, who imparted the importance of exploring the unknown. To Dr. Guelcher, who further enhanced the scope of my science and engineering work.

I am also extremely thankful for the members of the Harth group as they contributed significantly to my graduate school experience with meaningful feedback, collaborations and friendship. The group made a work environment that was very pleasant and welcoming, and I look forward to lifelong relationships with all of them.

As a testament to Vanderbilt University's truly collaborative environment, I was blessed to work with the most talented mentors and scientists and have incredible opportunities to develop deep technical skills along with leadership and professional experiences. Special thanks to Dr. Tony Hmelo of the Vanderbilt Institute for Nanoscale Science and Engineering for his input and

advice regarding the many instruments I utilized under his direction. To Dr. Phillips and Dr. Sutton for supervising my undergraduate teaching experiences, which offered unique opportunities to lead and manage others. And to Professor Joseph Rando of the Owens School of Management who contributed a complementary business education.

My success at Vanderbilt would not be possible without the support of my family. I would like to express thanks to my parents for raising me to work hard, be diligent, and for encouraging me throughout all my life's ventures. To my grandparents for always offering sage advice and spoiling me with kindness. And to the large extended network of family and friends who have offered me unconditional love and support over the years. Finally, I would like to thank my extraordinary and brilliant wife, Amy-Lee, who stood by my side throughout graduate school with unwavering love, patience and cheer along with our horse son Winston, and I can only hope to repay her generosity many times over throughout our future years together.

Lastly, I want to say many thanks to everyone who provide me with support and guidance throughout my graduate studies and in my scientific research.



## LIST OF FIGURES

Figure	Page
I-1. Overview of projects in this dissertation .....	6
II-1. Particle sizes and entrapment efficiencies for NP-4 and NP-8 particles .....	21
II-2. Cumulative free drug release of QT and TAM from NP-8% and NP-4% particles .....	22
II-3. Cumulative TAM and QT release from NP-4s in simulated gastrointestinal fluid .....	23
II-4. Percentage of parent TAM (encapsulated in NP-4 and NP-8) remaining after 2 h incubation with CYP3A4 enzyme .....	25
II-5. Percentage free QT (encapsulated in NP-4 and NP-8) remaining after 2 h incubation with UGT1A9 enzyme .....	25
II-6. Plots show cell viability after exposure to free TAM, free QT, combined free QT and TAM (1:1) or NP-TAM-QTs .....	26
II-7. IC50 of free TAM, free QT, combination of TAM and QT and NP-TAM-QTs upon treatment with 4T1 cells.....	27
III-1. Bulk hydrogels with semibranched poly-allyl-glycidyl-ether-glycidol.....	48
III-2. The two synthesis methods used to produce nanohydrogels (nHGs) involved step-wise and one-pot approaches. ....	48
III-3. Characterization of nanohydrogels (nHGs) made by one-pot approach (nHGs-OP).....	49
III-4. Stability of nanohydrogels.....	50
III-5. Lysozyme (LYS) assay.....	51
III-6. Cytocompatibility via MTT assay for liposomes (LUVs), step-wise nanogels (nHGs-SW), and one-pot nanogels (NGs-OP) using NIH 3T3 cells .....	52
III-7. Drug loading of nanogels .....	52
III-8. Nile red release .....	54
III-9. The <i>in vitro</i> releases of NR and LYS from nanogels and liposomes .....	55

III-10. Synthesis of polyglycidol-gemcitabine conjugate .....	59
III-11. Drug release in vitro at pH 6 at 37 °C using float-a-lyzer method .....	59
III-12. Drug combinations that are possible with nanogel platform .....	59
III-13. Full labeled <sup>1</sup> H-NMR (600 MHz, MeOD) spectrum of AGE/GLY polymer .....	64
III-14. Full labeled inverse-gated <sup>13</sup> C-NMR (600 MHz) spectrum of AGE/GLY polymer .....	65
IV-1. Table that includes advantages and drawbacks of the three current most common enzyme immobilization strategies for building enzymatic bio-sensing surfaces .....	85
IV-2. Determination of spin-coat parameters .....	87
IV-3. Bright field microscopy image of semi-branched polyglycidol dose test .....	88
IV-4. Vanderbilt University logo patterned by electron beam lithography .....	89
IV-5. Relative absorbance measurements or enzyme cascade in free solution .....	91
IV-6. Device fabrication schemes .....	92
IV-7. Results of enzyme cascade bioactivities .....	93
IV-8. Inverse-gated <sup>13</sup> C-NMR (600 MHz) spectrum of semi-branched polyglycidol .....	97
V-1. General graft mechanism .....	111
V-2. SEM imaging of time study graft process .....	111
V-3. SEM imaging at the dotted line .....	112
V-4. General procedure for pre-irradiation grafting of polyglycidols to UHMWPE .....	113
V-5. Contact angle, FTIR, XPS and fluorescence results .....	114
V-6. Results of biofilm characterization of poly(glycidol) films .....	116
V-7. Synthesis scheme of poly(glycidol)-Cy5 Dye conjugate.....	122
V-8. Labeled <sup>1</sup> H-NMR (400 MHz, d <sub>6</sub> -DMSO) spectrum of poly(glycidol)-Cy5 conjugate.....	123

## TABLE OF CONTENTS

	Page
DEDICATION .....	ii
ACKNOWLEDGEMENTS .....	iii
LIST OF FIGURES .....	v
Chapter	
I. Introduction .....	1
Dissertation Overview .....	5
References .....	10
II. Dual Drug Delivery of Tamoxifen and Quercetin with Polyester Nanosponges: Enhanced Bioavailability and Regulated Metabolism for Anti-Cancer Treatment	
Introduction .....	18
Results and Discussion .....	20
Synthesis, loading and release of tamoxifen and quercetin from nanosponges .....	20
In vitro enzyme metabolism of tamoxifen and quercetin loaded nanosponges .....	24
Cell cytotoxicity studies with dual drug-loaded nanosponges .....	26
Conclusion .....	27
Experimental .....	28
References .....	36
III. One-pot Polyglycidol Nanogels via Liposome Master Templates for Combination Drug Delivery	
Introduction .....	43
Results and Discussion .....	46
Synthesis and characterization of step-wise and one-pot nanogels .....	46
Nile Red <i>in vitro</i> release studies .....	53
Lysozyme <i>in vitro</i> release studies .....	56
Synthesis and application of one-pot nanogels loaded with gemcitabine, polyglycidol-gemcitabine conjugate and trastuzumab .....	59
Conclusion .....	60
Experimental .....	61
References .....	74

IV. Electron Beam Lithography of Polyglycidol Nanogels For Immobilization of Three-Enzyme Cascade

Introduction.....	84
Results and Discussion .....	86
Development of semi-branched poly(glycidol) as negative electron beam (EBL) resist.....	86
Optimization of enzyme cascade in free solution .....	90
Enzyme immobilization with nanogels.....	91
Conclusion .....	94
Experimental .....	95
References.....	101

V. Polyglycidol Coating on Ultra-High Molecular Weight Polyethylene for Reduced Biofilm Growth

Introduction.....	109
Results and Discussion .....	110
Radiation grafting and characterization .....	110
Biofilm <i>in vitro</i> assay.....	115
Conclusion .....	117
Experimental .....	118
References.....	126

VI. Future Directions .....130

Appendix

A. References of Adaption for Chapters.....	133
B. Curriculum Vitae .....	134

## CHAPTER I

### INTRODUCTION

Novel biomedical materials which improve human health through enhancing therapeutic efficacy, disease diagnostics or implant stability are in higher demand than ever. As most anti-cancer treatments involve therapeutics that are exceedingly hydrophobic, it creates serious limitations in terms of bioavailability, efficacy and often leads to higher dosage requirements and enhanced side effects. Innovative strategies to improve sensitivity and robustness of enzymatic biosensors is also of growing medical importance. Implants for hip and knee surgery are often rejected by the body due to biofilm growth and infections. Polymers are known to be one of the most versatile classes of macromolecules and can be applied extensively to a wide array of medical fields. The synthesis and development of functional macromolecular architectures is important to advancements in nanomaterials for versatile drug delivery systems, biosensing platforms, and antimicrobial films.

Recent progress in nanotechnology has enabled rapid expansion at the interface of polymeric systems and biomedicine such that synthetic nanocarriers can be capable of entrapment and tunable releases of chemotherapeutics, improved potential bioavailability and tumor targeting, as well as anti-cancer effects. For example, prolonged blood circulation and tumor accumulation can be achieved by the enhanced permeability and retention (EPR) effect of particles between 10 and 150 nm in diameter to yield more favorable pharmacokinetic profiles. Alternatively, the delivery system can provide enhanced efficacy by utilizing targeting peptides attached the surface.<sup>1</sup> Nanoscopic delivery systems have proven valuable for solubilizing BCS class IV (hydrophobic)

drugs but also co-delivering a synergistic combination of hydrophobic drugs, where one drug positively affects the activity of another drug when administered together. Several nanosized platforms including micelles,<sup>2,3</sup> traditional poly (ethylene glycol)-block-poly lactide (PEG-PLA) particles,<sup>4,5</sup> and poly (lactic-co-glycolic acid) (PLGA) particles<sup>6</sup> have been investigated. Other examples of nanoscale dual delivery vehicles include natural vitamin D3 nanoparticles,<sup>7</sup> nanocells,<sup>1</sup> layer-by-layer nanoparticles,<sup>8</sup> carbon nanotubes,<sup>9</sup> graphene-oxide,<sup>10</sup> gel-liposome<sup>11</sup> and mesoporous silica nanospheres<sup>12</sup> which have been explored for the treatment of a multitude of cancers. It should be noted that today's commercial medical use of nanoparticles has been limited to two technologies: iron oxide nanoparticles for imaging or liposomes for drug delivery. And with a global market value of 150 billion dollars and climbing, the economic opportunity to develop novel drug delivery systems is also growing tremendously. Most delivery time courses for single or multiple hydrophobic drugs are guided by degradation of the nanocarrier, which has led researchers to develop nanoparticles which respond to environmental factors like pH, temperature or sound. However, it can be seen in most of these platforms that drug release is complete in just 72 hours and limited control is observed.

Combination therapies which use hydrophobic and hydrophilic protein therapeutics have gained incredible traction in clinical treatments such as combined chemo-immunotherapy, particularly in malignant and drug-resistant cancers.<sup>13</sup> It has been shown that chemotherapy by itself is not sufficient to effectively eradicate cancer cells because they can mutate rapidly. Therefore, large hydrophilic molecules such as cytokines have been employed to induce systemic immune responses against cancer cells and promote the body's ability to eradicate the cancer. Despite promising recent clinical and experimental results, anti-cancer efficacy is still sub-optimal due to short drug and protein half-lives, systemic toxicity, and divergent *in vivo* pharmacokinetics and

distribution.<sup>14</sup> And despite the versatility of applying known delivery carriers such as liposomes, star polymers, micelles, polyester nanosponges and poly(lactic-co-glycolic acid) (PLGA) particles, the dual and co-delivery of multiple therapeutic agents such as hydrophilic large biologicals with small hydrophobic chemotherapeutics from the same nanocarrier can impose challenges due to varying size dimensions of the therapeutics and their adverse solubilities.<sup>15-16</sup> This was a key motivation in our focus to develop and investigate a novel nanocarrier architecture.

Due to physicochemical limitations of natural polymers, synthetic polymers are the preferred materials for creating tailorable architectures with advanced biomedical capabilities. There are only a small number of polymers that have been tested in the human body, and even less have been validated for systemic administration. Examples such as poly(vinylpyrrolidone) (PVP)<sup>17</sup>, *N*-(2-hydroxypropyl)methacrylamide (PHPMA)<sup>18</sup> and polyethylene glycol (PEG)<sup>19</sup> and their copolymers are hydrophilic and clinically validated, but fall short in terms of chemical versatility due to their mostly linear chemical structures.

A highly advanced and emerging biocompatible polymer called poly(glycidol), also known as poly(glycerol), has a similar polyether backbone to PEG. However, the branching and multiple hydroxyl groups in its chemical structure enable more versatility for bioconjugations, higher hydrophilicity, and outstanding potential in numerous biomedical nano, micro and surface material applications. Frey and coworkers<sup>20</sup>, along with Haag and coworkers<sup>21</sup>, have developed hyperbranched and dendritic polyglycerols for multiple surface coating and nano drug delivery applications. However, the hyperbranched topographies are a limiting feature due to the dense outer corona which inhibits crosslinking chemistries from reaching the interior parts of the molecular structure. Therefore, homogenous tailorable nanonetworks cannot be achieved with these hyperbranched systems. Recently, Harth and coworkers have developed unique semi-

branched polyglycidols from tin triflate-catalyzed polymerization of glycidol monomers with a synthetic technique that tunes the branching based on temperature.<sup>22</sup> The resulting topography enables more versatile functionality and efficient crosslinking to prepare nanogels, hydrogels and coating applications to name a few. The observed biocompatibility of semibranched polyglycidol make it an excellent building block for extended release applications of biologicals.

Along with delivery of biologicals, the need to stabilize biologically active of enzymes in biosensor applications has grown significantly in the last decade. Multiple enzymes that can interact with each other via the “cascade effect” by converting medically important substrates into easily measurable chemical markers will be the basis for future advanced diagnostics, lab-on-a-chip, and food production quality control applications. The knowledge advanced by Harth and coworkers<sup>23</sup> from studying polyglycidol and its ability to serve as a capable building block for sustained nanoparticle release of lysozyme inspired the possibility for incorporating it in the immobilization of enzyme cascades on a surface for biosensing applications. Maynard and coworkers<sup>24</sup> showed that PEG which is covalently attached to enzyme molecules and crosslinked by electron beam lithography irradiation can render the enzymes still active to an extent. Covalent attachment methods enable an improved binding to the substrate, but chemical modifications come in part with loss of enzyme activity through alterations. To date, there are very few examples where multiple enzymes have been entrapped on a surface for cascade reactions, and reusability is rarely addressed. Surface-patterning methods such as dip-pen lithography and bias-assisted atomic force microscopy (AFM) have been explored for imprinting biomolecules on a solid support by adsorption and covalence, but electron beam lithography (EBL) has emerged as a powerful tool for creating arbitrary micron and nanoscale patterns that entrap proteins within a polymeric negative resist.<sup>25-29</sup>



Another pressing biomedical concern is infections that form from biofilm growth on newly implanted hip and knee replacements, which leads to approximately 59,000 revision surgeries per year in the United States.<sup>30</sup> Ultra-high molecular weight polyethylene (UHMWPE) is a strong, inert, stable and the most commonly used polymeric material for artificial hip and knee replacements.<sup>31</sup> However, its strongly hydrophobic surface chemistry leaves it susceptible to bacterial adhesion and biofilm formation, which is known to be the first conditioning step for infections.<sup>32</sup> The vast majority of recent advances in biomaterial technology involve techniques that alter the surface chemistry from hydrophobic to hydrophilic with polymer coating techniques such as layer-by-layer (LBL) deposition or self-assembled monolayers (SMA), which use van der Waals secondary or electrostatic forces.<sup>33</sup> It has been more recently shown that a covalent bond however is more ideal to impart both physical stability and hydrophilicity to a biomedical implant surface.<sup>34</sup> Aside from the most prominent hydrophilic polymers like PEG or zwitterionic coatings<sup>34</sup>, it has been recently realized that poly(glycidol) has potential to achieve more advanced functionality due to its greater oxidative stability and hydrophilicity. The ability to form polymeric coatings to prevent adherence of bacteria on implants is an exciting avenue of research.

### Dissertation Overview

Cationic ring-opening polymerizations have been utilized to synthesize poly(glycidol) and poly(ester) as macromolecular building blocks for nano and macro architectures. The poly(ester) polymers were employed for the synthesis of nanosponges and investigated for sustained dual hydrophobic drug delivery and regulated metabolism. Poly(glycidol) architectures were employed for the genesis of a novel nanogel carrier for sustained combination delivery with small hydrophobic and large hydrophilic therapeutics. Through these investigations, poly(glycidol) was

employed for a biosensing platform that can immobilize multiple functioning enzymes for improved detection and reusability, and a hydrogel coating was synthesized to potentially reduce the growth of microbial infections as showing by Figure I-1.

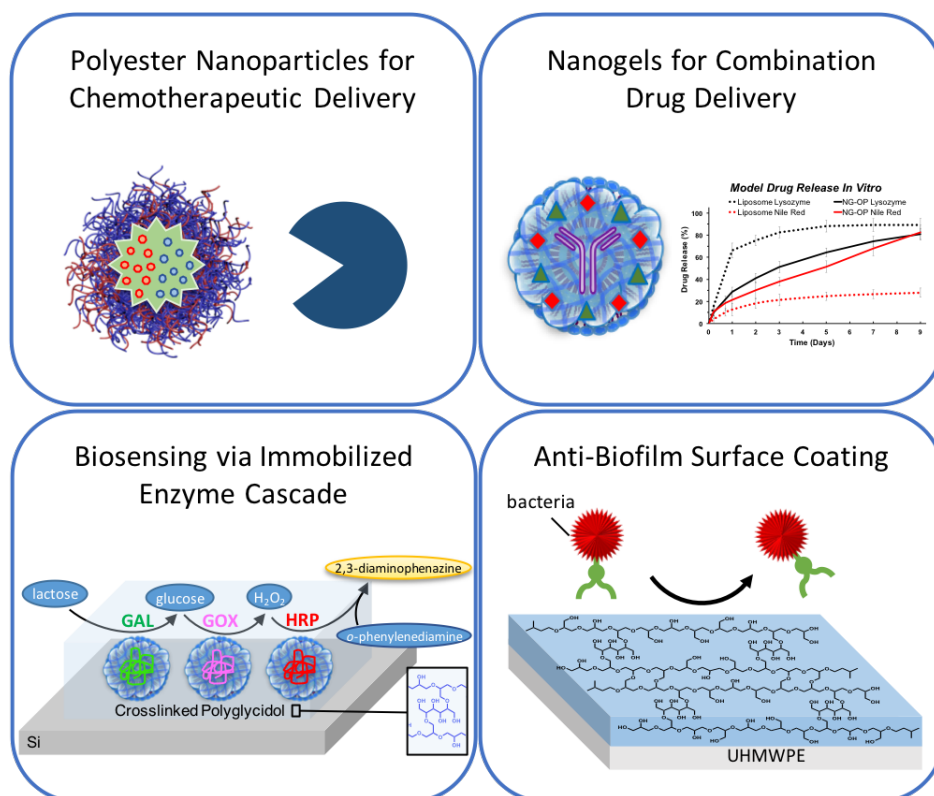


Figure I-1. Overview of projects in this dissertation.

The effect of nanoparticle architecture to influence or even regulate the metabolism of its therapeutic cargo has not been studied extensively. We hypothesized that the poly(ester) nanonetwork density in nanosponges (NP) might lead to an effect that is typically observed in prodrug approaches. In Chapter II, we chose to study the effect on dual drug release and metabolism with tamoxifen and quercetin as a model drug combination which well-known in synergistic anti-breast cancer treatments. Tamoxifen (TAM) has been the preeminent treatment

option for women with advanced breast cancer<sup>35</sup> but TAM is challenging to administer because of its hydrophobic solubility issues and extensive first-pass metabolism by the enzyme CYP3A4 in the liver.<sup>36</sup> This leads to low bioavailability and necessitates repetitive high doses. Quercetin (QT) on the other hand is a potent antioxidant and dietary flavanoid,<sup>37</sup> and has been shown to enhance the antitumor efficacy of TAM by promoting intestinal absorption<sup>38</sup> and reducing first-pass metabolism.<sup>39-41</sup> However, it is also not easily soluble in water and can be rapidly glucuronidated in the intestine which reduces its bioavailability drastically.<sup>42-43</sup> In the last few years, combination treatment of TAM with QT has been an effective way to improve the uptake of TAM and alleviate the hepatotoxicity generated throughout course of treatment.<sup>40</sup> To study this drug combination, two types of nanosponge particles (NP) with two crosslinking densities of 4% and 8% were synthesized and post-loaded with drugs TAM and QT (1:1) to evaluate the release kinetics, metabolism, gastric stability and cytotoxicity. To investigate the metabolism activity, specific P450 enzymes CYP3A4 and UGT1A9 were selected due to their high contributions in metabolizing TAM and QT, respectively. By increasing the crosslinking density, we demonstrated that the NP-TAM-QTs exhibit a tuned metabolism towards a slower rate, enhanced potential bioavailability, together with release kinetics that indicate that a dual loading does not alter the release kinetics of the individual drugs when released from a single carrier.<sup>44-46</sup>

While nanosponges work exceedingly well with hydrophobic drug releases and surface peptide conjugations<sup>44,47</sup>, we sought to generate a novel nanocarrier which can be loaded with both hydrophobic small molecules and large hydrophilic biologicals in the same vehicle. This is a challenging endeavor due to the adverse physiochemical properties but immensely important for future applications in combination chemotherapy with immunotherapy. We chose to utilize a liposomal template due to its dual amphiphilic nature to form a dual delivery system and aim for

a final product with unique features with no resemblance to the native carrier. In other words, the novel system attributes all its features from a newly created nanonetwork from liposomal templates which are significantly altered in the process. The reason this is important is because it has been shown that traditional liposome nanocarriers often do not release hydrophobic molecules completely, and release biologicals very fast in the first 24 h.<sup>48</sup> This unique nanomaterial was accomplished through the design and synthesis of tailored hydrophilic macromolecular building blocks, functionalized semi-branched poly(glycidol)s, and also through a developed one-pot extrusion technique. We report in Chapter III on the formation and characterization of a novel nanohydrogel (nHG) platform using a thiol-ene click cross-linking system composed of unique allyl-functionalized semi-branched polyglycidols and PEG dithiol (1 kDa). Two preparation methods are presented, one that in its methodology is comparable with traditional stepwise approaches and uses a prefabricated liposome as master template (nHG-SW) to form nanogels, and a second approach in which liposomal lipids are brought together with all components in one pot (nHG-OP) to yield a carrier with unique drug release characteristics that do not resemble liposomal delivery systems.

Through investigations of model *in vitro* release and therapeutic stability of the nanogels, we learned how the nanogels from the one-pot approach can entrap biologicals such as the lysozyme and still retain its activity. This was a basis of inspiration that enabled applications of the nanogel approach towards improving enzymatic biosensing systems.

We sought to create a sensing platform which employs enzyme-entrapped poly(glycidol) nanogel carriers to improve the spatial 3-D organization of multiple enzymes with a single EBL fabrication step and without harsh synthetic modifications as is often used in the literature<sup>49</sup>. As proof-of-concept, we spin-coated a three-enzyme cascade of  $\beta$ -galactosidase (GAL), glucose

oxygenase (GOX), and horseradish peroxidase (HRP) with and without nanogel pre-encapsulation and cross-linked the films within a semi-branched poly(glycidol) matrix by EBL as shown by Figure IV-6 in Chapter IV. Our previous work demonstrated that high enzyme loading and retained enzyme activity was feasible within the nano-networks of the poly(glycidol) nanogels we had developed previously,<sup>23-24</sup> and the three-enzyme cascade was chosen due to its important applications in the food and medical diagnostic industries.<sup>50</sup> Other attractive bioactive EBL resist materials have been tried such as aqueous-based silk and trehalose glycopolymers by Kaplan and Omenetto<sup>51</sup> and Maynard,<sup>52</sup> respectively. Herein Chapter IV, we demonstrate biosensing utility of the poly(glycidol) enzyme immobilization platform with improved performance, high reusability and storage stability via 3-D spatial arrangement of the three-enzyme cascade with nanogel entrapment compared to enzymes that were not nano-encapsulated. The resulting EBL patterns were investigated by bright-field microscopy and AFM, and the lactose enzyme cascade activity was determined by a chromogenic o-phenylenediamine indicator that was quantified by UV-vis spectrophotometry.

Through our investigations with poly(glycidol) (PG), it was realized that this polymer has potential to achieve bioinertness with even more advanced versatility towards implant coatings. While comparable in structure to poly(ethylene glycol) (PEG), PG offers tremendous advantages in terms of increased thermal stability, oxidative stability and can even form a hydrophilic barrier to biological adsorption.<sup>53</sup> Due to the chemical inertness of common biomaterials made from polyolefins, harsh activation methods such as UV-irradiation or plasma treatments are often required to modify those types of surfaces.<sup>54-55</sup> Haag and coworkers put forth an elegant “graft-to” approach using dendritic poly(glycidols) that were post-modified with amines in three synthetic steps, followed by grafting-to plasma-brominated polypropylene.<sup>56</sup> However, the highly branched

structures can limit surface coverage due to steric hindrance. Bucio and coworkers demonstrated that gamma-ray induced grafting of poly[2-(dimethylamino) ethyl methacrylate] (PDMAEMA) onto polyethylene (PE) films could be achieved by first exposing polyethylene to ionizing radiation, followed by exposure to high concentrations of monomer in solution.<sup>57</sup> Inspired by both Haag and Bucio, we sought to achieve an effective anti-biofilm coating with fewer processing steps using a “graft-from” approach with pre-irradiated PE and our unique semi-branched poly(glycidols) to coat the most commonly utilized biomaterials for hip-and-knee implants, ultra-high-molecular weight polyethylene (UHMWPE).<sup>58</sup> In Chapter V, advanced surface characterizations of the coatings along with resulting functional capabilities to resist bacterial biofilm growth can be found.

#### References

1. Sengupta, S.; Eavarone, D.; Capila, I.; Zhao, G. L.; Watson, N.; Kiziltepe, T.; Sasisekharan, R., Temporal targeting of tumour cells and neovasculature with a nanoscale delivery system. *Nature* **2005**, *436* (7050), 568-572.
2. Scarano, W.; de Souza, P.; Stenzel, M. H., Dual-drug delivery of curcumin and platinum drugs in polymeric micelles enhances the synergistic effects: a double act for the treatment of multidrug-resistant cancer. *Biomaterials Science* **2015**, *3* (1), 163-174.
3. Krishnamurthy, S.; Ke, X. Y.; Yang, Y. Y., Delivery of therapeutics using nanocarriers for targeting cancer cells and cancer stem cells. *Nanomedicine* **2015**, *10* (1), 143-160.
4. Wang, Q.; Bao, Y.; Ahire, J.; Chao, Y., Co-encapsulation of Biodegradable Nanoparticles with Silicon Quantum Dots and Quercetin for Monitored Delivery. *Advanced Healthcare Materials* **2013**, *2* (3), 459-466.

5. Soni, P.; Kaur, J.; Tikoo, K., Dual drug-loaded paclitaxel–thymoquinone nanoparticles for effective breast cancer therapy. *Journal of Nanoparticle Research C7 - 18* **2015**, *17* (1), 1-12.
6. Jain, A. K.; Thanki, K.; Jain, S., Co-encapsulation of Tamoxifen and Quercetin in Polymeric Nanoparticles: Implications on Oral Bioavailability, Antitumor Efficacy, and Drug-Induced Toxicity. *Molecular Pharmaceutics* **2013**, *10* (9), 3459-3474.
7. Palvai, S.; Nagraj, J.; Mapara, N.; Chowdhury, R.; Basu, S., Dual drug loaded vitamin D3 nanoparticle to target drug resistance in cancer. *Rsc Advances* **2014**, *4* (100), 57271-57281.
8. Deng, Z. J.; Morton, S. W.; Ben-Akiva, E.; Dreaden, E. C.; Shopsowitz, K. E.; Hammond, P. T., Layer-by-layer nanoparticles for systemic codelivery of an anticancer drug and siRNA for potential triple-negative breast cancer treatment. *ACS Nano* **2013**, *7* (11), 9571-84.
9. Chin, C. F.; Yap, S. Q.; Li, J.; Pastorin, G.; Ang, W. H., Ratiometric delivery of cisplatin and doxorubicin using tumour-targeting carbon-nanotubes entrapping platinum(iv) prodrugs. *Chemical Science* **2014**, *5* (6), 2265-2270.
10. Zhang, L.; Xia, J.; Zhao, Q.; Liu, L.; Zhang, Z., Functional graphene oxide as a nanocarrier for controlled loading and targeted delivery of mixed anticancer drugs. *Small* **2010**, *6* (4), 537-44.
11. Tripathy, N.; Ahmad, R.; Ko, H. A.; Khang, G.; Hahn, Y.-B., Enhanced anticancer potency using an acid-responsive ZnO-incorporated liposomal drug-delivery system. *Nanoscale* **2015**, *7* (9), 4088-4096.
12. Fang, Y.; Zheng, G. F.; Yang, J. P.; Tang, H. S.; Zhang, Y. F.; Kong, B.; Lv, Y. Y.; Xu, C. J.; Asiri, A. M.; Zi, J.; Zhang, F.; Zhao, D. Y., Dual-Pore Mesoporous Carbon@Silica Composite Core- Shell Nanospheres for Multidrug Delivery. *Angewandte Chemie International Edition* **2014**, *53* (21), 5366-5370.

13. Hu, C. M.; Zhang, L., Nanoparticle-based combination therapy toward overcoming drug resistance in cancer. *Biochemical Pharmacology* **2012**, *83* (8), 1104-11.
14. He, C.; Tang, Z.; Tian, H.; Chen, X., Co-delivery of chemotherapeutics and proteins for synergistic therapy. *Advanced Drug Delivery Reviews* **2016**, *98*, 64-76.
15. Wang, D. Y.; Sosman, J. A.; Johnson, D. B., Combination Immunotherapy: An Emerging Paradigm in Cancer Therapeutics. *Oncology (Williston Park, N.Y.)* **2015**, *29* (12).
16. Nars, M. S.; Kaneno, R., Immunomodulatory effects of low dose chemotherapy and perspectives of its combination with immunotherapy. *International Journal of Cancer* **2013**, *132* (11), 2471-8.
17. Ajani, J. A.; Hortobagyi, G. N.; Frye, D.; Levin, B.; Boman, B. M.; Faintuch, J. S., A randomized study of two schedules of copovithane in patients with advanced colorectal carcinoma. *American Journal of Clinical Oncology* **1987**, *10* (2), 139-40.
18. Duncan, R.; Gac-Breton, S.; Keane, R.; Musila, R.; Sat, Y. N.; Satchi, R.; Searle, F., Polymer-drug conjugates, PDEPT and PELT: basic principles for design and transfer from the laboratory to clinic. *Journal of Controlled Release* **2001**, *74* (1-3), 135-46.
19. Veronese, F. M.; Pasut, G., PEGylation, successful approach to drug delivery. *Drug Discovery Today* **2005**, *10* (21), 1451-8.
20. Wilms, D.; Stiriba, S. E.; Frey, H., Hyperbranched Polyglycerols: From the Controlled Synthesis of Biocompatible Polyether Polyols to Multipurpose Applications. *Accounts of Chemical Research* **2010**, *43* (1), 129-141.
21. Calderon, M.; Quadir, M. A.; Sharma, S. K.; Haag, R., Dendritic polyglycerols for biomedical applications. *Advanced Materials* **2010**, *22* (2), 190-218.



22. Spears, B. R.; Waksal, J.; McQuade, C.; Lanier, L.; Harth, E., Controlled branching of polyglycidol and formation of protein-glycidol bioconjugates via a graft-from approach with "PEG-like" arms. *Chemical Communications* **2013**, *49* (24), 2394-6.
23. Lockhart, J. N.; Beezer, D. B.; Stevens, D. M.; Spears, B. R.; Harth, E., One-pot polyglycidol nanogels via liposome master templates for dual drug delivery. *Journal of Controlled Release* **2016**, *244*, Part B, 366-374.
24. Mancini, R. J.; Paluck, S. J.; Bat, E.; Maynard, H. D., Encapsulated Hydrogels by E-beam Lithography and Their Use in Enzyme Cascade Reactions. *Langmuir* **2016**, *32* (16), 4043-4051.
25. Lee, K. B.; Lim, J. H.; Mirkin, C. A., Protein nanostructures formed via direct-write dip-pen nanolithography. *Journal of the American Chemical Society* **2003**, *125* (19), 5588-9.
26. Xing, C.; Zheng, Z.; Zhang, B.; Tang, J., Nanoscale patterning of multicomponent proteins by bias-assisted atomic force microscopy nanolithography. *Chemphyschem* **2011**, *12* (7), 1262-5.
27. Schnauber, P.; Schmidt, R.; Kaganskiy, A.; Heuser, T.; Gschrey, M.; Rodt, S.; Reitzenstein, S., Using low-contrast negative-tone PMMA at cryogenic temperatures for 3D electron beam lithography. *Nanotechnology* **2016**, *27* (19), 195301.
28. Lau, U. Y.; Saxer, S. S.; Lee, J.; Bat, E.; Maynard, H. D., Direct Write Protein Patterns for Multiplexed Cytokine Detection from Live Cells Using Electron Beam Lithography. *ACS Nano* **2016**, *10* (1), 723-9.
29. Zhang, J.; Cao, K.; Wang, X. S.; Cui, B., Metal-carbonyl organometallic polymers, PFpP, as resists for high-resolution positive and negative electron beam lithography. *Chemical Communications* **2015**, *51* (99), 17592-5.

30. Song, Z.; Borgwardt, L.; Hoiby, N.; Wu, H.; Sorensen, T. S.; Borgwardt, A., Prosthesis infections after orthopedic joint replacement: the possible role of bacterial biofilms. *Orthopedic Reviews* **2013**, *5* (2), 65-71.
31. Vu, N. B.; Truong, N. H.; Dang, L. T.; Phi, L. T.; Ho, N. T. T.; Pham, T. N.; Phan, T. P.; Pham, P. V., In vitro and in vivo biocompatibility of Ti-6Al-4V titanium alloy and UHMWPE polymer for total hip replacement. *Biomedical Research and Therapy* **2016**, *3* (3), 567-577.
32. Wei, Q.; Becherer, T.; Angioletti-Uberti, S.; Dzubiella, J.; Wischke, C.; Neffe, A. T.; Lendlein, A.; Ballauff, M.; Haag, R., Protein interactions with polymer coatings and biomaterials. *Angewandte Chemie International Edition* **2014**, *53* (31), 8004-31.
33. Banerjee, I.; Pangule, R. C.; Kane, R. S., Antifouling Coatings: Recent Developments in the Design of Surfaces That Prevent Fouling by Proteins, Bacteria, and Marine Organisms. *Advanced Materials* **2011**, *23* (6), 690-718.
34. Ngo, B. K. D.; Grunlan, M. A., Protein Resistant Polymeric Biomaterials. *ACS Macro Letters* **2017**, *6* (9), 992-1000.
35. Jain, A. K.; Swarnakar, N. K.; Godugu, C.; Singh, R. P.; Jain, S., The effect of the oral administration of polymeric nanoparticles on the efficacy and toxicity of tamoxifen. *Biomaterials* **2011**, *32* (2), 503-515.
36. Mugundu, G. M.; Sallans, L.; Guo, Y. Y.; Shaughnessy, E. A.; Desai, P. B., Assessment of the Impact of CYP3A Polymorphisms on the Formation of alpha-Hydroxytamoxifen and N-Desmethyltamoxifen in Human Liver Microsomes. *Drug Metabolism and Disposition* **2012**, *40* (2), 389-396.

37. Davis, J. M.; Carlstedt, C. J.; Chen, S.; Carmichael, M. D.; Murphy, E. A., The dietary flavonoid quercetin increases VO(2max) and endurance capacity. *International Journal of Sport Nutrition and Exercise Metabolism* **2010**, *20* (1), 56-62.
38. Caltagirone, S.; Ranelletti, F. O.; Rinelli, A.; Maggiano, N.; Colasante, A.; Musiani, P.; Aiello, F. B.; Piantelli, M., Interaction with type II estrogen binding sites and antiproliferative activity of tamoxifen and quercetin in human non-small-cell lung cancer. *American Journal of Respiratory Cell and Molecular Biology* **1997**, *17* (1), 51-9.
39. Osborne, C. K., Tamoxifen in the Treatment of Breast Cancer. *New England Journal of Medicine* **1998**, *339* (22), 1609-1618.
40. Shin, S.-C.; Choi, J.-S.; Li, X., Enhanced bioavailability of tamoxifen after oral administration of tamoxifen with quercetin in rats. *International Journal of Pharmaceutics* **2006**, *313* (1-2), 144-149.
41. Garcia-Saura, M. F.; Galisteo, M.; Villar, I. C.; Bermejo, A.; Zarzuelo, A.; Vargas, F.; Duarte, J., Effects of chronic quercetin treatment in experimental renovascular hypertension. *Molecular and Cellular Biochemistry* **2005**, *270* (1-2), 147-55.
42. Oliveira, E. J.; Watson, D. G., In vitro glucuronidation of kaempferol and quercetin by human UGT-1A9 microsomes. *FEBS Letters* **2000**, *471* (1), 1-6.
43. Graf, B. A.; Mullen, W.; Caldwell, S. T.; Hartley, R. C.; Duthie, G. G.; Lean, M. E. J.; Crozier, A.; Edwards, C. A., DISPOSITION AND METABOLISM OF [2-14C]QUERCETIN-4'-GLUCOSIDE IN RATS. *Drug Metabolism and Disposition* **2005**, *33* (7), 1036-1043.
44. Stevens, D. M.; Gilmore, K. A.; Harth, E., An assessment of nanosponges for intravenous and oral drug delivery of BCS class IV drugs: Drug delivery kinetics and solubilization. *Polymer Chemistry* **2014**, *5* (11), 3551-3554.

45. van der Ende, A. E.; Kravitz, E. J.; Harth, E., Approach to formation of multifunctional polyester particles in controlled nanoscopic dimensions. *Journal of the American Chemical Society* **2008**, *130* (27), 8706-13.
46. Rautio, J.; Kumpulainen, H.; Heimbach, T.; Oliyai, R.; Oh, D.; Jarvinen, T.; Savolainen, J., Prodrugs: design and clinical applications. In *Nature Reviews Drug Discovery*, England, 2008; Vol. 7, pp 255-70.
47. Hariri, G.; Edwards, A. D.; Merrill, T. B.; Greenbaum, J. M.; van der Ende, A. E.; Harth, E., Sequential targeted delivery of paclitaxel and camptothecin using a cross-linked "nanosponge" network for lung cancer chemotherapy. *Molecular Pharmaceutics* **2014**, *11* (1), 265-75.
48. Cipolla, D.; Wu, H.; Gonda, I.; Eastman, S.; Redelmeier, T.; Chan, H. K., Modifying the release properties of liposomes toward personalized medicine. *Journal of Pharmaceutical Sciences* **2014**, *103* (6), 1851-62.
49. Kolodziej, C. M.; Maynard, H. D., Electron-Beam Lithography for Patterning Biomolecules at the Micron and Nanometer Scale. *Chemistry of Materials* **2012**, *24* (5), 774-780.
50. Datta, S.; Christena, L. R.; Rajaram, Y. R., Enzyme immobilization: an overview on techniques and support materials. *3 Biotech* **2013**, *3* (1), 1-9.
51. Kim, S.; Marelli, B.; Brenckle, M. A.; Mitropoulos, A. N.; Gil, E. S.; Tsioris, K.; Tao, H.; Kaplan, D. L.; Omenetto, F. G., All-water-based electron-beam lithography using silk as a resist. *Nature Nanotechnology* **2014**, *9* (4), 306-10.
52. Bat, E.; Lee, J.; Lau, U. Y.; Maynard, H. D., Trehalose glycopolymer resists allow direct writing of protein patterns by electron-beam lithography. *Nature Communications* **2015**, *6*, 6654.

53. Siegers, C.; Biesalski, M.; Haag, R., Self-assembled monolayers of dendritic polyglycerol derivatives on gold that resist the adsorption of proteins. *Chemistry-A European Journal* **2004**, *10* (11), 2831-2838.
54. Deng, J. P.; Wang, L. F.; Liu, L. Y.; Yang, W. T., Developments and new applications of UV-induced surface graft polymerizations. *Progress in Polymer Science* **2009**, *34* (2), 156-193.
55. Farag, Z. R.; Friedrich, J. F.; Kruger, S., Adhesion promotion of thick fire-retardant melamine polymer dip-coatings at polyolefin surfaces by using plasma polymers. *Journal of Adhesion Science and Technology* **2014**, *28* (21), 2113-2132.
56. Lukowiak, M. C.; Wettmarshausen, S.; Hidde, G.; Landsberger, P.; Boenke, V.; Rodenacker, K.; Braun, U.; Friedrich, J. F.; Gorbushina, A. A.; Haag, R., Polyglycerol coated polypropylene surfaces for protein and bacteria resistance. *Polymer Chemistry* **2015**, *6* (8), 1350-1359.
57. Melendez-Ortiz, H. I.; Peralta, R. D.; Bucio, E.; Zerrweck-Maldonado, L., Preparation of Stimuli-Responsive Nanogels of Poly [2-(dimethylamino) Ethyl Methacrylate] by Heterophase and Microemulsion Polymerization Using Gamma Radiation. *Polymer Engineering and Science* **2014**, *54* (7), 1625-1631.
58. Jaganathan, S. K.; Balaji, A.; Vellayappan, M. V.; Subramanian, A. P.; John, A. A.; Asokan, M. K.; Supriyanto, E., Review: Radiation-induced surface modification of polymers for biomaterial application. *Journal of Materials Science* **2015**, *50* (5), 2007-2018.

## CHAPTER II

# DUAL DRUG DELIVERY OF TAMOXIFEN AND QUERCETIN WITH POLYESTER NANOSPONGES: ENHANCED BIOAVAILABILITY AND REGULATED METABOLISM FOR ANTI-CANCER TREATMENT

### Introduction

Substantial therapeutic benefits are observed from a combination of drugs, in which one drug affects the activity of another drug when administered together, also known as the synergistic effect.<sup>1</sup> Dual and multiple drug delivery must be carefully studied because overdosing or other side effects can occur due to the enhanced activity. Many of these drug combinations are described and studied for cancer chemotherapy<sup>2</sup> but are not limited to these disease profiles.<sup>3</sup> In fact, it can be witnessed that nanoscopic delivery systems are ideal not only to solubilize BCS class IV drugs but also provide opportunities to co-deliver a synergistic drug combination. Several nano-sized platforms including micelles,<sup>4,5</sup> squalene based micelles,<sup>6,7,8</sup> traditional poly (ethylene glycol)-block-poly lactide (PEG-PLA) particles,<sup>9,10</sup> and poly (lactic-co-glycolic acid) (PLGA) particles<sup>11</sup> have been investigated. Other examples of nanoscale dual delivery vehicles are vitamin D3 nanoparticles,<sup>12</sup> nanocells,<sup>13</sup> minicells,<sup>14</sup> drug-nano-particles,<sup>15</sup> micelleplexes,<sup>16</sup> layer-by-layer nanoparticles,<sup>17</sup> carbon nanotubes,<sup>18</sup> graphene-oxide,<sup>19</sup> gel-liposome<sup>20</sup> and mesoporous silica nanospheres<sup>21</sup> which have been explored for the treatment of a multitude of cancers. It is noted that the delivery platforms specialized to deliver two hydrophobic drugs are mainly guided by the degradation of the carrier and the location of these drugs within the nanoscale structure. When a more water-soluble drug is in the mix, in these cases a prodrug is formed to avoid a rapid escape from the carrier. Recently,

the response of a polymeric delivery carrier towards a stimulus such as pH or temperature has received a lot of attention to achieve a control over the time point and speed of delivery. These developments can be seen as a response to the often-limited control in degradation-guided delivery systems in which a fast release in the first 72 hours is observed. Degradation-guided delivery systems are traditionally prepared via solvent-change methods or salting out, leading to a self-assembled nanoscale particle containing the drug. Therefore, the degradation is guided by physicochemical properties only and limited control is observed. With the introduction of a chemical crosslinking that can be varied, we have developed the nanosponges (NP) to enhance the control over the degradation. In numerous examples, we have shown that the crosslinking density plays a main role in the delivery kinetics of these crosslinked nanonetworks. While we have conducted targeted drug delivery with one drug to be delivered per nanoparticle and also demonstrated the use of a sequential approach, we sought in this work to investigate the dual delivery of a synergistic drug combination to be combined into the same particle. Furthermore, the effect of the nanoparticle architecture to influence or even regulate the metabolism has not been studied extensively. We hypothesized that the nanonetwork density in nanosponges might lead to an effect that is typically observed in prodrug approaches. The incorporation of a drug combination which is protected by two different nanonetworks of varied composition is thought to lead to a different exposure to the metabolizing factors together with the aspects leading to degradation and release of the dual drug combination. In this work, we chose to study the effect on dual drug release and metabolism with tamoxifen and quercetin as drug combination known in synergistic anti-breast cancer treatments. Tamoxifen (TAM) has been the preeminent treatment option for women with advanced breast cancer<sup>22</sup> but TAM is challenging to administer because of solubility issues and undergoes extensive first-pass metabolism by CYP3A4 in the liver.<sup>23</sup> This causes a low

bioavailability and necessitates repetitive high doses. Quercetin (QT) on the other hand is a potent antioxidant and dietary flavanoid,<sup>24</sup> and has been shown to enhance the antitumor efficacy of TAM by promoting intestinal absorption<sup>25</sup> and reducing first-pass metabolism.<sup>26-28</sup> However, it is also not easily soluble in water and can be rapidly glucuronidated in the intestine which reduces its bioavailability drastically.<sup>29-30</sup> In the last few years, combination treatment of TAM with QT has been an effective way to improve the uptake of TAM and alleviate the hepatotoxicity generated throughout course of treatment.<sup>27</sup> To study this drug combination we sought to synthesize two types of nanosponge particles (NP) with two crosslinking densities of 4% and 8%, and postload them with TAM and QT (1:1) to evaluate the release kinetics, metabolism, gastric stability and cytotoxicity. To test the metabolism activity, the specific P450 enzymes CYP3A4 and UGT1A9 were selected due to their high contributions in metabolizing TAM and QT, respectively. In here, with increasing the crosslinking density we show that NP-TAM-QTs exhibit a tuned metabolism towards a slower rate, enhanced potential bioavailability, together with release kinetics that indicate that a dual loading does not alter the release kinetics of the individual drugs when released from a single carrier.<sup>31-33</sup>

## Results and Discussion

### **Synthesis, loading and release of tamoxifen and quercetin from nanosponges**

We first synthesized the nanoparticles via the intermolecular crosslinking reaction from linear poly(avl-evl) with 4 or 8 percent epoxide stemming from a complete oxidation of the allyl functionality in the corresponding poly(vl-avl). It has been observed that Sn(OTf)<sub>2</sub> with its high reactivity at room temperature needs to be carefully removed to not affect the subsequent oxidation step by an unwanted ring opening of the epoxide.<sup>34,35</sup> This can be done by efficient precipitation as



reported before<sup>31</sup> or in a more efficient way with SiliaMetS®Cysteine that is added at the end of the polymerization and filtered off before a final precipitation of the polymer into cold methanol. With this, we found that the subsequent epoxidation reaction is more robust. The nanosponge synthesis was adapted from the procedure by Stevens, et al.<sup>31</sup> After successful nanoparticle synthesis the particles were loaded with QT and TAM via a developed nanoprecipitation method. As shown in the table of Figure II-1, the entrapment efficiency improved from 69.1 to 72.7% for TAM and 77.2 to 78% for QT when comparing the post-loading for NP-4 particles to NP-8 particles.

<b>Formulation</b>	<b>NP-4</b>	<b>NP-8</b>
<b>Particle Size (nm)</b>	89.3 ± 14.8	91.5 ± 9.8
<b>Theoretical loading (%)</b>	20	20
<b>Total Practical Loading (%)</b>	14.63	15.06
<b>Practical Loading (%)</b>	TAM	6.91 ± 0.13
	QT	7.72 ± 0.15
<b>Loading Efficiency (%)</b>	TAM	69.11 ± 1.31
	QT	77.24 ± 1.54

Figure II-1. Particle sizes and entrapment efficiencies for NP-4 and NP-8 particles. \*Data represent means ± SD (n=3).

We attribute the higher loading efficiency to the denser network in the 8% crosslinked nanoparticles. The overall higher loading efficiency of QT in contrast to TAM might be the result of a higher a higher loading of hydrogen bonding between the hydroxyl groups of the QT molecule with the secondary amines in the crosslinker of the nanoparticle network. The particle size was very similar between the NP-8 and NP-4 as determined by transmission electron microscopy

(TEM) and around 100 nm. After determining the drug loading of around 14%, we sought to investigate whether the dual loading would influence the release of the individual drugs and a drug-drug interaction is occurring that results in an unexpected release profile. As shown in Figure II-2, there was an expected initial release of 22 and 25% from the NP-4 for a nanoparticle in the first day for TAM and QT, respectively, followed by a slow, linear release ending at 89 and 97% after 21 days.

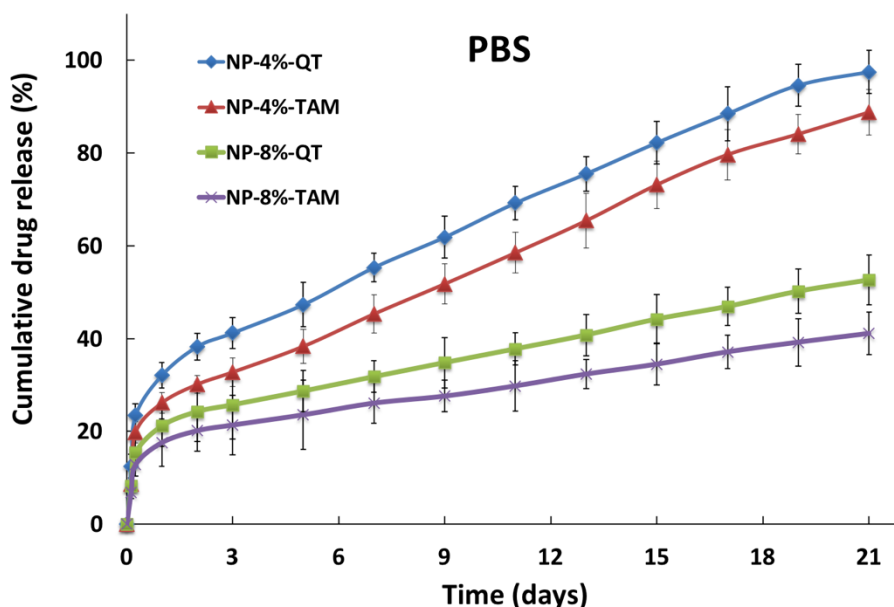


Figure II-2. Cumulative free drug release of QT and TAM from NP-8% and NP-4% particles in PBS at 37 °C over the course of 21 days.

The TAM release kinetics from our NP-4 and NP-8 were more consistent with previous reports of drug release by the anti-cancer drug Paclitaxel, which had an initial 1 day burst of 25% from the NP-4 and 12% release in the NP-10%.<sup>31</sup> Moreover, the release plot shows QT and TAM exhibited similar linear release kinetics with QT releasing slightly more on day 2 (38%) than TAM (30%).

We attribute this effect to the higher water solubility of QT versus TAM. A similar difference in release was noticed in the NP-8, when 30% of TAM and 52% QT was released after 21 days. It also can be said that the lower crosslinking density of the NP can provide a faster release where 50% drug is released in 9 days (NP-4), or slow release where 50% drug is released in 21 days (NP-8) as observed in the Paclitaxel release in comparable particle densities. Therefore, the dual release can be tailored for the desired application.

Free TAM and QT were monitored for its stability in the NP-4 formulation under conditions that mimic a gastro-intestinal environment and the stability test was run for 2 h which are standard conditions.<sup>36</sup> The resulting plot (see Figure II-3) shows that after 2 h, only 20% of TAM and 12% QT is released, which indicates a high stability of the NP-TAM and NP-QT formulations in SGF media.<sup>31</sup> Interestingly, more TAM than QT was released into the SGF media, indicating that TAM may be more likely to release at low pH conditions. Nonetheless, the nanoparticle formulation is stable in SGF and presents a promising platform application for combination oral drug delivery of TAM and QT.

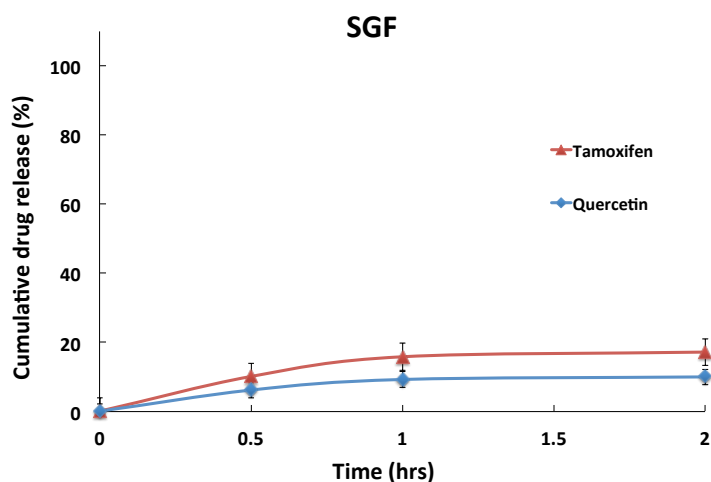


Figure II-3. Cumulative TAM and QT release from NP-4s in simulated gastrointestinal fluid (SGF) media at 37°C.

### ***In vitro* enzyme metabolism of tamoxifen and quercetin loaded nanosponges**

The bioavailability of tamoxifen and quercetin is limited because of fast metabolism in the liver.<sup>37</sup> We wanted to test our NP-4 and NP-8 dual drug formulations against enzymes under *in vitro* conditions consistent with experiments commonly cited in the literature for free TAM and QT.<sup>29,38</sup> TAM is extensively metabolized by the P450 CYP3A4 enzyme to metabolites N-desmethyltamoxifen, 4-hydroxytamoxifen and endoxifen.<sup>39</sup> QT is rapidly conjugated by UGT1A9 microsomes in the intestinal wall.<sup>40,30</sup> In order to detect how much free drug is metabolized in the NP formulations, we monitored the parent loss of TAM and QT in buffers under physiological temperature (37° C) and pH = 7.5. The quantity of free drug remaining after two hours for the NP-drug groups directly were compared with the free drug control groups. Figure II-4 illustrates a roughly 2-fold reduction in metabolism from 65% TAM (NP-4) to 36% TAM remaining, and a 77% (NP-8) to 35% TAM remaining after 2 h incubation with enzyme. The effect on QT was even more substantial with a 3 log reduction in metabolism from 74% QT (NP-4) to 19%, and a 4-fold reduction from 80 to 21% (NP-8) parent drug remaining (see Figure II-5). Each reaction set was run with a blank and control (no enzyme) to correct from any contact loss or compound degradation. It is apparent that the polymeric nanonetwork of the particle provides a protection effect for the drug, and the data suggests using a particle composition with higher crosslinking density can reduce metabolism further and improve bioavailability of the combination drug therapy.

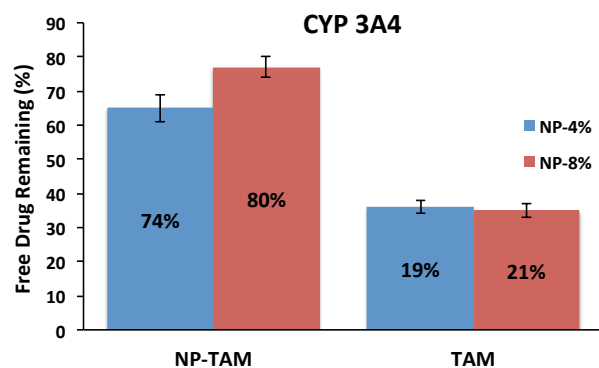


Figure II-4. Percentage of parent TAM (encapsulated in NP-4 and NP-8) remaining after 2 h incubation with CYP3A4 enzyme at 37°C.

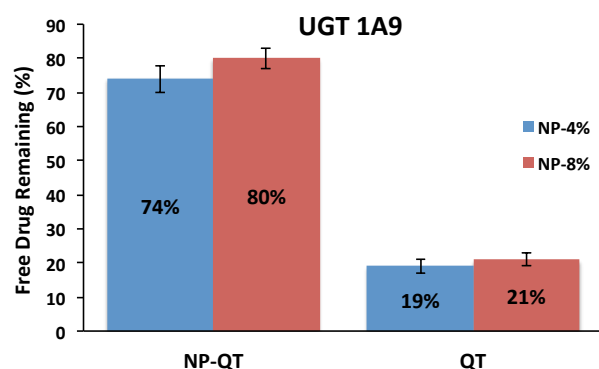


Figure II-5. Percentage free QT (encapsulated in NP-4 and NP-8) remaining after 2 h incubation with UGT1A9 enzyme at 37°C.

### Cell cytotoxicity studies with dual drug-loaded nanosponges

As the literature suggests,<sup>37</sup> the combination of QT and TAM exhibited increased anti-cancer cell activity in combination compared with either drug alone,<sup>41</sup> and our results indicate that free TAM+QT and NP-TAM-QT formulations imposed a similar effect on 4T1 cell viability after 24, 48 and 72 h of incubation (See Figure II-6) in MTT cytotoxicity assays. A time and concentration dependent decrease in cell viability against the 4T1 cell line was observed in all formulations tested. In this study, we only tested NP-4s because we anticipate that using NP-8s would result in

very similar results as the NP-4 because of the nearly identical composition. Regression analysis showed  $IC_{50}$  values in the table in Figure II-7 were similar between NP- drugs and free drugs ( $\sim 0.1 \mu\text{g/mL}$  at 72 h). On the other hand, recovery experiments revealed the  $IC_{50}$  value was significantly lower for NP-TAM-QTs ( $2.12 \mu\text{g/mL}$ ) compared with free drug ( $305.85 \mu\text{g/mL}$ ), which suggests the anti-cancer cell activity is preserved in the NP formulation and may even enhance the TAM and QT dual drug efficacy more than one hundred-fold.

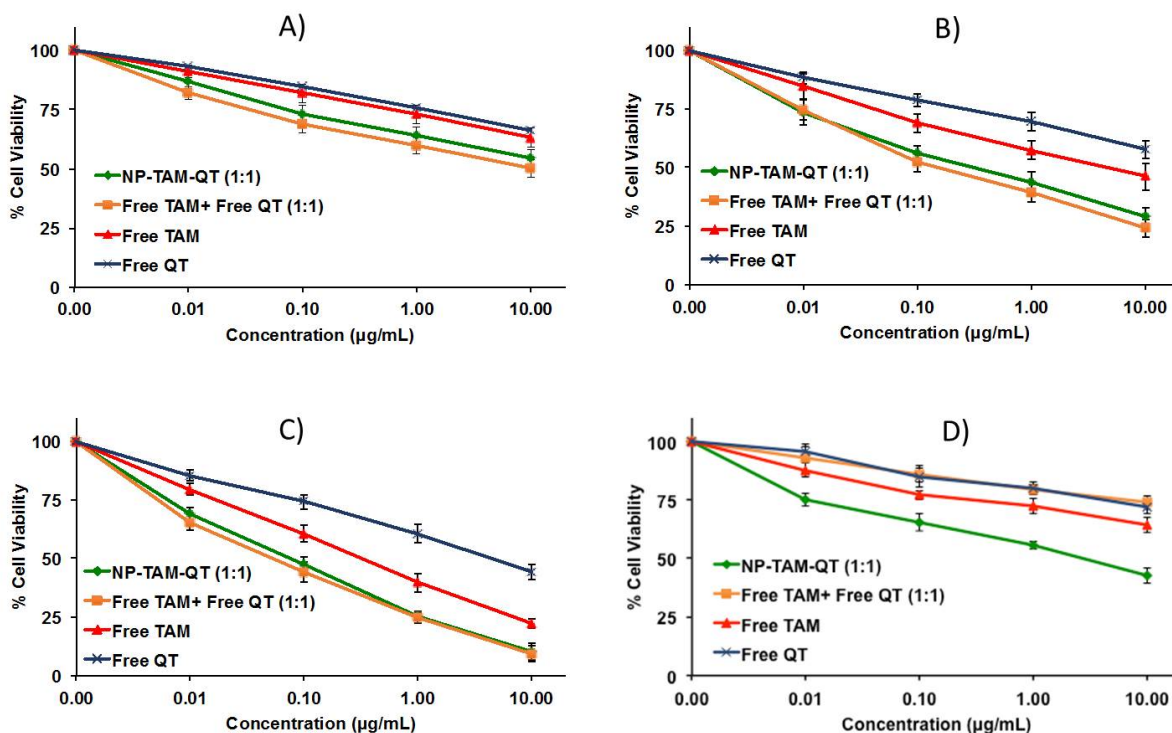


Figure II-6. Plots show cell viability after exposure to free TAM, free QT, combined free QT and TAM (1:1) or NP-TAM-QTs after (A) 24 h, (B) 48, (C) 72 and (D) recovery conditions. Each data point represents the mean  $\pm$  SD (n=3).

Formulation	IC <sub>50</sub> value (μg/mL)*			
	24h	48h	72h	Recovery
Free QT	65.32 ± 3.56	52.17 ± 2.23	4.90 ± 0.83	365.12 ± 14.54
Free TAM	42.39 ± 1.35	20.18 ± 1.28	0.35 ± 0.02	450.32 ± 16.23
Free TAM + QT (1:1)	10.82 ± 1.71	0.51 ± 0.03	0.088 ± 0.011	305.85 ± 10.87
NP-TAM-QTs	14.15 ± 1.19	0.27 ± 0.04	0.104 ± 0.013	2.12 ± 0.22

Figure II-7. IC<sub>50</sub> of free TAM, free QT, combination of TAM and QT and NP-TAM-QTs upon treatment with 4T1 cells. \*Data expressed as mean ± SD (n=3).

### Conclusion

We can summarize that this work supports a formulation strategy to synthesize and co-load a clinically relevant drug combination, TAM and QT, into a single dosage form. Previous reports have demonstrated how the targeting potential of our NPs can further enhance the therapeutic efficacy of cancer treatments.<sup>42</sup> The inclusion of an antioxidant helps in easing the oxidative stress induced by free radicals generated during the course of TAM therapy,<sup>43</sup> which is corroborated by our MTT cytotoxicity study. The NP-TAM-QT preparation posed higher cell cytotoxicity in contrast to the free drug combination. In the future, multiple dose kinetics and *in vivo* distribution studies can be performed to better understand the advantages of our combined formulation over any individual free drug regimen. NPs can be synthesized to encapsulate and protect TAM and QT and tune down the *in vitro* metabolism by up to 4-fold for QT and over 2-fold for TAM. There are many potential therapeutic applications where a slowed metabolism is beneficial.<sup>44</sup> Crosslinking density of our NPs can be modified to control the release and impact the metabolism of the encapsulated drug, and all particles were prepared in 100 nm size range, which is ideal for both

I.V. administration and oral delivery of drugs.<sup>45</sup> In summary, we hopefully have demonstrated the potential for tunable metabolism, improved therapeutic efficacy and controlled dual drug release functionality our NP-drug formulation can offer for breast cancer and many other potential therapeutic applications.

## Experimental

### Materials

TAM (Free Base), QT (anhydrous), Tween-80, 2,2'-(ethylenedioxy) diethylamine crosslinker, tin triflate, D- $\alpha$ -tocopherol polyethylene glycol 1000 succinate (Vit-E Peg), uridine diphosphoglucuronic acid (UDP-GluA) 1,1,1 tris-hydroxymethyl ethane, glucose-6-phosphate, and  $\beta$ -glucuronidase and were purchased from Sigma, USA.  $\delta$ -valerolactone and meta-chloroperoxybenzoic acid was also purchased from Sigma and purified via Kugelrohr distillation before use. The  $\alpha$ -allyl- $\delta$ -valerolactone was synthesized in-house according to a published protocol.<sup>46</sup> Tin scavenger SiliaMetS®Cysteine was purchased from Silicycle, USA. Phosphate buffered saline (PBS, 1X) was obtained from Gibco by Life Technologies, pH adjusted to 7.4, and supplemented with Tween-80 (0.1% v/v) for *in vitro* drug release studies. Dialysis tubing SpectraPor® (10k MWCO) was purchased from Spectrum Laboratories, Inc. Human CYP3A4 BACULOSOMES®, MTT reagent, and Human UGT-1A9 microsomes (20mg/mL) were purchased from Life Technologies, NADPH from Santa Cruz biotech, and Glucose-6-phosphate Dehydrogenase (G6P) was purchased from Millipore. All other solvents or reagents were purchased from Sigma Aldrich and used as received.



## Characterization

<sup>1</sup>H NMR spectra were obtained from a Bruker AV400 Fourier transform spectrometer with CDCl<sub>3</sub> as the solvent. High performance liquid chromatography (HPLC) was carried out using a Waters system equipped with a Waters 2996 variable wavelength photodiode array detector, a Waters 1525 binary HPLC pump, and a Thermo Synchronis C18 (100 x 4.6mm, 5μm) column. Runs were carried out using an isocratic gradient of methanol and water (70:30) with 0.1% TFA at a flow rate of 1.2 mL/min. Polyester nanoparticle samples for transmission electron microscopy (TEM) were prepared by dissolving 0.5 mg of nanoparticles in a 1 mL of cell culture water (GIBCO). Samples were sonicated for 5 min and then stained with 6 drops of 3% phosphotungstic acid. Carbon grids were prepared by dipping an Ultrathin Carbon Type-A 400 Mesh Copper Grid (Ted Pella, Inc., Redding, CA) into the particle solution three times, followed by drying overnight at room temperature. TEM images were obtained using a FEI Technai Osiris transmission electron microscope operated at 200 kV in bright field mode. Cell cytotoxicity was measured by a Synergy HT Microtiter Plate reader (BIO-TEK) at 540nm.

## Linear polymer synthesis poly(vl-avl)

A roughly 3000 Da ( $\alpha$ -allyl- $\delta$ -valerolactone,  $\delta$ -valerolactone) (AVL-VL, 4% AVL) polymer was synthesized in a N<sub>2</sub>-purged flame-dried 25-mL round bottom flask containing a catalytic amount (2.63 mg,  $1.97 \times 10^{-2}$  mol,  $3.2 \times 10^{-4}$  eq.) of tin triflate in the bottom of the round bottom flask, and then the flask was again purged with nitrogen. The 3-methyl-1-butanol initiator (73uL, 0.25 mmol, 0.37 eq) was added to the flask, and the mixture was stirred for 30 minutes to allow the catalyst to coordinate to the alcohol group on the initiator. The  $\delta$ -valerolactone (1.75 mL, 9.03 mmol, 13.3 eq) and the  $\alpha$ -allyl- $\delta$ -valerolactone (0.103 mL, 0.68 mmol, 1.0 eq) were added to the reaction

mixture along with the DCM (1.08 mL, 6.6 M), and the reaction was allowed to stir for 16-18 hours. After the reaction, a tin scavenger SiliaMetS®Cystein (Silicycle, 8 mol eq/mol tin) was added to the copolymer, stirred for 1 h, and removed by gravity filtration in DCM. The resulting polymer was purified by precipitation in methanol at -80°C and dried overnight. 1.6g yield (80%). <sup>1</sup>H NMR (400 MHz, CDCl<sub>3</sub>) δ: 0.92 (6H, d, CH<sub>3</sub>), 1.47-1.78 (8H, m, CH<sub>2</sub>), 1.86 (1H, m, CH), 2.14-2.52 (5H, m, CH<sub>2</sub>, CH), 3.65 (2H, t, CH<sub>2</sub>), 4.08 (4H, m, CH<sub>2</sub>), 5.04 (2H, m, CH<sub>2</sub>) 5.73 (1H, m, CH). A similar preparation was followed to synthesize the 8% AVL/VL polymer with VL (3.21 mL, 0.03456 mol), AVL (0.50mL, 0.003832 mol), 3-methyl-1-butanol (145μL, 0.1172 mol), and 1.97mL DCM (6.6 M). 3.3 g yield (83%). M<sub>w</sub>(NMR): 3245 g/mol. In a 6 dram vial, the VL/AVL polymer (0.500 g, 0.301 mmol, 1.0 eq) was added along with m-CPBA (62.4 mg, 0.362 mmol, 1.2 eq/allyl). CDCl<sub>3</sub> solvent was added to a final concentration of 6.5 x 10<sup>-3</sup> M. The vial was capped and allowed to stir at room temperature for 48 h. Oxidized polymer was purified by washing with saturated sodium bicarbonate (3 times) and brine (1 time), 65% yield. <sup>1</sup>H NMR (400MHz, CDCl<sub>3</sub>): In all cases, 100% conversion of allyl to epoxide was achieved as indicated by the disappearance of alkene proton shifts at 5.0 and 5.7 ppm and the presence of small broad peaks at 2.4, 2.7 and 2.9 ppm from the epoxide ring. M<sub>w</sub> (NMR): 3343 g/mol.

#### **Nanoparticle synthesis: 4% crosslinking with 1.5 of amines per epoxide**

A 340 mg amount of the oxidized poly (vl/evl) linear polymer with a M<sub>w</sub>(NMR) of 3400 g/mol was added to a 50-mL round bottom flask and dissolved in 35.8 ml DCM to reach a 3.24x10<sup>-3</sup> M concentration of the epoxide unit. 2,2'-(ethylenedioxy) diethylamine crosslinker, 12.7 μl (calculated for 0.75 eq of crosslinker molecules per epoxide, or 1.5 eq of amine per epoxide) was added via syringe to the polymer solution and refluxed at 46°C for 12 hours. The resulting particles

were purified by dialysis using Snakeskin Dialysis tubing (MWCO = 10,000) against DCM (changed 3 times daily) for 72 hours, and product was dried by rotovap and put overnight under vacuum. Particle size and morphology were determined by transmission electron microscopy at 200kV. Yield: 240 mg, 71% isolated nanoparticles as an off-white solid.

#### **Nanoparticle synthesis: 8% crosslinking with 1.5 amines per epoxide**

A 120 mg quantity of the oxidized poly (vl/evl) linear polymer with 8 wt % of epoxide and a  $M_w$  (NMR) of 3400 g/mol was added to a 50 mL round bottom flask and dissolved in 28.9 ml DCM to reach a  $3.24 \times 10^{-3}$  mol concentration of the epoxide unit. Then, 2,2'-(ethylenedioxy) diethylamine crosslinker, 10.3  $\mu$ L (calculated for 0.75 eq of crosslinker molecules per epoxide, or 1.5 eq of amine per epoxide) was added via microsyringe to the polymer solution and refluxed at 46°C for 12 hours. The resulting particles were purified by dialysis using Snakeskin Dialysis tubing (MWCO = 10,000) against DCM for 72 hours, and product was dried by rotovap and put overnight under vacuum. Particle size and uniformity were determined by transmission electron microscopy at 200kV. Yield: 98 mg, 82% isolated nanoparticles as an off-white solid.

#### **Post-loading TAM and QT into NPs**

A solution of 0.1% D- $\alpha$ -tocopherol polyethylene glycol 1000 succinate (0.40 g) was dissolved in distilled water (40.0 mL). To a separate tube, poly(vl-evl) nanoparticles (80.0 mg), TAM (10 mg) and QT (10 mg) were added and dissolved in minimal dimethyl sulfoxide (~100 $\mu$ L). The particle-drug solution was added dropwise to the vigorously stirring polyethylene glycol solution. The dual drug loaded particles were centrifuged for two cycles at 7830 rpm for 20 minutes/cycle. The resulting pellet was re-suspended in fresh distilled water and lyophilized to aid in the removal of

any residual dimethyl sulfoxide. Freeze-dried NP-TAM-QTs were stored at 4°C until use. The weight percent of post-loaded tamoxifen and quercetin was determined by HPLC by comparing the areas under the curves at 265nm to previously constructed calibration curves.

### **Dual drug release of NP-TAM-QTs**

Polyester nanoparticles (4% and 8% NPs) containing encapsulated QT and TAM were suspended in PBS (1X, pH 7.4, 0.1% Tween-80) to a final drug concentration of 0.3 mM TAM and QT (1:1). The mixture was stirred at 37°C, and buffer was collected and exchanged every 48 hours for 21 days. At each time point, the suspension was centrifuged at 7830 rpm for 15 minutes and the supernatant was collected and replaced with fresh buffer. Injections of 30µL of supernatants were made on the HPLC as described in the characterization section. The amount of drug released at each time point was calculated from a calibration curve, and all experiments were performed in triplicate. Tween-80 was used as surfactant to solvate the released TAM and prevent it from binding to the walls of the incubation container.<sup>31</sup>

### **Stability in Simulated gastro-intestinal (GI) fluid**

Simulated GI fluid was prepared by dissolving 2.0 grams NaCl in 7.0 mL concentrated HCl, diluting to 1.0 L of water, adjusted to pH 1.2 and supplemented with Tween-80 (0.1% v/v). Freeze-dried NP-TAM-QTs were suspended in GI media to a final drug concentration of 0.3 mM TAM and QT (1:1), and allowed to incubate at 37°C. At 30 min, 1h, and 2 h time points, the mixture was pelleted at 7830 rpm, and the supernatant was transferred, neutralized with sodium bicarbonate to pH 7 and extracted three times with 5 mL CH<sub>2</sub>Cl<sub>2</sub>. The CH<sub>2</sub>Cl<sub>2</sub> was evaporated and the resulting

solid was reconstituted in methanol/water (1:1 v/v). Drug content was quantified by HPLC, and all experiments were performed in triplicate.

### **Metabolism of NP-TAMs**

Procedure adapted from Kim, et al.<sup>38</sup> Tamoxifen was incorporated into 4% and 8% cross-linked NPs using a loading procedure as previously described.<sup>31</sup> Free TAM (0.5  $\mu$ M, 0.2mg/mL) and NP-TAM were incubated separately at 37°C for 2 h in 1X PBS, pH 7.4 (GIBCO), with 50 pmol of CYP3A4 BACULOSOMES® (Life Technologies), 1.3mM NADPH, 3.3mM glucose-6-phosphate, 3.3mM MgCl<sub>2</sub>, and glucose-6-phosphate dehydrogenase (0.4U/mL) in a 1.5-mL Eppendorf tubes with a total reaction volume of 0.5mL. The reaction mixture was pre-warmed at 37°C, and metabolism was started by the addition of enzyme (kept on ice until use). A control reaction with free TAM was run alongside with no enzyme added, and each reaction (NP-TAM, TAM, TAM control) was performed in triplicate. After 2h, the reaction was stopped by the addition of 500  $\mu$ L of cold methanol. The samples were mixed by vortex and then centrifuged at 7830 rpm for 15 min. 30  $\mu$ L of supernatant was injected directly onto the HPLC and peak areas were compared to a standard curve 6.25-100  $\mu$ g/mL in MeOH:Water (1:1) to quantify the amount of free TAM remaining after 2h.

### **Metabolism of NP-QTs**

QT metabolism procedure was adapted from Oliveira et al.<sup>29</sup> In a 1.5-mL Eppendorf tube, a 0.5mL reaction mixture contained 1 mg/mL UGT-1A9 microsomes, 4.5mM UDP-GluA, 100mM Tris Buffer (pH 7.5), 10mM MgCl<sub>2</sub>, and 300uM quercetin (0.1mg/mL). A separate reaction mixture contained 300uM quercetin encapsulated in 4% crosslinked nanoparticle, and another reaction

with 8% crosslinked nanoparticles with quercetin entrapped. The reactions started upon addition of cold UGT-1A9 microsomes to the pre-warmed (37°C) reaction mixtures. The mixtures were vortexed briefly before incubation. A control reaction with free drug and without enzyme was run in parallel, and each reaction was performed in triplicate. After 2h of incubation, the reactions were stopped by the addition of 0.5 mL of cold methanol, centrifuged at 4000 rpm for 20 min, and 30  $\mu$ L of supernatant was injected onto the HPLC. A standard curve of 6.25-100  $\mu$ g/mL in MeOH:Water (1:1) was constructed to determine the concentration of free drug remaining after 2h.

#### **4T1 cell culture experiments**

Mammalian breast cancer cells (4T1; ATCC® CRL-2539™, Manassas, VA, USA) were grown in tissue culture flasks (75 cm<sup>2</sup>) and maintained under 5% CO<sub>2</sub> atmosphere at 37 °C in complete growth media, which was made with RPMI-1640 (Corning, with glutamate, without phenol red) supplemented with 10% FBS (Gibco, USA). Growth media was changed every 2-3 days, and once 80% confluent, cultured cells were trypsinized and split (1:5 to 1:10 ratio) with 0.25% trypsin-0.53mM EDTA solution (Gibco, USA). For the MTT assay, 4T1 cells were seeded at a density of 10,000 cells/well in 96-well cell culture plates (BD Falcon, NJ, USA).

#### **Cell cytotoxicity assay**

A standard MTT (Life Technologies, USA) assay was used to determine the cell cytotoxicity of NP-TAM-QTs in mouse breast cancer cells (4T1, ATCC). The 4T1 cells were harvested from confluent cultures by trypsinization and adjusted to 600,000 cells/ml incomplete media. The suspension was added (0.2 ml/well) and incubated for 3 h for cell attachment. Following

attachment, the media was replaced with fresh complete media (0.2 ml/well) containing free TAM, free QT, a mixture of free TAM with QT (1:1 w/w), or NP-TAM-QTs in different wells to achieve net concentrations of 0.01, 0.1, 1, and 10  $\mu\text{g/mL}$  (equivalent to free TAM) and incubated for 24, 48, and 72 hours. After incubation was finished, the media containing drug formulation was aspirated, and cells were washed with PBS (1X, pH 7.4). Then, 150  $\mu\text{L}$  of MTT solution (500  $\mu\text{g/mL}$  in complete media) was added to each well and incubated for 3-4 h in order for the live cells to produce formazan crystals. Following incubation, all but 25  $\mu\text{L}$  were aspirated carefully. The formazan crystals were dissolved by addition of 50  $\mu\text{L}$  of DMSO with gentle mixing, and the absorbance (A) of each well was measured at 540 nm using a Synergy HT Microtiter Plater reader (BIO-TEK). Cell viability was assessed using the following equation:

$$\% \text{ cell viability} = \frac{A_{\text{test}} - A_{\text{blank}}}{A_{\text{control}} - A_{\text{blank}}} \times 100$$

**Recovery condition.** In a separate 96-well plate, free drugs or NP-drugs were incubated to estimate cell cytotoxicity in the recovery condition. In this experiment, 4T1 cells were dosed with free TAM, free QT, a mixture of free TAM and QT (1:1 wt/wt), or NP-TAM-QTs for 24 h at the same concentrations as other experiments, followed by washing with PBS (1X) and reincubation in fresh complete media up to 72 h. The cell cytotoxicity was measured by MTT under same protocol as above.

**Statistical analysis.** All results from experiments are expressed as mean  $\pm$  standard deviation (SD). Statistical analysis was performed in Microsoft Excel. Mean particle size and standard deviations were calculated using Image J software (Mac OSX).

## References

1. Lehar, J.; Krueger, A. S.; Avery, W.; Heilbut, A. M.; Johansen, L. M.; Price, E. R.; Rickles, R. J.; Short, G. F.; Staunton, J. E.; Jin, X. W.; Lee, M. S.; Zimmermann, G. R.; Borisy, A. A., Synergistic drug combinations tend to improve therapeutically relevant selectivity (vol 27, pg 659, 2009). *Nature Biotechnology* **2009**, *27* (9), 864-864.
2. Xu, M.; Xu, C. X.; Bi, W. Z.; Song, Z. G.; Jia, J. P.; Chai, W.; Zhang, L. H.; Wang, Y., Effects of endostar combined multidrug chemotherapy in osteosarcoma. *Bone* **2013**, *57* (1), 111-115.
3. Ndong, J. D.; Stevens, D. M.; Vignaux, G.; Uppuganti, S.; Perrien, D. S.; Yang, X. L.; Nyman, J. S.; Harth, E.; Elefteriou, F., Combined MEK Inhibition and BMP2 Treatment Promotes Osteoblast Differentiation and Bone Healing in Nf1(Osx)(-/-) Mice. *Journal of Bone and Mineral Research* **2015**, *30* (1), 55-63.
4. Scarano, W.; de Souza, P.; Stenzel, M. H., Dual-drug delivery of curcumin and platinum drugs in polymeric micelles enhances the synergistic effects: a double act for the treatment of multidrug-resistant cancer. *Biomaterials Science* **2015**, *3* (1), 163-174.
5. Krishnamurthy, S.; Ke, X. Y.; Yang, Y. Y., Delivery of therapeutics using nanocarriers for targeting cancer cells and cancer stem cells. *Nanomedicine* **2015**, *10* (1), 143-160.
6. Pond, S. M.; Tozer, T. N., First-pass elimination. Basic concepts and clinical consequences. *Clinical Pharmacokinetics* **1984**, *9* (1), 1-25.
7. He, W.; Lv, Y.; Zhao, Y.; Xu, C.; Jin, Z.; Qin, C.; Yin, L., Core-shell structured gel-nanocarriers for sustained drug release and enhanced antitumor effect. *International Journal of Pharmaceutics* **2015**, *484* (1-2), 163-171.



8. Li, Q.; Lv, S.; Tang, Z.; Liu, M.; Zhang, D.; Yang, Y.; Chen, X., A co-delivery system based on paclitaxel grafted mPEG-b-PLG loaded with doxorubicin: preparation, in vitro and in vivo evaluation. *International Journal of Pharmaceutics* **2014**, *471* (1-2), 412-20.
9. Wang, Q.; Bao, Y.; Ahire, J.; Chao, Y., Co-encapsulation of Biodegradable Nanoparticles with Silicon Quantum Dots and Quercetin for Monitored Delivery. *Advanced Healthcare Materials* **2013**, *2* (3), 459-466.
10. Soni, P.; Kaur, J.; Tikoo, K., Dual drug-loaded paclitaxel–thymoquinone nanoparticles for effective breast cancer therapy. *Journal of Nanoparticle Research C7 - 18* **2015**, *17* (1), 1-12.
11. Jain, A. K.; Thanki, K.; Jain, S., Co-encapsulation of Tamoxifen and Quercetin in Polymeric Nanoparticles: Implications on Oral Bioavailability, Antitumor Efficacy, and Drug-Induced Toxicity. *Molecular Pharmaceutics* **2013**, *10* (9), 3459-3474.
12. Palvai, S.; Nagraj, J.; Mapara, N.; Chowdhury, R.; Basu, S., Dual drug loaded vitamin D3 nanoparticle to target drug resistance in cancer. *Rsc Advances* **2014**, *4* (100), 57271-57281.
13. Sengupta, S.; Eavarone, D.; Capila, I.; Zhao, G. L.; Watson, N.; Kiziltepe, T.; Sasisekharan, R., Temporal targeting of tumour cells and neovasculature with a nanoscale delivery system. *Nature* **2005**, *436* (7050), 568-572.
14. Giacalone, M. J.; Sabbadini, R. A.; Chambers, A. L.; Pillai, S.; Berkley, N. L.; Surber, M. W.; McGuire, K. L., Immune responses elicited by bacterial minicells capable of simultaneous DNA and protein antigen delivery. *Vaccine* **2006**, *24* (33-34), 6009-17.
15. Barua, S.; Mitragotri, S., Synergistic targeting of cell membrane, cytoplasm, and nucleus of cancer cells using rod-shaped nanoparticles. *ACS Nano* **2013**, *7* (11), 9558-70.

16. Sun, T. M.; Du, J. Z.; Yao, Y. D.; Mao, C. Q.; Dou, S.; Huang, S. Y.; Zhang, P. Z.; Leong, K. W.; Song, E. W.; Wang, J., Simultaneous delivery of siRNA and paclitaxel via a "two-in-one" micelleplex promotes synergistic tumor suppression. *ACS Nano* **2011**, *5* (2), 1483-94.
17. Deng, Z. J.; Morton, S. W.; Ben-Akiva, E.; Dreaden, E. C.; Shopsowitz, K. E.; Hammond, P. T., Layer-by-layer nanoparticles for systemic codelivery of an anticancer drug and siRNA for potential triple-negative breast cancer treatment. *ACS Nano* **2013**, *7* (11), 9571-84.
18. Chin, C. F.; Yap, S. Q.; Li, J.; Pastorin, G.; Ang, W. H., Ratiometric delivery of cisplatin and doxorubicin using tumour-targeting carbon-nanotubes entrapping platinum(iv) prodrugs. *Chemical Science* **2014**, *5* (6), 2265-2270.
19. Zhang, L.; Xia, J.; Zhao, Q.; Liu, L.; Zhang, Z., Functional graphene oxide as a nanocarrier for controlled loading and targeted delivery of mixed anticancer drugs. *Small* **2010**, *6* (4), 537-44.
20. Tripathy, N.; Ahmad, R.; Ko, H. A.; Khang, G.; Hahn, Y.-B., Enhanced anticancer potency using an acid-responsive ZnO-incorporated liposomal drug-delivery system. *Nanoscale* **2015**, *7* (9), 4088-4096.
21. Fang, Y.; Zheng, G. F.; Yang, J. P.; Tang, H. S.; Zhang, Y. F.; Kong, B.; Lv, Y. Y.; Xu, C. J.; Asiri, A. M.; Zi, J.; Zhang, F.; Zhao, D. Y., Dual-Pore Mesoporous Carbon@Silica Composite Core-Shell Nanospheres for Multidrug Delivery. *Angewandte Chemie-International Edition* **2014**, *53* (21), 5366-5370.
22. Jain, A. K.; Swarnakar, N. K.; Godugu, C.; Singh, R. P.; Jain, S., The effect of the oral administration of polymeric nanoparticles on the efficacy and toxicity of tamoxifen. *Biomaterials* **2011**, *32* (2), 503-515.
23. Mugundu, G. M.; Sallans, L.; Guo, Y. Y.; Shaughnessy, E. A.; Desai, P. B., Assessment of the Impact of CYP3A Polymorphisms on the Formation of alpha-Hydroxytamoxifen and N-

Desmethyltamoxifen in Human Liver Microsomes. *Drug Metabolism and Disposition* **2012**, *40* (2), 389-396.

24. Davis, J. M.; Carlstedt, C. J.; Chen, S.; Carmichael, M. D.; Murphy, E. A., The dietary flavonoid quercetin increases VO<sub>2</sub>(max) and endurance capacity. *International Journal of Sport Nutrition and Exercise Metabolism* **2010**, *20* (1), 56-62.

25. Caltagirone, S.; Ranelletti, F. O.; Rinelli, A.; Maggiano, N.; Colasante, A.; Musiani, P.; Aiello, F. B.; Piantelli, M., Interaction with type II estrogen binding sites and antiproliferative activity of tamoxifen and quercetin in human non-small-cell lung cancer. *American Journal of Respiratory Cell and Molecular Biology* **1997**, *17* (1), 51-9.

26. Osborne, C. K., Tamoxifen in the Treatment of Breast Cancer. *New England Journal of Medicine* **1998**, *339* (22), 1609-1618.

27. Shin, S.-C.; Choi, J.-S.; Li, X., Enhanced bioavailability of tamoxifen after oral administration of tamoxifen with quercetin in rats. *International Journal of Pharmaceutics* **2006**, *313* (1-2), 144-149.

28. Garcia-Saura, M. F.; Galisteo, M.; Villar, I. C.; Bermejo, A.; Zarzuelo, A.; Vargas, F.; Duarte, J., Effects of chronic quercetin treatment in experimental renovascular hypertension. *Molecular and Cellular Biochemistry* **2005**, *270* (1-2), 147-55.

29. Oliveira, E. J.; Watson, D. G., In vitro glucuronidation of kaempferol and quercetin by human UGT-1A9 microsomes. *FEBS Letters* **2000**, *471* (1), 1-6.

30. Graf, B. A.; Mullen, W.; Caldwell, S. T.; Hartley, R. C.; Duthie, G. G.; Lean, M. E. J.; Crozier, A.; Edwards, C. A., DISPOSITION AND METABOLISM OF [2-14C]QUERCETIN-4'-GLUCOSIDE IN RATS. *Drug Metabolism and Disposition* **2005**, *33* (7), 1036-1043.

31. Stevens, D. M.; Gilmore, K. A.; Harth, E., An assessment of nanosponges for intravenous and oral drug delivery of BCS class IV drugs: Drug delivery kinetics and solubilization. *Polymer Chemistry* **2014**, *5* (11), 3551-3554.
32. van der Ende, A. E.; Kravitz, E. J.; Harth, E., Approach to formation of multifunctional polyester particles in controlled nanoscopic dimensions. *Journal of the American Chemical Society* **2008**, *130* (27), 8706-13.
33. Rautio, J.; Kumpulainen, H.; Heimbach, T.; Oliyai, R.; Oh, D.; Jarvinen, T.; Savolainen, J., Prodrugs: design and clinical applications. In *Nature Reviews Drug Discovery*, England, 2008; Vol. 7, pp 255-70.
34. Dechy-Cabaret, O.; Martin-Vaca, B.; Bourissou, D., Controlled ring-opening polymerization of lactide and glycolide. *Chemical Reviews* **2004**, *104* (12), 6147-76.
35. Stevens, D. M.; Watson, H. A.; LeBlanc, M.-A.; Wang, R. Y.; Chou, J.; Bauer, W. S.; Harth, E., Practical polymerization of functionalized lactones and carbonates with Sn(OTf)<sub>2</sub> in metal catalysed ring-opening polymerization methods. *Polymer Chemistry* **2013**, *4* (8), 2470-2474.
36. Jain, A. K.; Swarnakar, N. K.; Godugu, C.; Singh, R. P.; Jain, S., The effect of the oral administration of polymeric nanoparticles on the efficacy and toxicity of tamoxifen. In *Biomaterials*, 2010 Elsevier Ltd: England, 2011; Vol. 32, pp 503-15.
37. Crewe, H. K.; Notley, L. M.; Wunsch, R. M.; Lennard, M. S.; Gillam, E. M., Metabolism of tamoxifen by recombinant human cytochrome P450 enzymes: formation of the 4-hydroxy, 4'-hydroxy and N-desmethyl metabolites and isomerization of trans-4-hydroxytamoxifen. *Drug Metabolism and Disposition: The Biological Fate of Chemicals* **2002**, *30* (8), 869-74.

38. Kim, S. Y.; Suzuki, N.; Santosh Laxmi, Y. R.; Rieger, R.; Shibutani, S.,  $\alpha$ -Hydroxylation of Tamoxifen and Toremifene by Human and Rat Cytochrome P450 3A Subfamily Enzymes. *Chemical Research in Toxicology* **2003**, *16* (9), 1138-1144.
39. Antunes, M. V.; Rosa, D. D.; Viana Tdos, S.; Andreolla, H.; Fontanive, T. O.; Linden, R., Sensitive HPLC-PDA determination of tamoxifen and its metabolites N-desmethyltamoxifen, 4-hydroxytamoxifen and endoxifen in human plasma. *Journal of Pharmaceutical and Biomedical Analysis* **2013**, *76*, 13-20.
40. Ader, P.; Wessmann, A.; Wolfram, S., Bioavailability and metabolism of the flavonol quercetin in the pig. *Free Radical Biology and Medicine* **2000**, *28* (7), 1056-1067.
41. Ma, Z. S.; Huynh, T. H.; Ng, C. P.; Do, P. T.; Nguyen, T. H.; Huynh, H., Reduction of CWR22 prostate tumor xenograft growth by combined tamoxifen-quercetin treatment is associated with inhibition of angiogenesis and cellular proliferation. *International Journal of Oncology* **2004**, *24* (5), 1297-304.
42. Hariri, G.; Edwards, A. D.; Merrill, T. B.; Greenbaum, J. M.; van der Ende, A. E.; Harth, E., Sequential targeted delivery of paclitaxel and camptothecin using a cross-linked "nanosponge" network for lung cancer chemotherapy. *Molecular Pharmaceutics* **2014**, *11* (1), 265-75.
43. Lee, Y. H.; Kang, B. S.; Bae, Y. S., Premature senescence in human breast cancer and colon cancer cells by tamoxifen-mediated reactive oxygen species generation. *Life Sciences* **2014**, *97* (2), 116-22.
44. Huttunen, K. M.; Raunio, H.; Rautio, J., Prodrugs--from serendipity to rational design. In *Pharmacological Reviews*, United States, 2011; Vol. 63, pp 750-71.

45. Jana, S.; Mandlekar, S.; Marathe, P., Prodrug design to improve pharmacokinetic and drug delivery properties: challenges to the discovery scientists. In *Current Medicinal Chemistry*, Netherlands, 2010; Vol. 17, pp 3874-908.
46. Parrish, B.; Quansah, J. K.; Emrick, T., Functional polyesters prepared by polymerization of  $\alpha$ -allyl(valerolactone) and its copolymerization with  $\epsilon$ -caprolactone and  $\delta$ -valerolactone. *Journal of Polymer Science Part A: Polymer Chemistry* **2002**, *40* (12), 1983-1990.

Portions of this chapter were reprinted with permission from Lockhart, J. N.; Stevens, D. M.; Beezer, D. B.; Kravitz, A.; Harth, E., Dual drug delivery of tamoxifen and quercetin: Regulated metabolism for anticancer treatment with nanosponges. *Journal of Controlled Release* 2015, *220*, 751-757. Copyright 2015 Elsevier.

## CHAPTER III

# ONE-POT POLYGLYCIDOL NANOGELS VIA LIPOSOME MASTER TEMPLATES FOR COMBINATION DRUG DELIVERY

### Introduction

Combination therapy using dual synergistic drug delivery systems has become a leading approach for treating malignant and drug-resistant cancers.<sup>1</sup> The inability of chemotherapy to eradicate cancer cells can be due to rapid mutations within subgroups of tumor cells which evade cytotoxic drugs.<sup>2</sup> It is well known that a tumor suppresses anti-cancer immune responses within its microenvironment in order to facilitate growth, progression, and metastasis.<sup>3</sup> On the other hand, protein therapeutics, such as cytokines and antibodies, can induce an effective anticancer response by stimulating the immune system. A combined chemo-immunotherapy approach can promote synergy against cancer cells and suppress drug resistance through unique mechanisms of action.<sup>4</sup> Despite promising recent clinical and experimental results, anti-cancer efficacy is still sub-optimal due to short drug and protein half-lives, systemic toxicity, and divergent *in vivo* pharmacokinetics and distribution.<sup>5</sup>

Polymeric nanotechnology has opened unprecedented opportunities to develop controlled delivery nano vehicles, which have resulted in a number of benefits to deliver small molecule chemotherapeutic drugs. For example, prolonged blood circulation and tumor accumulation can be achieved by the enhanced permeability and retention (EPR) effect of particles between 10 and 150 nm in diameter to yield more favorable pharmacokinetic profiles. Alternatively, the delivery system can provide enhanced efficacy by utilizing targeting peptides.<sup>6</sup> Despite the versatility of

known nanoparticle delivery carriers such as liposomes, star polymers, micelles, nanosponges and PLGA particles, the dual and co-delivery of multiple therapeutic agents, such as hydrophilic large biologicals with small hydrophobic chemotherapeutics from the same nanocarrier can impose challenges. Contributing factors include varying size dimensions of the therapeutics and their adverse solubility.<sup>7,8</sup> Current designs either separate two drugs in a core-shell structure like in hyaluronic acid (HA) nanogel-enveloped liposomes<sup>9</sup>, or use a double-emulsion technique with spatial co-localization of oil-water droplets within a larger surfactant stabilized carrier.<sup>10</sup> Designs of delivery systems with no spatial separation of the two therapeutics include porous silicon nanoparticles<sup>11</sup>, or lipogels<sup>12</sup>, also known as liposome-enveloped nanogels.<sup>13-14</sup>

A common theme in all of these systems is the implementation of traditional carriers already tested for a small molecule delivery which are improved or modified for a co-delivery application. One of these traditional carriers are liposomes, which are prepared in a facile process and feature high stability. However, some of the reported disadvantages include prolonged circulation times and incomplete or rapid release rates of therapeutics.<sup>15</sup> Although HA nanogel-enveloped liposomes are recognized as novel drug delivery systems, the liposome component is still the dominant factor in the observed release kinetics, mainly due to the intact liposomal drug delivery core. However, more recently, liposomes are employed as suitable templates to develop carriers, such as liposome-enveloped nanogels or lipogels in which the incorporated nanogel structure plays a greater role in the overall improved release characteristics of this liposome based nanocarrier. One example from the Fahmy group prepares a nanogel from a linear crosslinker (PLA-PEG-PLA) in which the cytokine and the drug loaded acrylate-modified cyclodextrin forms a unique incorporated gel using UV-light illumination to achieve the crosslinking of the acrylate functional endgroups.<sup>13</sup> The small molecule and the cytokine delivery kinetics correspond still to a



liposomal system but are influenced by the nanogel core component to achieve a more controlled release of the two therapeutics. It should be noted that the exposure to UV-light and the generated free radicals do not seem to impair the activity of the incorporated cytokines because a high efficacy in *in vivo* studies was observed. The lack of versatile, hydrophilic nanogel components that can be shuttled into liposome templates and provide tailored crosslinking densities for a more controlled release of all types of therapeutics is limiting the clinical relevance for some of these nanogels.

In this work, we sought to utilize a liposomal carrier to form a dual delivery system and aim for a final product with unique features with no resemblance to the native carrier. In other words, the novel system attributes all its features from a created nanonetwork from liposomal templates which are significantly altered in the process. This will be accomplished for one, through the design and synthesis of tailored hydrophilic macromolecular building blocks such as functionalized semi-branched polyglycidols, and also through a developed one-pot technique. We report on the formation and characterization of a novel nanohydrogel (nHG) platform using a thiol-ene click cross-linking system composed of unique allyl-functionalized semi-branched polyglycidols, poly(GLY/AGE), and PEG dithiol (1 kDa). Two preparation methods are presented, one that is in its methodology comparable with traditional stepwise approaches and uses a prefabricated liposome as master template (nHG-SW) to form nanogels, and a second approach in which liposomal lipids are brought together with all components in one pot (nHG-OP) to yield a carrier giving unique characteristics that are not resembling liposomal delivery systems.

## Results and Discussion

### **Synthesis and characterization of step-wise and one-pot nanogels**

Liposomes have been one of the first nanocarriers approved for the clinic and are still in practice today despite several drawbacks.<sup>16</sup> Disadvantages include a too rapid or slow release of therapeutics and difficulties to find means to tailor the release for these type of carriers. However, the ability to easily prepare precise nanoscopic sizes depending on the intended application is one of the advantages in using liposomes and has sparked interest using them as templates for the preparation of nanogels. For example, hydrophilic therapeutics such as siRNA or polymers can be shuttled into the interior using the liposome as a nanogel scaffold.<sup>16</sup> However, the efficacy of the trafficking and the non-tailorable release rates are still one of the challenges and improvements are desired. We sought to optimize the quality of the nanogels by introducing branched polyglycidols into the interior for providing a tighter and adjustable network but also seek alternative routes for implementing the liposomal lipid components in an investigated one-pot approach.

Nanohydrogels (nHGs) were prepared in two methods *via* liposome master template method as shown in Figure III-2. The traditional step-wise approach to prepare nanogels from liposome templates involves producing freeze-dried large unilamellar liposomes (LUVs) first, followed by hydration with pre-gel components in aqueous buffer and gelation upon exposure to UV light (see Figure III-2, nHGs-SW). This sequence was encouraging, however, only yielded 10% by mass with high polydispersity (PDI = 0.2, DLS) and poor morphology of nanogel structures was observed. We attributed the low yield in conventional synthesis to the extra freeze-dry step which has been well-documented to disrupt the liposome bilayer.<sup>17-19</sup> In an attempt to improve upon synthesis yield and characterization, we attempted a new approach by adding the pre-gel components in one pot to the lipid mixture before extrusion (Figure III-2, nHG-OP). After

hydration of the lipid thin film (i.e. lipid mix) with the gel precursors we form so-called multilammellar vesicles (MLVs - GPs) containing gel components throughout the structure. Extrusions of the MLVs - GPs through polycarbonate membrane filters of decreasing pore sizes enabled a hypothesized self-assembly of the bilayer components containing the gel precursors with narrow size distribution.<sup>20-21</sup> The prepared so-called MLVs - GPs with pre-gel components are dialyzed to remove any non-entrapped material and diluted 4-fold to mitigate the risk of macro-scale gelation before exposure to UV light. Upon UV irradiation, the hydrogel precursors are cross-linked by thiol-ene click chemistry as demonstrated with the model hydrogel (Figure III-1). It is anticipated that for the one-pot approach portions of gel precursors co-locate within the lipid bilayer fragments and upon become incorporated within the gel nanonetwork. The new method greatly improved the yield (25%) and uniformity (PDI = 0.07, DLS).

The surface charge and hydrodynamic diameter ( $d_h$ ) of the nanohydrogels were determined by zeta potential and dynamic light scattering (DLS) measurements in aqueous solution. As shown by Figure III-3 A, the nHG-OP had a hydrodynamic diameter 149 nm with a polydispersity index (PDI) of 0.07. Values of PDI obtained from the Zetasizer ZS that are <0.1 indicate a narrow, monomodal size distribution.<sup>22</sup> The size and PDI of nHG-OP are very close to those of liposomes prepared under the same conditions (122 nm, PDI = 0.05). TEM images of the nHG-OP in Figure III-3 B-D indicate well-defined spherical particles with an average diameter of  $132 \text{ nm} \pm 32$ , which is slightly less than obtained particle size values from the DLS measurements due to the dry sample preparation.<sup>23-24</sup>

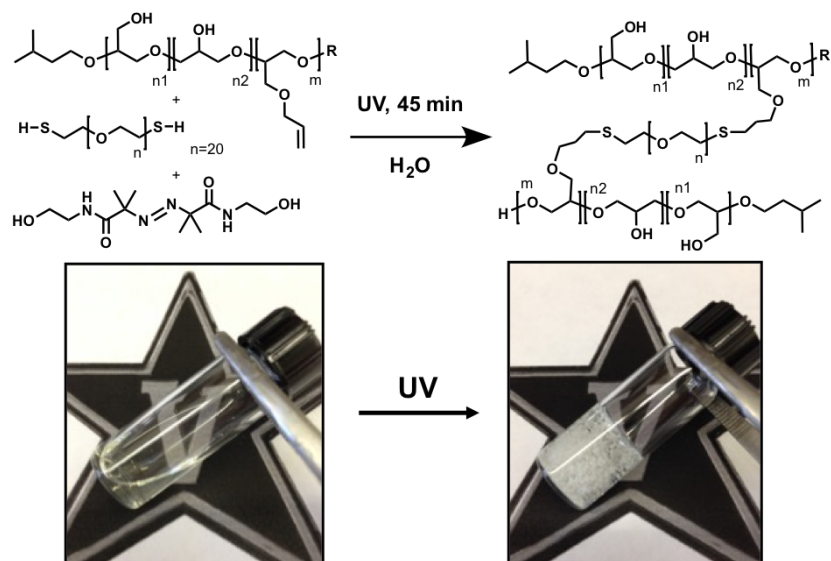


Figure III-1. Bulk hydrogels were using unique semibranch poly-allyl-glycidyl-ether-glycidol (poly-AGE/GLY, 20/80) with 1 kDa PEG dithiol linker in the presence of VA-086 photoinitiator and long wave (365 nm) UV light.

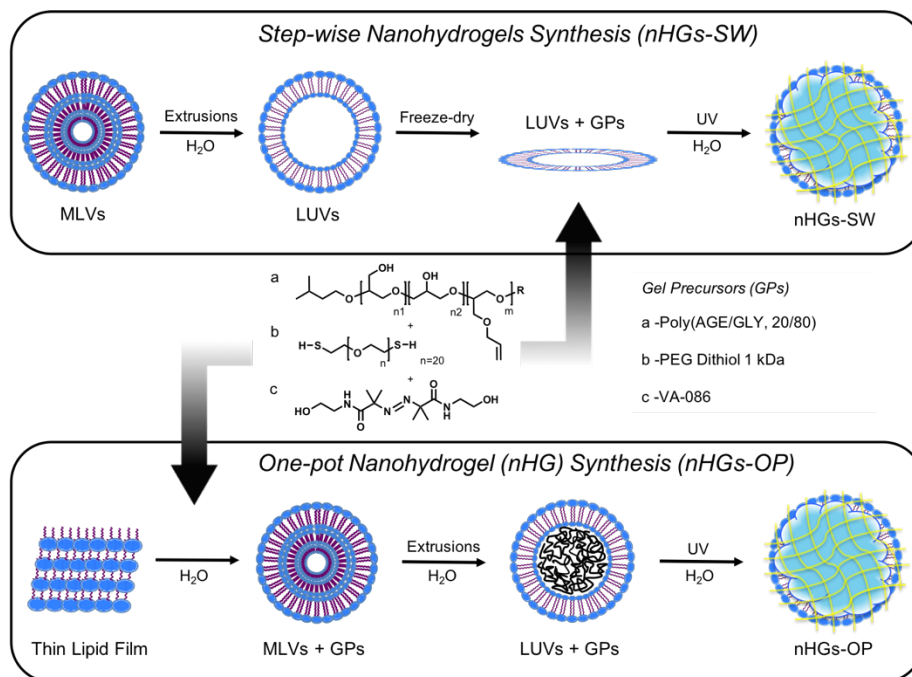


Figure III-2. The two synthesis methods used to produce nanohydrogels (nHG) involved step-wise and one-pot approaches. In step-wise, the unilamellar liposomes were generated first, followed by rehydration with pre-gel components and UV-irradiation. In the one-pot approach, pre-gel components were added to hydrate the thin film lipid mix, followed by extrusions and UV-irradiation.

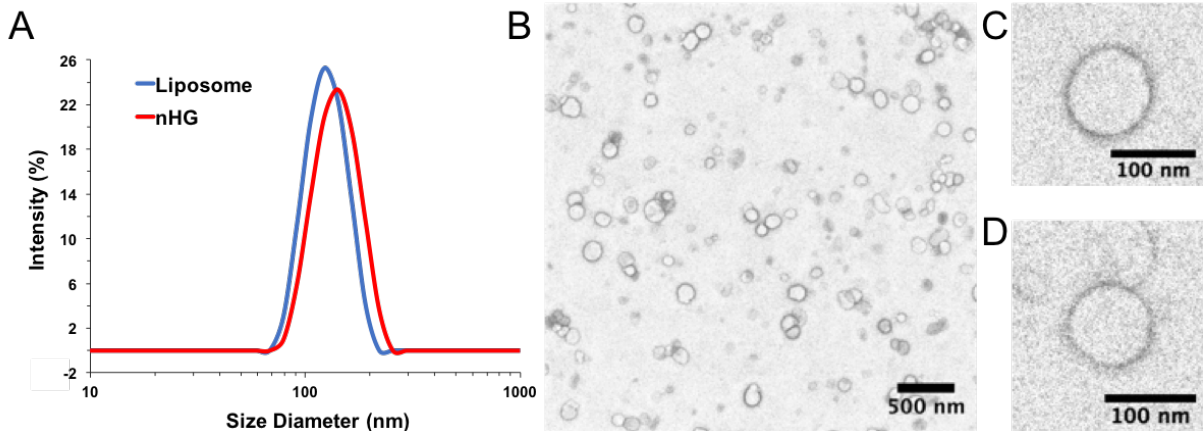


Figure III-3. Characterization of nanohydrogels (nHG) made by one-pot approach (nHG-OP). A) Dynamic Light Scattering (DLS) of nHG-OP and liposome templates. Average nHG diameter ( $D_w$ ) = 149 nm  $\pm$  37, and polydispersity index (PDI) = 0.07. B) Negative stain transmission electron microscopy (TEM) image of nHG at 22,000x magnification. C & D) Negative stain images of nHG at 81,000 x magnification. The average TEM diameter measured 132 nm  $\pm$  32. D)

Stability measurements of nHG-OP nanohydrogels were taken by DLS at three different temperatures in PBS and also in the presence of detergent. The results in Figure III-4 indicate negligible changes in hydrodynamic size or polydispersity between 25 and 50°C, which suggests the nHG-OP do not aggregate at physiologically relevant temperatures. The plot in Figure III-4 shows a comparison between liposomes and nHG-OP when treated with 10% Tween-80. A significant reduction in the liposome hydrodynamic diameter (132 to 7 nm) was observed, while the nHG-OP diameter was only slightly reduced (149 to 145 nm). These data confirm that the gel components were successfully crosslinked and incorporated within liposomal bilayer fragments to form a unique nanohydrogel network that is not destabilized by detergent.<sup>25</sup>

Although biologically active nanogels have been prepared in the past using photo-initiated crosslinking reactions and UV illumination for 10 min, it did not seem to significantly affect the biological therapeutic efficacy. However, our procedure used exposure times that were 4 times longer. Therefore, to confirm that the activity of the lysozyme protein was not impaired by the

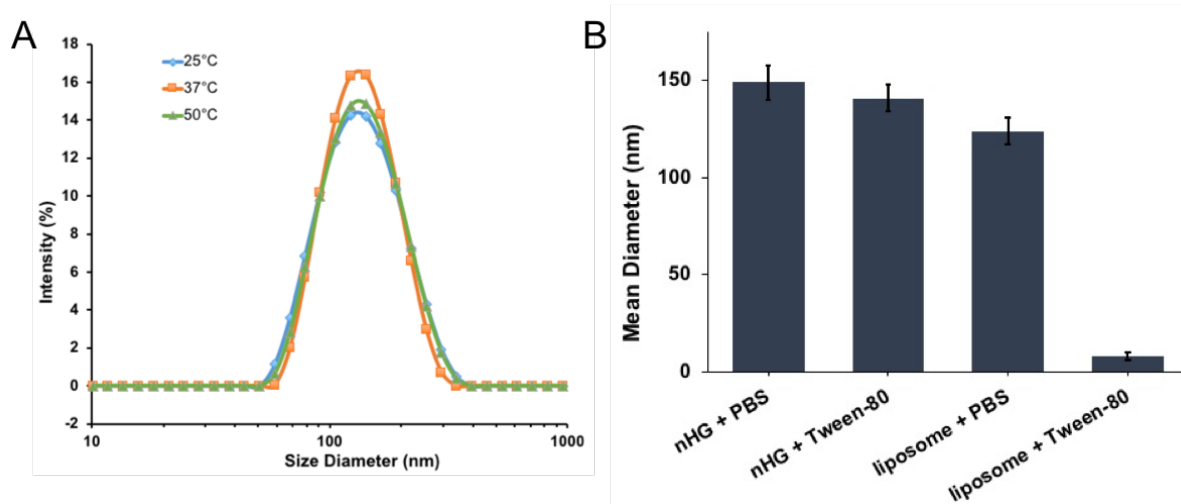


Figure III-4 Stability of nanohydrogels. A) Dynamic Light Scattering (DLS) analysis of the hydrodynamic size of a nanohydrogel sample in PBS (1X) at varying temperatures. Note that size and polydispersity remains stable from 25-50°C. Data is representative of at least 11 measurements by Malvern Zetasizer DLS instrument. B) Stability of nanohydrogels (nHGs) and liposomes was evaluated in PBS (1X, pH 7.4) and Tween-80 (10% in PBS) via DLS characterization of hydrodynamic diameter. Data on right is shown as mean diameter  $\pm$  SD for triplicate samples.

crosslinking process using long wave (365 nm) UV light in the presence of free radicals, we performed a lysozyme activity assay. We evaluated the lysozyme activity in four different treatment conditions: a.) illumination for 10 min and b.) 45 min, c.) in the presence of free radical initiator VA -086 with 10 min illumination, and d.) VA -086 with 45 min illumination. We found that a prolonged exposure of UV light had a minimal impact to the retained activity of the lysozyme. However, the addition of the initiator amplified this effect slightly. The two ten-minute treatment groups a.) and c.) displayed a 14 % reduction of the activity when the initiator is added. Treatment groups b.) and d.) showed a 19.7% loss of activity. In conclusion, this experiment revealed significant retention of activity even though we apply longer exposure times in the crosslinking process.

The cytocompatibility was tested with a MTT cell viability and proliferation assay, testing the prepared nanogels towards a liposome control group with concentrations reaching from 0.01-10

mg/ml in Figure III-6. It was observed that liposomes showed a drastic increase of toxicity starting at 1 mg/ml. NHGs-SW were less toxic than the master template of liposomes they were prepared with, indicating that the liposomal character of the nanogels in weakened and the gel components exhibit a reduced toxicity.

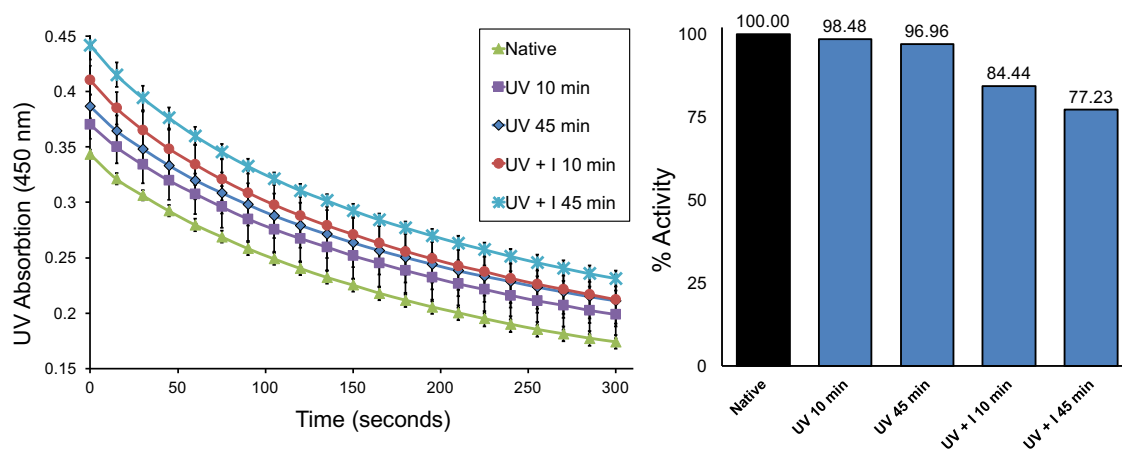


Figure III-5. Lysozyme (LYS) assay. The rate of lysis of *Micrococcus lysodeikticus* in 0.1 M potassium phosphate buffer (pH=7.0) was determined in triplicate by spectrophotometric monitoring of optical density at 450 nm using a BioTek Synergy H2 microplate reader over the course of 5 minutes at 15 second intervals as shown in the left-hand plot. Prior to activity monitoring, LYS was treated by UV light (365 nm, 6W) for two different time intervals, with and without VA-086 initiator present. Percent activity retention of each treatment group was calculated using the optical density slope over time and compared to the native lysozyme activity (black bar) in the plot on the right.

However, the toxicity increased with 5 mg/ml documented a slight influence of the liposomal character in the nHP-SW. Nanogels prepared with the one-pot procedure (nHP-OPs) did not exhibit any liposomal character, as observed as well in the release studies, but showed excellent cytocompatibility at high concentrations of 10mg/ml (See Figure III-6). In can be concluded that the one-pot process is the superior method for the preparation of dual release systems.

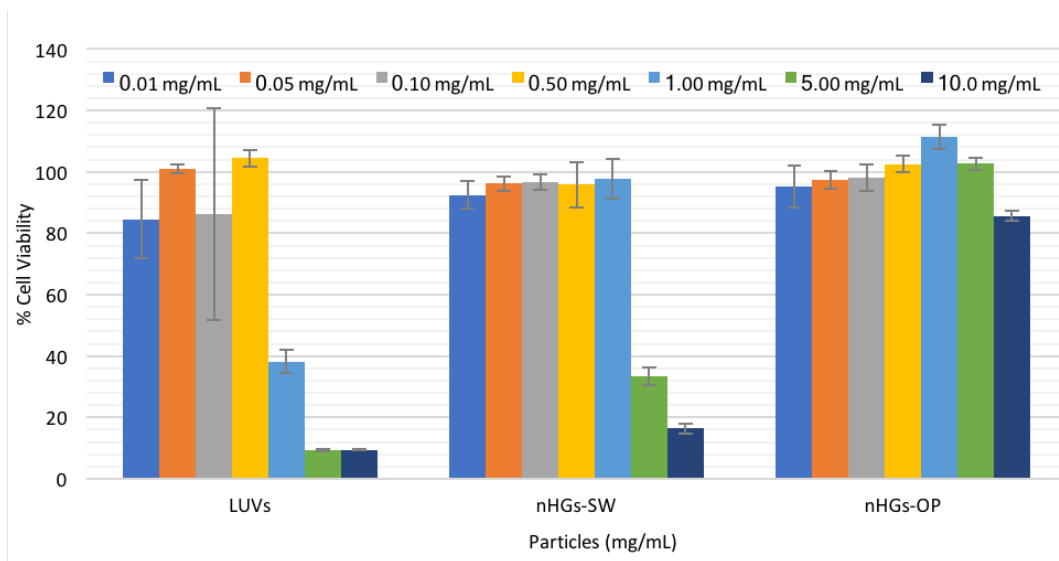


Figure III-6. Cytocompatibility via MTT assay for liposomes (LUVs), step-wise nanogels (nHG-SW), and one-pot nanogels (NGs-OP) using NIH 3T3 cells. Data reported as the mean and standard deviation of three independent trials for each test condition.

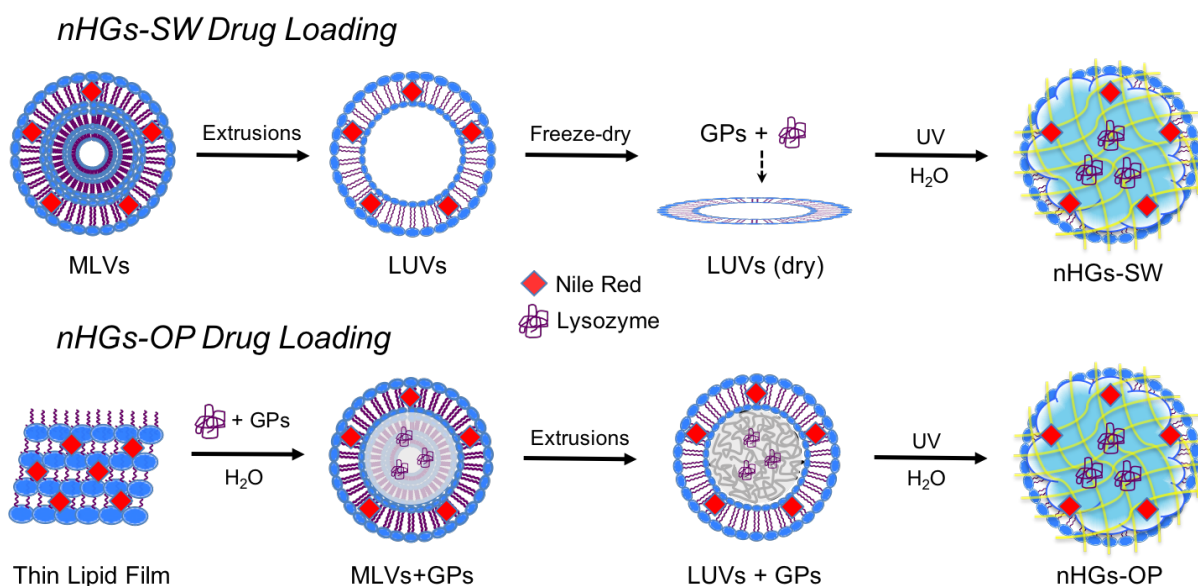


Figure III-7. Drug loading of nanogels by step-wise method involves making the multilamellar liposomes (MLVs) with hydrophobic drug first, followed by extrusions to make unilamellar liposomes (LUV), freeze-drying and rehydrating with gel precursors with lysozyme in water. The drug loading for one-pot synthesis involves adding pre-gel components with biological to a container of thin film lipid mix (pre-loaded with hydrophobic drug), followed by extrusions and UV crosslinking.



## Nile red *in vitro* release studies

Nile red (NR, logP = 3-5) was chosen as a model hydrophobic drug for *in vitro* release studies because of its similar size and physicochemical properties to common chemotherapeutic molecules like paclitaxel (logP = 3.96).<sup>26</sup> Another advantage to using Nile red is that it can easily be detected by spectrophotometric methods due to its absorbance in the 550-580 nm region, which is not interfered by any other components in the nanohydrogel system or release media. It has been reported that hydrophobic drug release is measured using organics in the release media to solvate the drug. Problems can arise however when the nanoparticle system degrades too quickly in organics and thus does not represent the true release of drug from the particle.<sup>27</sup> In order to conduct a study that is more closely aligned to physiologically relevant conditions while dissolving Nile red, we employed hydrophilic cyclodextrins (hydroxypropyl  $\beta$ -cyclodextrin, HBC) in the release media.<sup>28-31</sup> Measuring drug release *in vitro* from nanoparticles is often a challenge because nanoparticles must be separated from the release medium,<sup>32</sup> and ultra-centrifugation is often used.<sup>33</sup> However, it is a time consuming process that occurs at high centrifugal forces, which may destroy the nanoparticles, especially nanogels which get softer over time as degradation proceeds.<sup>35</sup> We chose the dialysis method using Float-A-Lyzers® from SpectraPore for monitoring drug release from liposomes and nanohydrogels due to the ability to easily separate the drug from nanocarriers without destroying the formulation architecture during the experiment.<sup>36</sup>

In order to measure the true release rates of drug from nanocarriers, its movement through a dialysis membrane must be rapid.<sup>30,37</sup> We first experimented with Float-A-Lyzer dialysis tubes of three different pore sizes to better understand the diffusion of free NR across the membrane. As shown in Figure III-8, NR release was nearly complete after 3 h using the 300 kDa pore size and is comparable to a similar diffusion experiment by Saarinen-Savolainen, et al<sup>30</sup>. At the same 3 h

time point, only 20 and 10% of NR was released using 20 kDa and 10 kDa pore sizes, respectively. This data convinced us to move forward using the 300 kDa dialysis membranes because it minimally affects movement of NR across the dialysis membrane. It was also determined by DLS that this pore size was small enough to keep liposomes and nHGs inside.

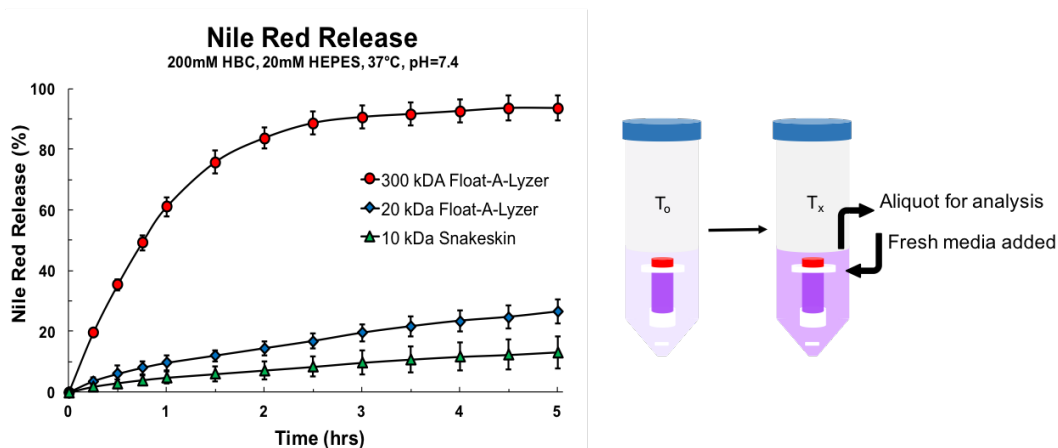


Figure III-8 Nile red release by dialysis method (bottom right) monitored by Nanodrop 2000c at 580 nm. Dialysis control bags of various molecular weight cut-offs (10 kDa, 20 kDa and 300 kDa) were filled with 1 mL Nile red (500  $\mu$ g) in sink media. Nile red was monitored for appearance in external sink (18 mL) over the course of 5 hours. Sink conditions were 200 mM hydroxypropyl beta-cyclodextrin in 20 mM HEPES (pH 7.4) maintained at 37°C by an electrostatic temperature-control stir plate. Release plot data (left) represents mean (n=3)  $\pm$  1 standard deviation.

Release of NR was monitored from liposomes, nanohydrogels made with the step-wise method (nHGs-SW) and nanohydrogels made with the one-pot method (nHGs-OP), Figure III-9. The liposomes showed the slowest release for the Nile red, with only 29% after 9 days. Moreover, after an initial 20% release in a 3 day period the kinetic slowed down and only 5% was released in the following 6 days. It underlines that traditional liposomal carriers are safe but still suffer from an incomplete release of the bilayer and need to be optimized. Release kinetics from carriers using the liposome as a template with a nanogel core made from the shuttling-in-approach (nHG-SW) showed a much different kinetic which was almost the opposite of the liposome. The release occurs

to be rapid with an exponential release in which 50 % of the Nile red is released in a 3 day period with 70% percent released after 9 days. We attribute this behavior as the result of transporting the gel components through the bilayer. We hypothesize that some of the gel components do not completely pass and intercalate the bilayer. We observed in some of our initial studies that the nanogel is formed from the outside to the inside leading to a “doughnut” gel structure if the

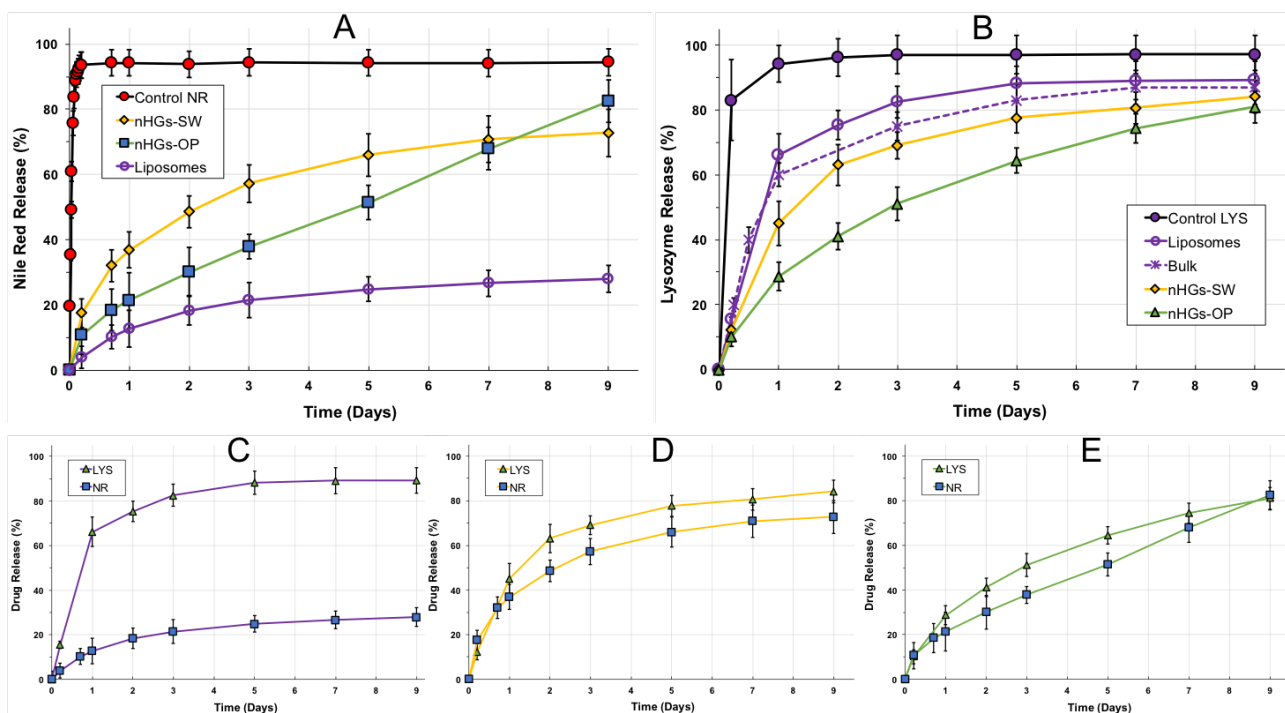


Figure III-9. The *in vitro* release of A) Free Nile red (NR) control, and NR from liposomes, nanohydrogels-step wise (nHG-SW) and nanohydrogels-one pot (nHG-OP) over time (days) via dialysis method. B) In vitro release of Lysozyme (LYS) free drug control, and LYS from liposomes, nHG-OP, nHG-SW and bulk gel via dialysis method. C) Plot of LYS and NR release from liposomes D) LYS and NR release from nHG-SW and E) LYS and NR release from nHG-OP. Release media for Nile red experiments consisted of 20 mM HEPES, pH 7.4, 200 mM hydroxypropyl cyclodextrin at 37°C. Lysozyme experiments consisted of PBS 1X, pH 7.4 maintained at 37°C. All data represent the mean of triplicate samples  $\pm$  1 standard deviation. Note: The results shown in Figure 2C, D, E stem from individual loadings and release experiments of hydrophobic and hydrophilic drugs Nile red and lysozyme, summarized in Figure A and B, respectively. Due to overlapping UV absorbance regions of the two model drugs in this study, individual release experiments were conducted to model the dual release capacity as proof-of-concept. If one were to analyze their release from the same carrier in the same media, additional separation techniques will be required.

polymer loading was set to be too low. Therefore, we assume that the nHG's after curing, leave an imperfect bilayer behind which is less densely packed as compared to the native liposome which results in a faster release of the Nile red. However, the contribution of the polyglycidol components influence the release rates towards a more controlled and slower kinetic than reported comparable nanogels that contain networks made from linear polymer precursors and result in an even more rapid release of hydrophobic small molecule drugs (80% released in 3 days).

The nHG-OP release kinetics support the superiority of the one-pot synthesis strategy. 50% of drug was released in 5 days and complete *in vitro* release was achieved in 9 days. The release curve is nearly linear with a minimal burst in the first few hours, followed by a sustained linear release. This is in contrast with the nHG-SW which released 35% NR in 1 day and then exhibited an exponential release pattern. We can conclude that the one-pot nanogels show superior release kinetics in contrast to the traditional liposomes and nanogels made in a step wise approach. These results underline that the structure of the one-pot nanogels suggests a much tighter and more homogenous network in contrast to the step-wise nanogel network.

### **Lysozyme in vitro release studies**

Lysozyme was used as a model protein drug with similar molecular size and hydrophilicity to therapeutic biologicals. Its release from liposomes, bulk gel, and nanohydrogels (nHG-OP, nHG-SW) was monitored over a period of 9 days under physiologically relevant *in vitro* conditions (PBS 1X, pH 7.4, 37 °C) as shown in Figure III-9. First, we tested if lysozyme is released sufficiently from the dialysis tubing into the sink to confirm the suitability of our developed analytical method. We noticed the free lysozyme releases rapidly (~95% in 24 h) from the dialysis

tubing, which indicates minimal impedance or binding of drug to the dialysis membrane. The fastest release of lysozyme was observed from liposomal carriers with 65% released in the first day and is in contrast to the release of Nile red from the same carrier. It demonstrates again that liposomal release strongly depends on the physicochemical character of the drug, and an effective synergistic dual release from liposomes is difficult to achieve as shown in Figure III-9 C. In comparison, cumulative release of lysozyme from the two prepared nanogel platforms demonstrated that loading of lysozyme in nanohydrogels enables a more sustained release of the model protein. The lysozyme release from the nHGs-SW appeared to be very similar to the release of the NR with a comparable exponential release kinetic but appeared to be slightly faster with 63% released on day 2. However, we can conclude that both release kinetics are suitable for a release of two drugs to give a synergistic effect, Figure 2 D. Although both model drugs are released relatively rapidly, the release is overall slower as compared to nanogels prepared in a similar fashion. For example, the nanosized liposomal polymer gels described by the Fahmy group released 80% of its biological drug (IL-2) in 4 days.<sup>13</sup>

The *in vitro* release of lysozyme from nHGs-OP was slower than protein releases in gel systems found in the literature. Release of BSA from hydrophobically-modified alginate hydrogels was nearly complete in 3 days.<sup>38</sup> The liposome-crosslinked hybrid gels reported by the Kiick group demonstrated complete cytochrome c release in 6 days.<sup>39</sup> To the best of our knowledge, nHGs prepared *via* one-pot method (nHGs-OP) released lysozyme in the most sustained fashion from currently studied carriers. The kinetics were slightly exponential but less pronounced with 50% of the drug released on day 3. Comparing the release kinetics for the small molecule and protein for the nHGs-OP, we observed the most controlled kinetics from all our studied carriers and are the most suitable for a dual release when a synergistic effect is desired. The one-pot method

provides an opportunity to prepare nanonetworks that give release profiles that do not seem to account for the quite different size and solubility of the model drugs. The integrated lipophilic liposomal bilayer fragments might contribute to a higher residence time of both the small hydrophobic but also hydrophilic drug together with forming a more homogenous network.

### **Synthesis of one-pot nanogels loaded with gemcitabine, polyglycidol-gemcitabine and trastuzumab**

After showing release properties of small and large model therapeutics from nanogels, we sought to utilize the platform for a relevant immunotherapy-chemotherapy drug combination, trastuzumab (TRA) and gemcitabine (GEM). Gemcitabine is a small molecule nucleoside analog that is also hydrophilic and used as chemotherapy for breast cancer treatment. Trastuzumab (TRA), commercially known as Herceptin®, is a large molecular weight monoclonal antibody which binds to HER2 receptors in breast cancer cells and slows down replication. Since it is known that hydrophilic small molecules tend to release rapidly from nano carriers, we decided to create a unique gemcitabine-conjugate with polyglycidol (PG-GEM) per synthesis scheme in Figure III-10 in order to delay the diffusion of gemcitabine from the nanogel after loading. Inspired by Nicolas and coworkers,<sup>90</sup> Gemcitabine was derivatized with levulinic acid to create a functional ketone site for fast and efficient hydrazone chemistry with a hydrazine-functionalized-polyglycidol polymer. We can easily characterize the end product by proton NMR, looking for unique aromatic protons around 5.9 and 7.8 ppm after purification. TRA, GEM or PG-GEM were all loaded with the hydrophilic hydrogel precursors in the first step like lysozyme as depicted in Figure III-7 (one-pot method). Release aliquots of TRA and GEM were measured from the same carrier via HPLC and BCA assay according to procedures established during the model release. As shown in Figure III-

11, it was observed that all therapeutic loadings into nanogels provided an extended release up to 9 days, which is two days longer than what has been seen by release studies of any biologicals from a nanocarrier. Moreover, the conjugated gemcitabine (NG Conjugate-Gem) exhibited a release that was indicative of a more controlled linear profile compared to the non-conjugated gemcitabine release (NG Free GEM).

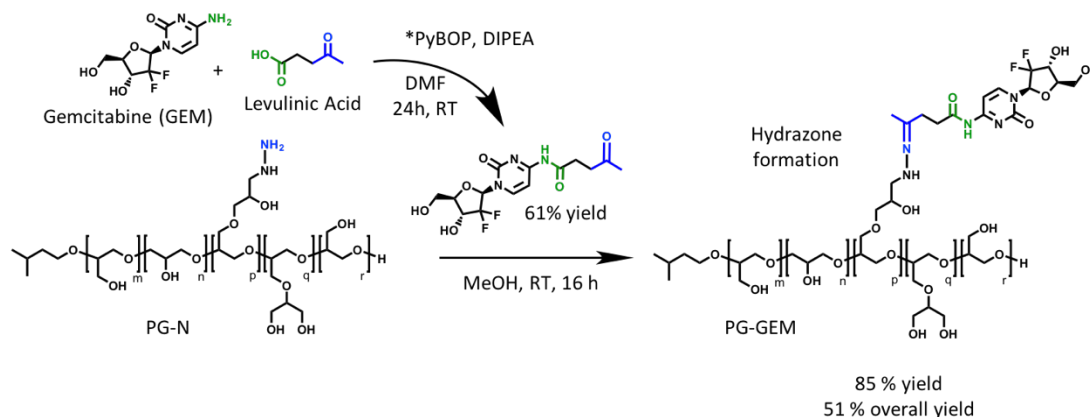


Figure III-10. Synthesis of polyglycidol-gemcitabine conjugate.

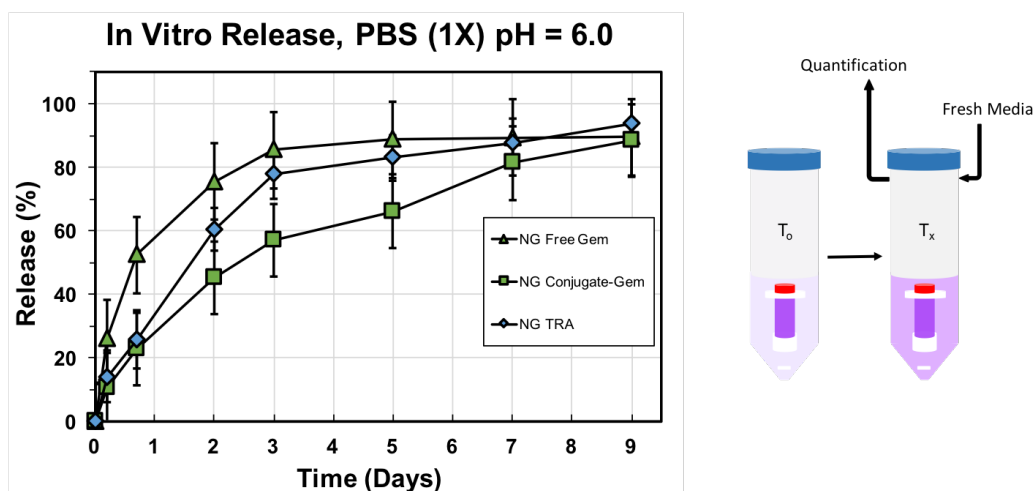


Figure III-11. Drug release *in vitro* at pH 6 at 37 °C using float-a-lyzer method. Free gemcitabine (GEM) and trastuzumab (TRA) were loaded into the same carrier and monitored for release, while the polyglycidol-gemcitabine conjugate was monitored for individual loading from the others.

## Conclusion

Precise size-controlled nanohydrogels (nHGs) have been developed *via* photo-initiated thiol-ene reactions using liposome templates under mild synthetic conditions in a step-wise and one-pot approach nHG-OP. Nanogels prepared in a step-wise approach (nHG-SW) exhibited release rates that are more controlled than other reported nanogels. This can be attributed to the implementation of branched polyglycidols to form tighter networks in the liposomal core than would be possible with linear crosslinking materials. In a one-pot approach, a lipid bilayer mix was preformed and allowed to self-assemble with pre-gel components before the thiol-ene crosslinking process. These structures (nHG-OP) afforded the most controlled release kinetics and showed the highest cytocompatibility of all our prepared carriers and the integration of bilayer structures seems to interpenetrate the hydrogel network in a favorable way to not only provide a controlled release of small hydrophobic but also biological therapeutics such as trastuzumab, small hydrophilic such as gemcitabine and polyglycidol-conjugated drugs such as the polyglycidol-gemcitabine construct. These nHGs may serve as promising strategy for dual nano-delivery of hydrophobic drugs and biologicals for applications such as immunotherapy with chemotherapy among other possible combination (see Figure III-12). In future studies, we plan to tailor the nanonetwork pore sizes by tuning the allyl-functionality ratio in the polyglycidols and study the influence of incorporated lipids.



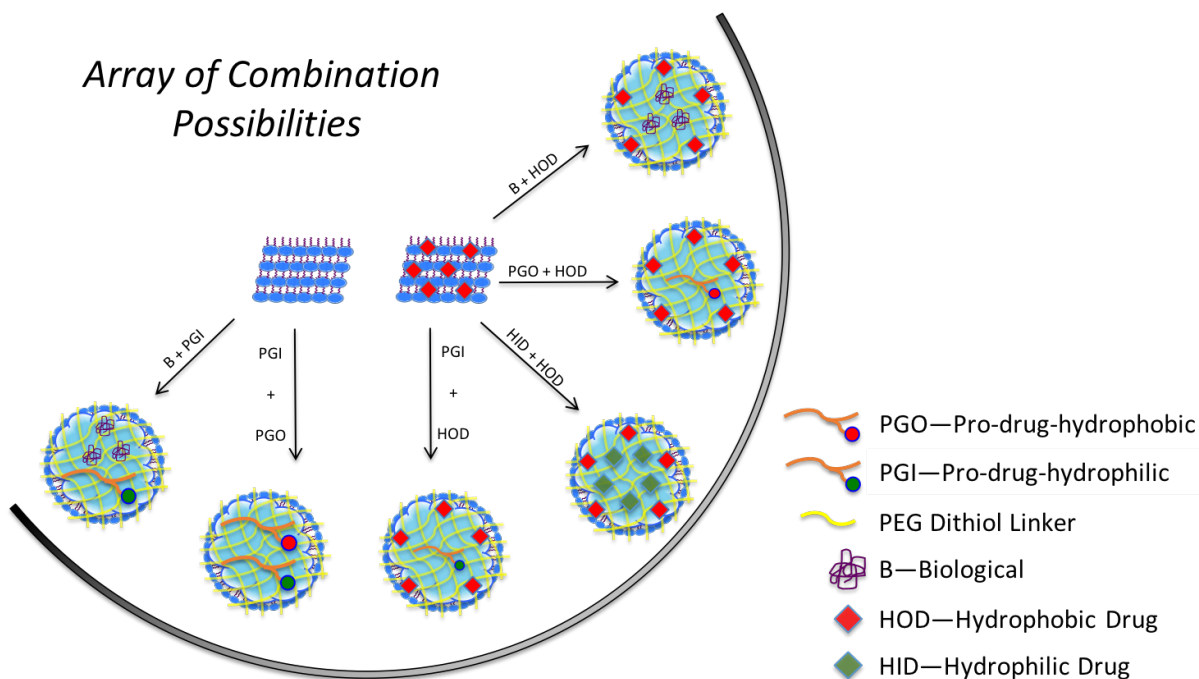


Figure III-12. Drug and drug-conjugate combinations that are possible with this nanoparticle platform.

## Experimental

### Materials

L- $\alpha$ -phosphatidylcholine (Egg-PC) was purchased from Avanti Polar Lipids (Alabaster, AL, USA). Cholesterol, Poly(ethylene glycol) dithiol (PEG dithiol,  $M_n$  1000 g mol<sup>-1</sup>), Nile Red (NR, technical grade), lysozyme from chicken egg white, Allyl glycidyl ether (AGE), and (2-Hydroxypropyl)- $\beta$ -cyclodextrin (HBC) were purchased from Sigma, USA. Glycidol (GLY) was also purchased from Sigma and purified via Kugelrohr distillation before use. VA-086, 2,2-Azobis(2-methyl-*N*-(2-hydroxyethyl)propionamide), 98% was purchased from Wako Chemicals USA, Inc. and used without further purification. *Micrococcus lysodeikticus* cells (M1) ATCC No. 4698 were purchased from Sigma, USA. HEPES buffer (1M Solution) was purchased from Corning (Corning, NY), diluted to 20mM in DI water, pH adjusted to 7.4 and supplemented with

200mM HCB for *in vitro* release studies. Phosphate buffered saline (PBS, 1X, pH 7.4) and Standard MTT reagent were obtained from Gibco by Life Technologies. Dialysis tubing SnakeSkin® (molecular weight cutoff (MWCO): 10 kD, 16 mm dry I.D.), Spectra/Por® G2 Float-A-Lyzers® (1 mL volume, MWCO: 20 kD and 300 kD) were purchased from Spectrum Laboratories, Inc. (Rancho Dominguez, CA). All other solvents or reagents were purchased from Sigma Aldrich unless mentioned otherwise and used as received.

### **Characterization**

<sup>1</sup>H and <sup>13</sup>C NMR spectra of poly(glycidol allylglycidyl ether), poly(GLY/AGE) were obtained from a Bruker AV600 Fourier transform spectrometer with deuterated methanol as the solvent. Gel permeation chromatography-size exclusion chromatography (GPC-SEC) of the poly(GLY/AGE) copolymer was performed in dimethyl formamide (DMF, with 1 mg/mL LiBr) at 45°C with a flow rate of 1.0 mL/min (Waters 1525 binary HPLC pump); columns: 7.8 x 300mm; Styragel HR 5 DMF, Styragel HR 4E, and Styragel HR 3: molecular weight range 50,000 to 4x10<sup>6</sup>, 50 to 100,000, and 500 to 30,000 g/mol. GPC detection was accomplished using a Waters 2414 refractive index detector at 410 nm. Molecular weights ( $M_n$  and  $M_w$ ) and polydispersity were determined from PEG standards provided by Varian. The average size and size distribution (polydispersity index, PDI) of the nanogels were analyzed *via* dynamic light scattering (DLS), and the zeta potential ( $\zeta$ ) determined *via* analysis of electrophoretic light scattering on a Malvern Zetasizer Nano ZS apparatus with Malvern Instruments DTS software (v.6.0d1) (Malvern Instruments, UK). Measurements were collected on solutions of nanogels and liposomes in DI water at 25°C. Temperature stability measurements of nanogels were conducted in PBS (1X, pH 7.4) at varying temperatures. The mean hydrodynamic diameter ( $d_h$ ) was computed from the intensity of the

scattered light using Malvern software based on Brownian motion and the Stokes-Einstein equation. Zeta potential ( $\zeta$ ) of the nanogels was analyzed using the electrophoretic light scattering spectrometer of the instrument. Transmission electron microscopy (TEM) images were captured using a FEI Technai Osiris FEI operating at 200 kV. Grids were prepared by dipping an Ultrathin Carbon Type-A 400 Mesh Copper Grid (Ted Pella, Redding, CA) into the sample solution ( $0.01 \text{ mg mL}^{-1}$ ) twice, followed by addition of 1 drop ( $\sim 3 \mu\text{L}$ ) of 2% uranyl acetate (Electron Microscopy Sciences, Hatfield, PA) to the carbon side of grid, and excess solution was wicked away after 3 minutes using a piece of filter paper. Grids were allowed to dry for 3 hours on benchtop at room temperature before imaging. Nile red was detected *via* UV-vis absorbance at 550nm (DMSO) or 580nm (HBC-HEPES media) after 2  $\mu\text{L}$  of sample was loaded on a Nanodrop 2000c spectrophotometer (Thermo, Wilmington, DE, USA) using instrument software NanoDrop 2000/2000c (v1.4.1). Blank samples of solvent, liposome and nanogels were analyzed to ensure no other compounds absorbed in this region. Lysozyme was quantified with BCA Assay and a Synergy HT Microtiter Plate reader (BIO-TEK) at 562 nm. The retained activity of lysozyme was determined by an activity assay with a protocol adapted from Worthington, Inc.

### **Synthesis of poly(glycidol allylglycidyl ether)**

Copolymerization of allyl glycidyl ether (AGE) and glycidol (GLY) was performed by cationic ring-opening polymerization with a 25/75 feed of AGE/GLY.  $\text{Sn}(\text{OTf})_2$  (5.2 mg;  $8.52 \times 10^{-6} \text{ mol}$ ; 0.00035 eq) and 3-methyl butanol (54  $\mu\text{L}$ ;  $3.33 \times 10^{-4} \text{ mol}$ ; 0.066 eq) were added to a  $\text{N}_2$ -purged, flame dried 25-mL round bottom reaction flask with small magnetic stir bar and lowered in to an ice bath at  $0^\circ\text{C}$ . After 15 minutes of stirring, the AGE (1.06 mL; 8.91 mmol; 0.25 eq) was added dropwise to the stirring flask, followed by slow dropwise addition of glycidol (GLY, 1.44 g; 26.7

mmol; 0.75 eq) over a period of 30 minutes. After stirring was completely impeded (~16h), the crude viscous polymer product was dissolved in a minimal amount of methanol and precipitated into vigorously stirring ethyl acetate at room temperature, which was then decanted to afford the pure GLY/AGE polymer product as translucent viscous material. The product was collected in methanol, transferred to a massed 6-dram vial, and excess solvent was removed. Yield: 2.6 g (88%). The polymer was stored at 4°C in 25 wt% MeOH to prevent crosslinking during storage. The degree of the allyl monomers incorporated into the polymer was determined *via*  $^1\text{H}$  NMR in MeOD with a value of 20% and a degree of branching of 0.23<sup>41-42</sup>.  $^1\text{H}$ -NMR (600 MHz, MeOD)  $\delta$  : 5.92 (1H), 5.21 (2H), 4.04 (2H), 3.38-3.94 (27.30H).  $^{13}\text{C}$ -NMR (150 MHz, MeOD)  $\delta$  : 136.31, 117.42, 81.56, 80.01, 74.09, 73.43, 72.51, 70.87, 64.60, 62.69. GPC  $M_n$  = 2900 Da using PEG standards. See Figure III-13 and III-14 for full labeled spectra.

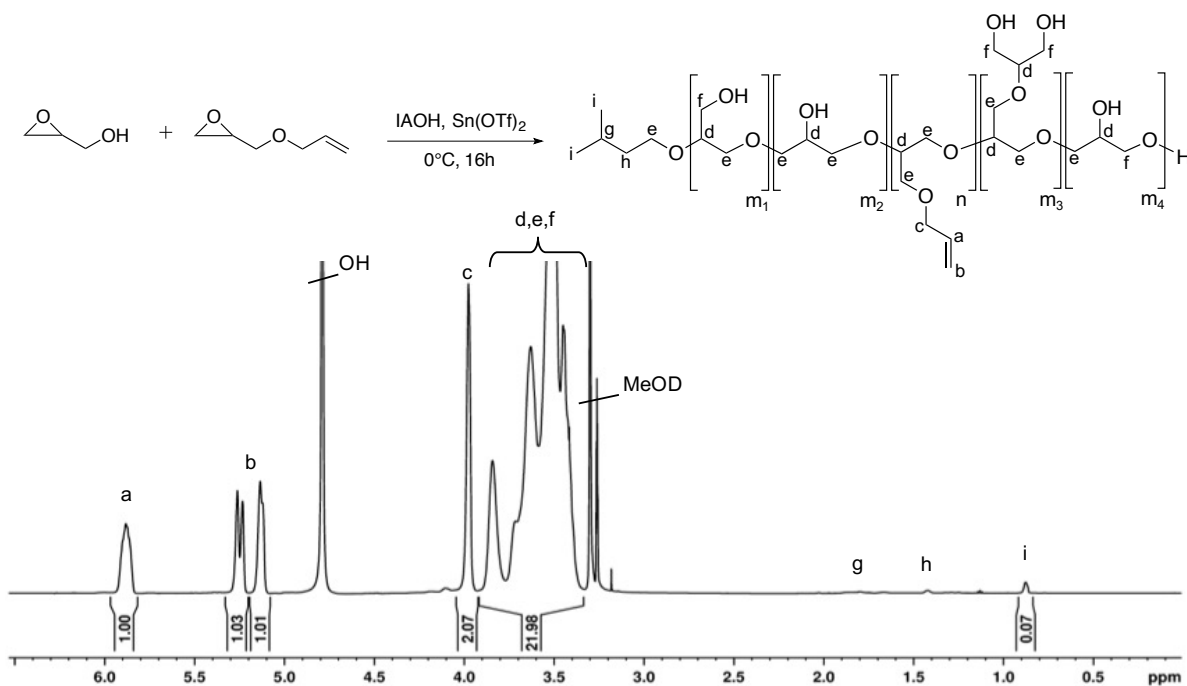


Figure III-13. Full labeled  $^1\text{H}$ -NMR (600 MHz, MeOD) spectrum of AGE/GLY polymer formed *via* cationic ring opening polymerization<sup>43</sup>.

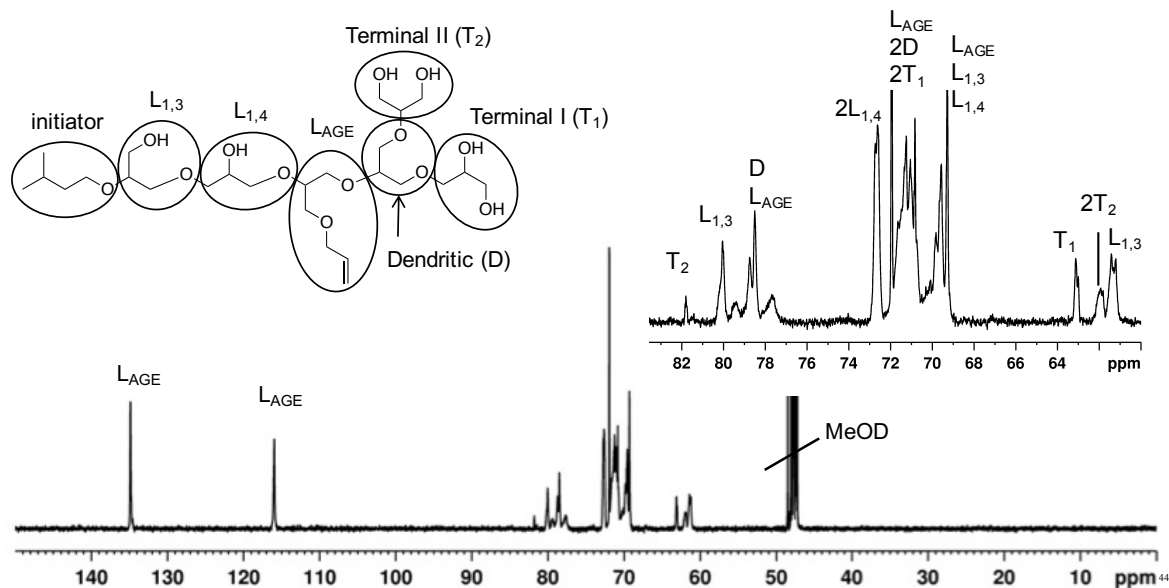


Figure III-14. Full labeled inverse-gated  $^{13}\text{C}$ -NMR (600 MHz) spectrum of AGE/GLY polymer in deuterated methanol with inset of 62-83 ppm region (top right). Relaxation time (D) was 10 sec, and number of scans (NS) was 1024. Degree of branching was calculated as 0.23 (semi-branched) based on relative integration values of dendritic units (D) compared with linear backbone units ( $L_{1,3}$ ,  $L_{1,4}$ , and  $L_{AGE}$ ) as previously described in the literature<sup>45-48</sup>.

### Synthesis of gemcitabine-levulinoate derivative

A 300 mg amount of gemcitabine (free base, 1.15 mmol) was combined with 199  $\mu\text{L}$  of *N,N*-Diisopropylethylamine (DIPEA, 1.14 mmol) with 5 mL dry dimethylformamide (DMF) in a flame-dried, nitrogen-purged 15-mL round bottom flask and stirred for 3 h at 900 rpm in ambient conditions. Additionally, 593 mg of (Benzotriazol-1-yloxy)tripyrrolidinophosphonium hexafluorophosphate (PyBOP, 1.14 mmol) was combined with 116  $\mu\text{L}$  of levulinic acid (1.14 mmol), 397  $\mu\text{L}$  of DIPEA (dry, 2.28 mmol) and 5 mL of DMF in a flame-dried, nitrogen-purged 25-mL round bottom flask and allowed to stir for at least 3 h at 900 rpm in ambient conditions to create the activated ester. Then, all contents from the gemcitabine mixture were added dropwise to the levulinic acid mixture and allowed to stir at room temperature for 24 h at 900 rpm. The DMF

was reduced *in vacuo* and the product was taken up in 50 mL ethyl acetate (EtOAc), transferred to a separatory funnel and washed with 100 mL HCl (10%, 2x), 100 mL of saturated sodium bicarbonate (2x), 100 mL of brine (1x). The organic layer was dried thoroughly and purified by column chromatography. The gemcitabine-levulinoate derivative was characterized by <sup>1</sup>H NMR in d<sub>6</sub>-DMSO and confirmed by the characteristic ethylene protons shifted in the 2.4-2.65 ppm region and disappearance of the amine hydrogen peak at 7.45 ppm. Dry yield = 61%.

### **Synthesis of polyglycidol-gemcitabine conjugate**

The synthesis of polyglycidol (allyl glycidyl-hydrazide) ether (7% allyl, 9 % amine) proceeded in 3 steps before adding the gemcitabine-ketone derivative. First, the poly(glycidol allylglycidyl) (20% allyl) was converted to partial epoxide functionality using 1.2 equivalents of purified meta-chloroperoxybenzoic acid (mcpba) in methanol (MeOH, 0.4 M), stirred at 1100 rpm for 48 h at room temperature in a sealed, flame-dried, N<sub>2</sub>-purged 6-DRAM vial. The product was dialyzed in 1 kDa MWCO tubing for 24 h against 500 mL methanol (changed six times), and dried *in vacuo* overnight (dry yield = 85%, 9% allyl, 13% epoxide by H<sup>1</sup>-NMR calculated ratio). A 100 mg sample of the partial epoxides in polymer were converted to Boc-hydrazide groups *via* nucleophilic amine-epoxide ring-opening with 1.4 equivalents of *tert*-Butyl carbazate, 0.17 M MeOH stirred at 800 rpm in a flame-dried, N<sub>2</sub>-purged 6 DRAM vial heated to 50 °C for 16 h. The product was purified by dialysis in 1 kDa MWCO tubing against 500 mL MeOH for 3 days (changed twice daily) and dried *in vacuo* overnight (dry yield = 254 mg [85%], 7% allyl, 9% N-N-Boc by H<sup>1</sup>-NMR calculated ratio). Just before addition of the gemcitabine-ketone derivative, the N-Boc group was deprotected with 569 equivalents of trifluoroacetic acid (TFA) mixed in 50 % (v/v) MeOH (0.02 M) stirring at 800 rpm at 25 °C for 24 h in a 6DRAM vial open to the air. The resulting product was diluted 5x

in MeOH and dried by rotovap four times to remove all TFA and further purified by passing through a glass pipet column made with 20 mg Sephadex® G-25 (Sigma) in MeOH. The product was collected in a 6 DRAM vial, dried overnight, and characterized by dry weight (dry yield = 95%, 7% allyl, 9% amine, 3 amines/polymer as determined by NMR). <sup>1</sup>H-NMR (400 MHz, MeOD) δ: 8.33 (3H), 5.92 (1H), 5.29 (2H), 4.11 (2H), 4.07 (4H), 3.08-3.94 (33H), 0.98 (6H) ppm. A 1.4 mol equivalent of gemcitabine-ketone derivative was added to 100 mg of the polyglycidol (allyl glycidyl hydrazide) ether with 20 mg of sodium bicarbonate (0.24 mmol) in 2 mL of MeOH in a 6 DRAM vial and stirred for 16 h at 800 rpm, purified in 1 kDa MWCO against MeOH (24 h, 6 changes). The purified product was collected in a 6DRAM, dried *in vacuo* and characterized by dry yield and proton NMR. A shift in the aromatic peak at 7.9 ppm indicated successful attachment of the gemcitabine to polyglycidol. Dry yield = 51 mg (51% yield).

### **General procedure for synthesis of bulk polyglycidol hydrogels**

Polyglycidol model hydrogels were prepared by a photo-initiated thiol-ene reaction of 1 kDa PEG dithiol (170 mg, 0.170 mmol, 0.5 eq) with poly(glycidol-allylglycidyl ether), (150 mg, 0.341 mmol, 1.0 eq, 15% solution) and a water soluble photoinitiator VA-086 (49 mg, 0.5 eq) in 1 mL DI water and vortexed well. Bulk gels for biological release were prepared with lysozyme (6.3 mg, 0.443 μmol) added to the pre-gel mixture. Exposure to long wave UV light (365 nm) for 45 min yielded an opaque crosslinked hydrogel. Yield = 94-98% (See Figure III-1).

### **Synthesis of step-wise nanohydrogels (nHG-SW)**

Multilammellar liposomes (MLVs) were first prepared using a thin film method as described in the literature<sup>49,51</sup>. A solution of chloroform (1 mL) with egg-PC (50 mg, 5 mol eq) and cholesterol

(5 mg, 1 mol eq) was prepared in a 6 DRAM vial and vortexed. For hydrophobic drug loading, Nile red (0.55 mg, 1.7  $\mu\text{mol}$ ) was added to the mixture in this step. Chloroform was then evaporated *via* nitrogen stream, and the lipid or lipid-drug mix was dried under vacuum overnight to yield a thin off-white film in the vial. One milliliter of DI water was added to hydrate the lipids through 10 alternating cycles of 30 s vortexing followed by 5 min resting at room temperature to allow for complete MLV formation. The resulting MLVs were extruded through 0.8, 0.2 and 0.1  $\mu\text{m}$  polycarbonate membranes (Whatman, Piscataway, NJ, USA) 11 times each using an Avanti® Mini-Extruder (Avanti Polar Lipids, Inc., Alabaster, AL, USA) to produce large unilamellar vesicles (LUVs) of 100 nm diameter and were subsequently lyophilized overnight to yield a white spongy solid. An aqueous solution of 15 wt% poly(GLY/AGE), 150 mg, was prepared in a separate 1 DRAM vial with 170 mg 1kDa PEG dithiol, 49 mg VA-086<sup>st</sup> and 1 mL of DI water in the same equivalences described in the model bulk gel preparation. The aqueous solution was used to hydrate the film through 10 alternating cycles of 30 s vortexing and 5 min resting at room temperature to allow for complete liposome hydration with pre-gel components shuttled into the interior of the vesicles<sup>13</sup>. The LUVs with pre-gel components were then diluted 4-fold to prevent macro scale gelation, dialyzed in 10 kDa MWCO Snakeskin tubing in fresh DI water for 6 hours to remove un-entrapped materials, transferred to a 1DRAM, and irradiated under long UV light (365 nm, 6 W) for 45 min. Dry yield = 49 mg (13%). Nanogels were stored at 4°C until use.

### **Synthesis of one-pot nanohydrogels (nHGs-OP)**

A solution of chloroform (1 mL) with egg-PC (50 mg, 5 mol eq) and cholesterol (5 mg, 1 mol eq) was prepared in a 6 DRAM vial and vortexed. For hydrophobic drug loading, Nile red (0.55 mg, 1.7  $\mu\text{mol}$ ) was added to the mixture in this step. Chloroform was then evaporated *via* nitrogen



stream, and the lipid or lipid-drug mix was dried under vacuum overnight to yield a thin off-white film in the vial. A 15 wt% GLY/AGE polymer (150 mg) solution was prepared in a separate 1 DRAM vial with 170 mg 1KDa PEG dithiol, 49 mg VA-086 and 1 mL of water in the same equivalences described under bulk gel preparation. The aqueous solution containing the pre-gel components was used to hydrate the film through 10 alternating cycles of 30 s vortexing and 5 min resting at room temperature to allow for complete multilammellar liposome hydration with pre-gel components. The resulting MLVs-PG were extruded through 0.8, 0.2 and 0.1  $\mu\text{m}$  polycarbonate membranes (Whatman, Piscataway, NJ, USA) 11 times each using an Avanti® Mini-Extruder (Avanti Polar Lipids, Inc., Alabaster, AL, USA) to produce what we called large unilamellar vesicles (LUVs-PG) of about 100 nm diameter<sup>14,53,54</sup>. The LUVs with pre-gel components were diluted 4-fold to prevent macro scale gelation, dialyzed in 10 kDa MWCO Snakeskin tubing in DI water for 6 hours, transferred to a 1 DRAM vial, and irradiated under long UV light (365 nm, 6W) for 45 min. Dry yield = 95 mg (25%) after lyophilization. Nanogels were stored at 4°C until use. Empty liposomes and NR-loaded liposomes were prepared in parallel using pure DI water for hydration.

### **Lysozyme activity retention assay**

Activity of Lysozyme (LYS) was determined with *Micrococcus lysodeikticus* cells. Lysozyme (from chicken egg, Sigma) was first prepared in 10 mg/mL DI water as a stock solution. Dilutions were made in 6 DRAM vials (1:10) to a final concentration of 1 mg/mL LYS in 10 mL of DI water. Four additional vials were prepared at 1 mg/mL. Two vials were treated with VA-086 photo-initiator to a final concentration of 4.9 mg/mL (equivalent to amount used in nanogel preparation). All four vials were subjected to long-wave UV light (365 nm, 6W) for either 10 or 45 minutes at

room temperature. Following treatment, each test group (including native LYS) was diluted 20-fold into 1 mL DI water in a 1.5-mL Eppendorf tube and kept cool until use with the assay<sup>55</sup>. A suspension of 15 mg of dried *Micrococcus lysodeikticus* (ATCC No. 4698, Sigma, MI) with 45 mL of 0.1 M potassium phosphate buffer<sup>56</sup> was prepared in a 50-mL Falcon (Fisher) tube. In a 96-well plate, 200  $\mu$ L of MI cell suspension were pipetted into test wells and allowed to rest at room temperature to equilibrate for 5 minutes. Then, 25  $\mu$ L of each LYS test group (n=3) were added to the MI suspensions, and the microplate was immediately loaded into a BioTek Synergy H2 microplate reader. The optical density was recorded every 15 seconds over the course of 5 minutes at 450 nm. The activity of LYS was calculated by the following equation<sup>55</sup>:

$$Units/mg = \frac{\Delta A_{450/min} \times 1000}{mg \text{ enzyme in reaction mix}}$$

where the absolute slope of the optical density over time was taken as  $\Delta A_{450/min}$ , the activity of native LYS was taken as 100%, and the treated LYS test group activities were compared directly to the native value to determine percent activity retention.<sup>57</sup>

### **Measurement of cytocompatibility of liposomes, nHG-SW and nHG-OP**

NIH 3T3 mouse fibroblast cells were purchased from Sigma Aldrich and cultured in Dulbecco's modified eagle medium with 10% bovine growth serum and 1% penicillin/streptomycin. They were cultured at 37 °C with 5% CO<sub>2</sub> using standard protocol. The cell compatibility of the liposome, nHG-SW and nHG-Ops to NIH 3T3 mouse fibroblast cells was evaluated using a MTT assay. The cells were cultured and seeded in a 96 well plate at a density of approximately 7,000 cells per well and incubated for 24 hrs at 37 °C. Afterwards, the media was removed and replaced

with 100  $\mu\text{L}$  of fresh complete growth media, supplemented with concentrations of 0.01, 0.05, 0.1, 0.5, 1, 5 and 10 mg/mL of liposome, nHG-SW or nHG-Ops respectively. The cells were incubated for 24 hrs. At the end of this time period, the media was removed and the wells were washed gently with 100  $\mu\text{l}$  of DPBS. Then, 100  $\mu\text{L}$  of fresh media was added followed by 20  $\mu\text{L}$  of MTT solution (5 mg/mL in DPBS) was added to each well and cells were incubated at 37 °C for 2 hours. Then, 100  $\mu\text{L}$  of 10% sodium dodecyl sulfate was added to each well and incubated for 5 hrs at 37 °C. The absorbance was measured at 562 nm using a Synergy HT Microtiter plate reader. Experiments were done in triplicates. Cell viability was assessed using the following equation:

$$\% \text{ Cell Viability} = \frac{A_{test} - A_{blank}}{A_{control} - A_{blank}} \times 100$$

The data was reported as the mean and standard deviation of three independent trials for each test condition.

### **Loading of liposomes, nHGs-SW, and nHGs-OP with Nile red and lysozyme**

Nile red (0.55 mg, 1.7  $\mu\text{mol}$ ) was always added to the lipid mix with chloroform prior to thin lipid film formation during the synthesis of liposomes, nHGs-SWs and nHGs-OPs as described earlier. Lysozyme (10  $\mu\text{g}/\text{mg}$  material, 1 wt%) was loaded in to liposomes, nHGs-SW and nHGs-OP at different stages. For liposomes and nanogels prepared by step-wise addition, lysozyme was added with water or pre-gel components during the hydration of dry LUVs (see Scheme 3). In the case of nanogels prepared by the one pot approach, lysozyme was added with pre-gel components to the thin lipid film, followed by extrusions and crosslinking. Drug-loaded nano-carriers were purified using 50 kDa MWCO dialysis tubing (Spectrum Laboratories, CA) in DI water for 6 hours to removed non-entrapped protein material.

### **Determination of Nile Red encapsulation in Liposomes, nHG-SW and nHG-OP nanohydrogels**

A 5 mg sample of nanogel or liposome containing the NR was mixed in 1 mL of DMSO. The solution was sonicated for 10 minutes, and a small aliquot (2  $\mu$ L) was analyzed directly on the nanodrop as described in the characterization section. The sample absorbance was used to calculate Nile Red quantity *via* prepared standard curve of Nile Red in DMSO. The encapsulation efficiency was determined according to the following equation:

$$\frac{Drug_{Entrapped}}{Drug_{feed}} \times 100 = Encapsulation\ Efficiency\ (\%)$$

### **Determination of lysozyme encapsulation in liposomes, nHG-SW and nHG-OP nanohydrogels**

To determine the loading efficiency, it is not applicable to directly measure the loaded amount of lysozyme using the same method as established for the Nile Red loading. Lysozyme absorbs in water at the same wavelength as the polymer backbone. For the same reason, a Pierce® BCA protein assay kit is used to form Cu-BCA chelates in the presence of the lysozyme and are detected at 580 nm. However, the complexation and detection is only reliable when the lysozyme is in free form and not entrapped in the nanostructure. However, we did not attempt to extract the lysozyme by degrading or destroying the nanostructure and could potentially damage the protein and lead to an inaccurate quantification. Instead, we opted for the Float-A-Lyzer dialysis membrane, here we can separate the protein from the nanogels, in 9-11 days, and apply the release aliquots to the detection kit. The loading efficiency of lysozyme in liposomes, nHGs-SWs and nHGs-OP is with this method calculated through the maximum cumulative release of protein. This value can be taken as the minimum loading efficiency because it is also the total detected release. This

calculation method gives the most conservative readout for the loading efficiency of a biological in these systems.

### ***In vitro* release of Nile red from liposomes, nHG-SW, nHG-OP**

The *in vitro* release of Nile red was determined using Float-A-Lyzer dialysis tubing to ensure a constant separation between the selected nanocarrier and released drug in the sink media. Float-A-Lyzer dialysis tubing devices were treated with 10% isopropanol/water for 15 minutes to remove the glycerol preservative, followed by careful rinsing with DI water and overnight soak in release media to ensure thorough wetting of the membranes before use<sup>37</sup>. As a control, one milliliter of free Nile red (0.5 mg, 1.57 mM) was dissolved in HBC-HEPES (200 mM HBC, 20 mM HEPES, pH 7.4) and transferred to a Float-A-Lyzer (MWCO: 300 kD) dialysis pod, placed in a 50-mL Falcon tube with 18 mL of fresh HBC-HEPES media (1:18 gradient ratio) and capped to prevent evaporation of release media. Liposomes (200 mg, 1.57 mM NR), nanogels prepared by step-wise (nHG-SW, 178.5 mg, 1.57 mM NR) and nanogels prepared by one-pot (nHG-OP, 161.2 mg, 1.57 mM NR) were prepared in a similar fashion. Release media were agitated (150 rpm) continuously using small magnetic stir bars to prevent the formation of an unstirred water layer at the membrane/outer solution interface<sup>38</sup>. Release experiments were kept at a constant temperature of 37°C using a water bath and an electrostatic temperature control stir plate. Samples of 10 µL were withdrawn from the sink at fixed time intervals of 5 and 17 hours, then again at 2, 3, 5, 7 and 9 days and analyzed directly on the Nanodrop. Equivalent amounts of fresh release media were added to maintain sink conditions. Nile red release was determined by standard curve (1-100 µg/mL) in HBC-HEPES solution. All experiments were performed in triplicate.

### **In vitro release of lysozyme from liposomes, nHG-SW, nHG-OP nanohydrogels.**

Float-A-Lyzers (300 kD MWCO, 1.0 mL) were treated with 10% isopropanol to remove the glycerol preservative and were allowed to soak in release media (PBS 1X, pH 7.4) overnight to thoroughly wet the membrane<sup>27 59 60</sup>. A control bag was prepared with 1.0 mL of free lysozyme (0.5 mg, 500  $\mu\text{g mL}^{-1}$ ) in PBS and transferred to 18 mL of PBS (1:18 ratio) similarly to the Nile red release setup (See Figure III-8). Samples of liposome (50 mg, 10  $\mu\text{g/mL}$  LYS), nHG-SW (50,  $\mu\text{g/mL}$  LYS) and nHG-OP (50 mg, 10  $\mu\text{g/mL}$  LYS) were prepared with equivalent amounts of lysozyme and run in parallel. Release containers were incubated in a water bath set to 37°C. At fixed time intervals of 5 hours, 1, 2, 3, 5, 7 and 9 days, 30  $\mu\text{L}$  aliquots of sink media were removed and replaced with equal volumes of fresh PBS (1X, pH 7.4) to maintain sink conditions. The aliquots were analyzed for lysozyme content using a Pierce® BCA Protein Assay kit following the manufacturer instructions. All experiments were performed in triplicate.

### References

1. Hu, C. M.; Zhang, L., Nanoparticle-based combination therapy toward overcoming drug resistance in cancer. *Biochemical Pharmacology* **2012**, 83 (8), 1104-11.
2. Win, L. L.; Powis, J.; Shah, H.; Feld, J. J.; Wong, D. K., Death from Liver Failure despite Lamivudine Prophylaxis during R-CHOP Chemotherapy due to Rapid Emergence M204 Mutations. *Case Reports in Hepatology* **2013**, 2013, 454897.
3. Kim, R.; Emi, M.; Tanabe, K.; Arihiro, K., Tumor-driven evolution of immunosuppressive networks during malignant progression. *Cancer Research* **2006**, 66 (11), 5527-5536.

4. van der Weijden, J.; Paulis, L. E.; Verdoes, M.; van Hest, J. C. M.; Figdor, C. G., The right touch: design of artificial antigen-presenting cells to stimulate the immune system. *Chemical Science* **2014**, *5* (9), 3355-3367.
5. He, C.; Tang, Z.; Tian, H.; Chen, X., Co-delivery of chemotherapeutics and proteins for synergistic therapy. *Advanced Drug Delivery Reviews* **2016**, *98*, 64-76.
6. Hariri, G.; Edwards, A. D.; Merrill, T. B.; Greenbaum, J. M.; van der Ende, A. E.; Harth, E., Sequential targeted delivery of paclitaxel and camptothecin using a cross-linked "nanosponge" network for lung cancer chemotherapy. *Molecular Pharmaceutics* **2014**, *11* (1), 265-75.
7. Wang, D. Y.; Sosman, J. A.; Johnson, D. B., Combination Immunotherapy: An Emerging Paradigm in Cancer Therapeutics. *Oncology (Williston Park, N.Y.)* **2015**, *29* (12).
8. Nars, M. S.; Kaneno, R., Immunomodulatory effects of low dose chemotherapy and perspectives of its combination with immunotherapy. *International Journal of Cancer* **2013**, *132* (11), 2471-8.
9. Jiang, T.; Mo, R.; Bellotti, A.; Zhou, J.; Gu, Z., Gel-Liposome-Mediated Co-Delivery of Anticancer Membrane-Associated Proteins and Small-Molecule Drugs for Enhanced Therapeutic Efficacy. *Advanced Functional Materials* **2014**, *24* (16), 2295-2304.
10. Roy, A.; Singh, M. S.; Upadhyay, P.; Bhaskar, S., Combined chemo-immunotherapy as a prospective strategy to combat cancer: a nanoparticle based approach. *Molecular Pharmaceutics* **2010**, *7* (5), 1778-88.
11. Shahbazi, M. A.; Shrestha, N.; Makila, E.; Araujo, F.; Correia, A.; Ramos, T.; Sarmiento, B.; Salonen, J.; Hirvonen, J.; Santos, H. A., A prospective cancer chemo-immunotherapy approach mediated by synergistic CD326 targeted porous silicon nanovectors. *Nano Research* **2015**, *8* (5), 1505-1521.

12. Kazakov, S., Liposome-Nanogel Structures for Future Pharmaceutical Applications: An Updated Review. *Current Pharmaceutical Design* **2016**, *22* (10), 1391-1413.
13. Park, J.; Wrzesinski, S. H.; Stern, E.; Look, M.; Criscione, J.; Ragheb, R.; Jay, S. M.; Demento, S. L.; Agawu, A.; Limon, P. L.; Ferrandino, A. F.; Gonzalez, D.; Habermann, A.; Flavell, R. A.; Fahmy, T. M., Combination delivery of TGF-beta inhibitor and IL-2 by nanoscale liposomal polymeric gels enhances tumour immunotherapy. *Nature Materials* **2012**, *11* (10), 895-905.
14. An, S. Y.; Bui, M.-P. N.; Nam, Y. J.; Han, K. N.; Li, C. A.; Choo, J.; Lee, E. K.; Katoh, S.; Kumada, Y.; Seong, G. H., Preparation of monodisperse and size-controlled poly(ethylene glycol) hydrogel nanoparticles using liposome templates. *Journal of Colloid and Interface Science* **2009**, *331* (1), 98-103.
15. Joo, K. I.; Xiao, L.; Liu, S.; Liu, Y.; Lee, C. L.; Conti, P. S.; Wong, M. K.; Li, Z.; Wang, P., Crosslinked multilamellar liposomes for controlled delivery of anticancer drugs. *Biomaterials* **2013**, *34* (12), 3098-109.
16. Allen, T. M.; Cullis, P. R., Liposomal drug delivery systems: From concept to clinical applications. *Advanced Drug Delivery Reviews* **2013**, *65* (1), 36-48.
17. Yin, F.; Guo, S.; Gan, Y.; Zhang, X., Preparation of redispersible liposomal dry powder using an ultrasonic spray freeze-drying technique for transdermal delivery of human epithelial growth factor. *International Journal of Nanomedicine* **2014**, *9*, 1665-76.
18. He, W.; Lv, Y.; Zhao, Y.; Xu, C.; Jin, Z.; Qin, C.; Yin, L., Core-shell structured gel-nanocarriers for sustained drug release and enhanced antitumor effect. *International Journal of Pharmacognosy* **2015**, *484* (1-2), 163-171.



19. Wang, T.; Deng, Y.; Geng, Y.; Gao, Z.; Zou, J.; Wang, Z., Preparation of submicron unilamellar liposomes by freeze-drying double emulsions. *Biochimica et Biophysica Acta* **2006**, *1758* (2), 222-31.
20. Kazakov, S.; Kaholek, M.; Kudasheva, D.; Teraoka, I.; Cowman, M. K.; Levon, K., Poly(N-isopropylacrylamide-co-1-vinylimidazole) hydrogel nanoparticles prepared and hydrophobically modified in liposome reactors: Atomic force microscopy and dynamic light scattering study. *Langmuir* **2003**, *19* (19), 8086-8093.
21. Kazakov, S.; Kaholek, M.; Teraoka, I.; Levon, K., UV-induced gelation on nanometer scale using liposome reactor. *Macromolecules* **2002**, *35* (5), 1911-1920.
22. Fowler, C. I.; Muchemu, C. M.; Miller, R. E.; Phan, L.; O'Neill, C.; Jessop, P. G.; Cunningham, M. F., Emulsion Polymerization of Styrene and Methyl Methacrylate Using Cationic Switchable Surfactants. *Macromolecules* **2011**, *44* (8), 2501-2509.
23. Liang, Y.; Kiick, K. L., Multifunctional lipid-coated polymer nanogels crosslinked by photo-triggered Michael-type addition. *Polymer Chemistry* **2014**, *5* (5), 1728-1736.
24. Wang, Y.; Tu, S.; Pinchuk, A. N.; Xiong, M. P., Active drug encapsulation and release kinetics from hydrogel-in-liposome nanoparticles. *Journal of Colloid and Interface Science* **2013**, *406* (0), 247-255.
25. Seddon, A. M.; Curnow, P.; Booth, P. J., Membrane proteins, lipids and detergents: not just a soap opera. *Biochimica et Biophysica Acta* **2004**, *1666* (1-2), 105-17.
26. Surapaneni, M. S.; Das, S. K.; Das, N. G., Designing Paclitaxel drug delivery systems aimed at improved patient outcomes: current status and challenges. *International Scholarly Research Notices Pharmacology* **2012**, *2012*, 623139.

27. de Andrade, D. F.; Zuglianello, C.; Pohlmann, A. R.; Guterres, S. S.; Beck, R. C., Assessing the In Vitro Drug Release from Lipid-Core Nanocapsules: a New Strategy Combining Dialysis Sac and a Continuous-Flow System. *AAPS PharmSciTech* **2015**, *16* (6), 1409-17.
28. Albers, E.; Muller, B. W., Cyclodextrin derivatives in pharmaceuticals. *Critical Reviews in Therapeutic Drug Carrier Systems* **1995**, *12* (4), 311-37.
29. Hirayama, F.; Uekama, K., Cyclodextrin-based controlled drug release system. *Advanced Drug Delivery Reviews* **1999**, *36* (1), 125-141.
30. Saarinen-Savolainen, P.; Jarvinen, T.; Taipale, H.; Urtti, A., Method for evaluating drug release from liposomes in sink conditions. *International Journal of Pharmaceutics* **1997**, *159* (1), 27-33.
31. Thompson, D. O., Cyclodextrins--enabling excipients: their present and future use in pharmaceuticals. *Critical Reviews in Therapeutic Drug Carrier Systems* **1997**, *14* (1), 1-104.
32. Washington, C., Drug Release from Microdisperse Systems - a Critical-Review. *International Journal of Pharmaceutics* **1990**, *58* (1), 1-12.
33. Varela, M. C.; Guzman, M.; Molpeceres, J.; del Rosario Aberturas, M.; Rodriguez-Puyol, D.; Rodriguez-Puyol, M., Cyclosporine-loaded polycaprolactone nanoparticles: immunosuppression and nephrotoxicity in rats. *European Journal of Pharmaceutical Sciences* **2001**, *12* (4), 471-8.
34. Jiao, Y. Y.; Ubrich, N.; Marchand-Arvier, M.; Vigneron, C.; Hoffman, M.; Lecompte, T.; Maincent, P., In vitro and in vivo evaluation of oral heparin-loaded polymeric nanoparticles in rabbits. *Circulation* **2002**, *105* (2), 230-235.

35. Molpeceres, J.; Aberturas, M. R.; Guzman, M., Biodegradable nanoparticles as a delivery system for cyclosporine: preparation and characterization. *Journal of Microencapsulation* **2000**, *17* (5), 599-614.
36. Guzman, M.; Aberturas, M. R.; Rodriguez-Puyol, M.; Molpeceres, J., Effect of nanoparticles on digitoxin uptake and pharmacologic activity in rat glomerular mesangial cell cultures. *Drug Delivery* **2000**, *7* (4), 215-22.
37. Modi, S.; Anderson, B. D., Determination of drug release kinetics from nanoparticles: overcoming pitfalls of the dynamic dialysis method. *Molecular Pharmaceutics* **2013**, *10* (8), 3076-89.
38. Leonard, M.; De Boisseson, M. R.; Hubert, P.; Dalencon, F.; Dellacherie, E., Hydrophobically modified alginate hydrogels as protein carriers with specific controlled release properties. *Journal of Controlled Release* **2004**, *98* (3), 395-405.
39. Liang, Y.; Kiick, K. L., Liposome-Cross-Linked Hybrid Hydrogels for Glutathione-Triggered Delivery of Multiple Cargo Molecules. *Biomacromolecules* **2016**, *17* (2), 601-14.
40. Nicolas, J., Drug-Initiated Synthesis of Polymer Prodrugs: Combining Simplicity and Efficacy in Drug Delivery. *Chemistry of Materials* **2016**, *28* (6), 1591-1606.
41. Holter, D.; Frey, H., Degree of branching in hyperbranched polymers .2. Enhancement of the DB: Scope and limitations. *Acta Polymerica* **1997**, *48* (8), 298-309.
42. Holter, D.; Burgath, A.; Frey, H., Degree of branching in hyperbranched polymers. *Acta Polymerica* **1997**, *48* (1-2), 30-35.
43. Matyjaszewski, K., *Cationic Polymerizations: Mechanisms, Synthesis & Applications*. CRC Press: 1996.

44. Zhuang, X.; Wu, T.; Zhao, Y.; Hu, X.; Bao, Y.; Guo, Y.; Song, Q.; Li, G.; Tan, S.; Zhang, Z., Lipid-enveloped zinc phosphate hybrid nanoparticles for codelivery of H-2K(b) and H-2D(b)-restricted antigenic peptides and monophosphoryl lipid A to induce antitumor immunity against melanoma. *Journal of Controlled Release* **2016**, *228*, 26-37.
45. Spears, B. R.; Marin, M. A.; Montenegro-Burke, J. R.; Evans, B. C.; McLean, J.; Harth, E., Aqueous Epoxide Ring-Opening Polymerization (AEROP): Green Synthesis of Polyglycidol with Ultralow Branching. *Macromolecules* **2016**, *49* (6), 2022-2027.
46. Spears, B. R.; Waksal, J.; McQuade, C.; Lanier, L.; Harth, E., Controlled branching of polyglycidol and formation of protein-glycidol bioconjugates via a graft-from approach with "PEG-like" arms. *Chemical Communications* **2013**, *49* (24), 2394-6.
47. Schull, C.; Gieshoff, T.; Frey, H., One-step synthesis of multi-alkyne functional hyperbranched polyglycerols by copolymerization of glycidyl propargyl ether and glycidol. *Polymer Chemistry* **2013**, *4* (17), 4730-4736.
48. Wilms, D.; Stiriba, S. E.; Frey, H., Hyperbranched Polyglycerols: From the Controlled Synthesis of Biocompatible Polyether Polyols to Multipurpose Applications. *Accounts of Chemical Research* **2010**, *43* (1), 129-141.
49. Moghimipour, E.; Handali, S., Utilization of thin film method for preparation of celecoxib loaded liposomes. *Advanced Pharmaceutical Bulletin* **2012**, *2* (1), 93-8.
50. Kong, X.; Lu, D.; Wu, J.; Liu, Z., Spreading of a Unilamellar Liposome on Charged Substrates: A Coarse-Grained Molecular Simulation. *Langmuir* **2016**.
51. Li, K.; Wang, S., Preparation, Pharmacokinetic Profile, and Tissue Distribution Studies of a Liposome-Based Formulation of SN-38 Using an UPLC-MS/MS Method. *AAPS PharmSciTech* **2016**.

52. Occhetta, P.; Visone, R.; Russo, L.; Cipolla, L.; Moretti, M.; Rasponi, M., VA-086 methacrylate gelatine photopolymerizable hydrogels: A parametric study for highly biocompatible 3D cell embedding. *Journal of Biomedical Materials Research Part A* **2015**, *103* (6), 2109-2117.
53. Kant Shashi, K. S., Prashar Bharat, A Complete Review On: Liposomes. *International Research Journal of Pharmacy* **2012**, *3* (7), 10.
54. Vemuri, S.; Rhodes, C. T., Preparation and characterization of liposomes as therapeutic delivery systems: a review. *Pharmaceutica Acta Helvetica* **1995**, *70* (2), 95-111.
55. Worthington, K., and Worthington, V. Worthington Enzyme Manual 2011. <http://www.worthington-biochem.com/pap/default.html>.
56. Preparation of 0.1 m Potassium Phosphate Buffer at 25°C. *Cold Spring Harbor Protocols* **2006**, *2006* (1), pdb.tab19.
57. Lucius, M.; Falatach, R.; McGlone, C.; Makaroff, K.; Danielson, A.; Williams, C.; Nix, J. C.; Konkolewicz, D.; Page, R. C.; Berberich, J. A., Investigating the Impact of Polymer Functional Groups on the Stability and Activity of Lysozyme-Polymer Conjugates. *Biomacromolecules* **2016**, *17* (3), 1123-34.
58. D'Souza, S. S.; DeLuca, P. P., Development of a dialysis in vitro release method for biodegradable microspheres. *AAPS PharmSciTech* **2005**, *6* (2), E323-8.
59. Krieter, D. H.; Fink, S.; Dorsch, O.; Harenberg, J.; Melzer, N.; Wanner, C.; Lemke, H. D., Pharmacokinetics of Certoparin During In Vitro and In Vivo Dialysis. *Artificial Organs* **2015**, *39* (11), 951-9.
60. Breynaert, A.; Bosscher, D.; Kahnt, A.; Claeys, M.; Cos, P.; Pieters, L.; Hermans, N., Development and Validation of an in vitro Experimental GastroIntestinal Dialysis Model with

Colon Phase to Study the Availability and Colonic Metabolisation of Polyphenolic Compounds.

*Planta Medica* **2015**, *81* (12-13), 1075-83.

Portions of this chapter were reprinted with permission from Lockhart, J. N.; Beezer, D. B.; Stevens, D. M.; Spears, B. R.; Harth, E., One-pot polyglycidol nanogels via liposome master templates for dual drug delivery. *Journal of Controlled Release* 2016, *244*, Part B, 366-374. Copyright 2016 Elsevier.

## CHAPTER IV

### ELECTRON BEAM LITHOGRAPHY OF POLYGLYCIDOL NANOGELS FOR IMMOBILIZATION OF THREE-ENZYME CASCADE

#### Introduction

Enzyme cascade immobilization has become increasingly valuable in chemical synthesis, bioreactor, and biosensor applications.<sup>1-4</sup> The high substrate selectivity, specificity, and reusability of enzymes make them cost-effective analytical tools, but enzyme longevity and spatial control present ongoing development challenges.<sup>5-6</sup> As shown by Figure IV-1, the three current most common immobilization strategies for building enzymatic biosensor surfaces include physical adsorption, covalence (e.g. crosslinking with glutaraldehyde), and encapsulation within a gel or polymeric matrix atop a solid support. The physical adsorption method typically does not include a matrix which makes the process easy, but significant drawbacks like a fast desorption of the enzymes are observed. Covalent attachment methods enable an improved binding to the substrate, but chemical modifications come in part with loss of enzyme activity through alterations. Enzyme entrapment into polymer matrices do not alter the enzyme but are prone to enzyme leakage. Enabling methods to support these techniques are for example surface-patterning methods such as dip-pen lithography and bias-assisted atomic force microscopy (AFM) have been explored for imprinting biomolecules on a solid support by adsorption and covalence, but electron beam lithography (EBL) has emerged as a powerful tool for creating arbitrary micron and nanoscale patterns that entrap proteins within a polymeric negative resist.<sup>7-11</sup> Much EBL work has been focused on linear poly(ethylene glycol) (PEG) for hydrogel entrapment of single proteins.<sup>12-17</sup> In this

approach, a high-energy beam of electrons causes hydrogen abstraction on the PEG backbone, followed by radical-mediated inter-chain and chain-surface crosslinking. Krsko *et al.* was the first to show how EBL can be used to make arbitrary micro-hydrogel patterns ~50-100 nm thick on silicon.<sup>17-18</sup> In an elegant work from the Maynard and coworkers, a core-shell poly(ethylene glycol) cross-linked hydrogel structure can be created using EBL to confine into selected matrix regions, necessary for an enzyme cascade reaction.<sup>28</sup> This approach led to improved 3-D spatial control over immobilization of two enzymes and with modest retention of bioactivity. This work inspired us to investigate ways to confine enzyme into specific regions using alternative methods.

To date, there are very few examples where multiple enzymes have been entrapped on a surface for cascade reactions, and reusability is rarely addressed. We sought to create a novel bio-

Strategy	Binding Method	Advantages	Drawbacks	References
Physical Adsorption	Van der Waals, affinity, hydrophobic, ionic or hydrogen bonding between enzyme and support	<ul style="list-style-type: none"> <li>• Simple</li> <li>• Easy to regenerate enzyme</li> </ul>	<ul style="list-style-type: none"> <li>• Desorption</li> <li>• Non-specific protein binding</li> </ul>	19-21
Covalent Attachment	Cross-linking or other chemical bonding between enzyme and support	<ul style="list-style-type: none"> <li>• No diffusion barrier</li> <li>• Short response time</li> </ul>	<ul style="list-style-type: none"> <li>• High enzyme bioactivity loss</li> <li>• Enzyme cannot be regenerated easily</li> </ul>	17, 22-23
Encapsulation	Entrapment of the enzyme within a gel or polymer matrix atop support	<ul style="list-style-type: none"> <li>• No chemical reaction between enzyme and polymer</li> <li>• Multiple different enzymes can be easily immobilized in the same matrix</li> </ul>	<ul style="list-style-type: none"> <li>• Diffusion barrier for substrates</li> <li>• Enzyme leakage leads to reduced activity over time</li> </ul>	10, 13-14, 24-26

Figure IV-1. Table that includes advantages and drawbacks of the three current most common enzyme immobilization strategies for building enzymatic bio-sensing surfaces.

sensing platform which employs enzyme-entrapped poly(glycidol) nanogel carriers to improve the spatial 3-D organization of multiple enzymes with a single EBL fabrication step and without harsh synthetic modifications. As proof-of-concept, we spin-coated a three-enzyme cascade of  $\beta$ -



galactosidase (GAL), glucose oxygenase (GOX), and horseradish peroxidase (HRP) with and without nanogel pre-encapsulation and cross-linked the films within a semi-branched poly(glycidol) matrix by EBL as shown by Figure IV-6. Our previous work demonstrated that high enzyme loading and retained enzyme activity was feasible within the nano-networks of the poly(glycidol) nanogels we had developed previously,<sup>14,27</sup> and the three-enzyme cascade was chosen due to its important applications in the food and medical diagnostic industries.<sup>28</sup> Moreover, poly(glycidol) was chosen to be developed as a novel EBL resist due to its aqueous solubility, superior storage stability, biocompatibility, high packing efficiency and non-fouling characteristics.<sup>29</sup> Other attractive bioactive EBL resist materials have been used such as aqueous-based silk and trehalose glycopolymers by Kaplan and Omenetto<sup>30</sup> and Maynard,<sup>26</sup> respectively. Herein, we demonstrate biosensing utility of the poly(glycidol) enzyme immobilization platform with improved performance, high reusability and storage stability via 3-D spatial arrangement of the three-enzyme cascade with nanogel entrapment compared to enzymes that were not nano-encapsulated. The resulting EBL patterns were investigated by bright-field microscopy and AFM, and the lactose enzyme cascade activity was determined by a chromogenic o-phenylenediamine indicator that was quantified by UV-vis spectrophotometry.

## Results and Discussion

### **Development of semi-branched poly(glycidol) as negative electron beam (EBL) resist**

The use of poly(glycidol) as a bio-stabilizing EBL resist has not been shown in the literature to date. The only known account for exposing a related poly(glycidol) to EBL using a mixture with poly(ethylene oxide), and the hyper-branched structure of the PG differs from ours due to its dissimilar synthetic method.<sup>31</sup> Therefore, we determined the optimal spin coat parameters

necessary for obtaining a uniform and reproducible thickness with the intent of encapsulating 100-150 nm nanogels on the silicon surface. Prior to spin-coating, the silicon surface needed to be cleaned thoroughly to improve coating uniformity. We tried cleaning methods with methanol, the basic KOH clean,<sup>32</sup> and finally a piranha clean method.<sup>33</sup> Ultimately, we found that the piranha cleaning method provided the most ideal hydrophilic surface for spin-coating semi-branched poly(glycidol) due to improved wettability and increased hydrophilic interactions between the silicon surface and the hydroxyl groups of poly(glycidol) (see Figure IV-2). The two most important parameters in determining spin-coat film thickness are viscosity and spin speed. Therefore, we varied the viscosity of the PG spin-coat solution by preparing concentrations of 1,2,3 and 5% PG and monitored the resultant film thickness by ellipsometry to produce Figure IV-2 left-hand plot. We found that the 5% PG solution gave us the best uniformity, so we proceeded

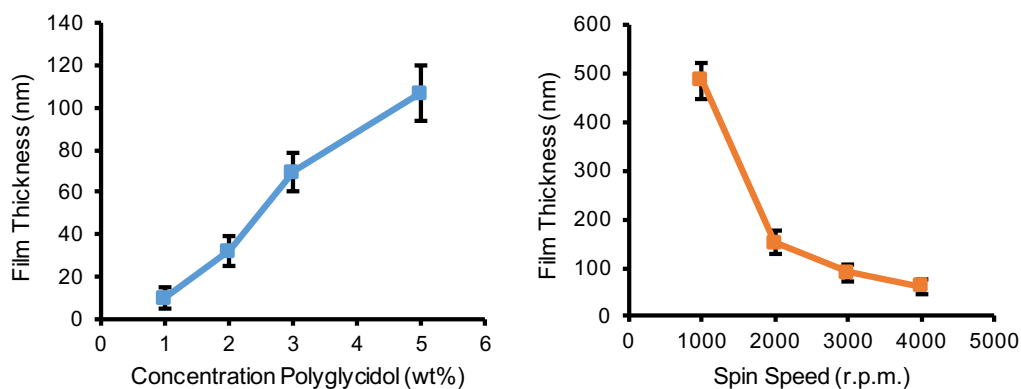


Figure IV-2. Left plot represents dry film thickness resulting from various concentrations of semi-branched polyglycidol (wt% in DI water) after spin-coating 50  $\mu$ L on to piranha clean 10 x 10 mm silicon chips at 3000 rpm for 60 s, followed by drying overnight. The bottom plot represents film thickness as a result of spin-coating 50  $\mu$ L of 5 wt% polyglycidol in DI water onto clean silicon at varying spin speeds (1000-4000 r.p.m. for 60 s) followed by drying overnight. Film thickness was measured by ellipsometry, and all experiments were performed in triplicate. Error bars represent standard deviation (n=3).

to test at varying spin speeds from 1000-5000 r.p.m. at that concentration. The resulting data in the right-hand plot of Figure IV-2 indicated that a film thickness in the 100-150 nm range could be obtained with 2000 and 3000 r.p.m. However, the 3000 r.p.m. was chosen as the optimal spin-coat speed due to better uniformity.

A polymer resist can undergo chain scission or a crosslinking chemical change when electron beam energy is deposited by irradiation.<sup>16-15</sup> It has also been shown that linear polyethylene glycol polymers indicate crosslinking reactive doses in the range of 20-120  $\mu\text{C}/\text{cm}^2$ .<sup>13-14</sup> Since poly(glycidol) has a similar polyether backbone, we generated square dose testing patterns in the linear range of 1-400  $\mu\text{C}/\text{cm}^2$  as a starting point in order to find the minimum dose required to generate well-defined structures as detected by atomic force microscopy (AFM). After exposure, the chips were developed briefly in  $\text{H}_2\text{O}$ , which washed away any non-crosslinked polymer material, leaving behind raised features of cross-linked poly(glycidol) as represented in Figure IV-3. As anticipated, the cross-linked poly(glycidol) exhibited a dose-dependent feature height which could be measured by AFM.

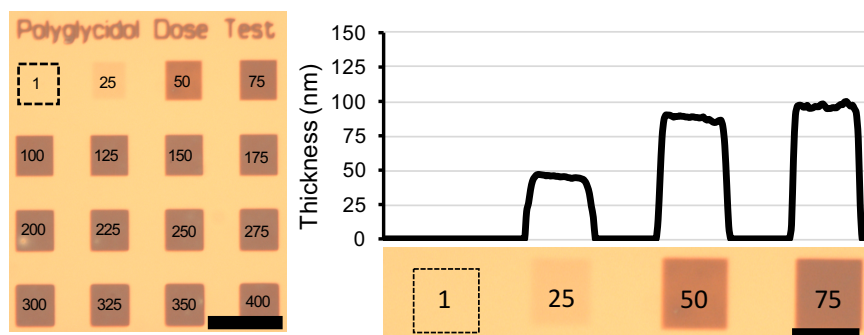


Figure IV-3. Left: Bright field microscopy image of semi-branched polyglycidol dose test from 1-400  $\mu\text{C}/\text{cm}^2$  captured at 20 x magnification. black bar represents 20  $\mu\text{m}$ . Right: Atomic force microscopy plot (top) which indicates crosslinked polyglycidol film thickness post-development at varying electron beam irradiation doses ( $\mu\text{C}/\text{cm}^2$ ). Corresponding dose squares (bottom) were captured with a bright field microscope equipped with a camera, and the black bar represents 10  $\mu\text{m}$ .

The resulting heights for  $25 \mu\text{C}/\text{cm}^2$  was 48 nm,  $50 \mu\text{C}/\text{cm}^2$  was 85 nm, and  $75 \mu\text{C}/\text{cm}^2$  was 98 nm. Additionally, we were able to pattern well-defined micron features from doses up to  $300 \mu\text{C}/\text{cm}^2$  as exemplified by the AFM image in Figure IV-4. A Vanderbilt logo was patterned by dots in 400 nm spacing at  $300 \mu\text{C}/\text{cm}^2$  and examined under AFM to measure its height and surface features. Interestingly, we found an initial dense bottom layer of crosslinked poly(glycidol) approximately 110 nm high, and on top there were 40-50 nm spikes. We attribute this “stalagmite effect” to the movement of secondary electrons outward from the resist, generating crosslinking along the way with the density of crosslink-able polymer material diminishing near the surface of the resist. Presence of these spikes may indicate potential utility for on-chip single cell immobilization or anti-fouling applications.<sup>34-36</sup> Other research groups

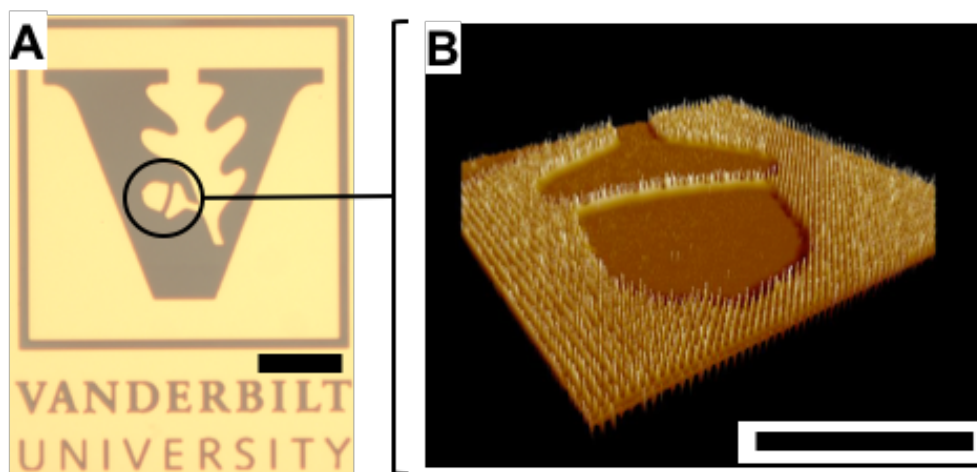


Figure IV-4. A) Vanderbilt University logo patterned by electron beam lithography after spin-coating an aqueous solution of 5 wt% semi-branched poly(glycidol), irradiated at  $300 \mu\text{C}/\text{cm}^2$  on silicon, and imaged at 50x magnification by bright field microscopy. B) Atomic Force Microscopy image of acorn showing the raised features from the silicon surface. The black scale bars represent 20 microns. Permission to use logo was granted by the Vanderbilt University Trademark Licensing Office.

require up to 10 times higher accelerations voltages to obtain crosslinking of resists such as with silk (100 keV) or polyethylene glycol (30 keV).<sup>14,30</sup> We hypothesize that the requirement for less acceleration voltage to reach crosslinking may be attributed to the semi-branched structure of poly(glycidol) compared to other more linear chemical resists.

### **Optimization of enzyme cascade in free solution**

Before attempting to spin coat and perform EBL with enzymes and enzyme-loaded nanogels, we first optimized an enzymatic cascade reaction known for detection of lactose in free solution as our proof-of-concept. Enzyme cascade reactions have long been utilized in signal amplification strategies for colorimetric detection of biologically relevant analytes.<sup>37</sup> The final indicator step is key in detection of any enzyme cascade.<sup>38</sup> In our case, the colorimetric indicator for horseradish peroxidase (HRP), o-phenylenediamine (OPD), was chosen due to its strong literature precedence, reliability, along with cost-effectiveness compared to alternatives such as Amplex Red or 3,3',5,5'-Tetramethylbenzidine (TMB). Another important parameter we established was the starting concentration of free enzyme in solution to determine what concentration to use during spin-coating. Walde and coworkers presented a set of enzymes for cascade reactions in free solution,<sup>39</sup> which we optimized by varying the ratios of GAL, GOX and HRP concentrations (1:1:1, 1:2:1, and 3:2:1). Results of this study can be found in Figure IV-5. One can note the significant gain in signal (3.1 au) by using the enzyme ratio 3:2:1 over all others tested (2.7 and 2.4 au for 1:2:3 and 1:1:1, respectively). This can be explained by the kinetics of GAL being much slower in specific activity (12.1 U/mg) compared with GOX (281 U/mg) and HRP (179 U/mg). Note: Unit is defined as 1  $\mu$ mol substrate turnover per min. When we increased the available enzyme for the slow step,

the overall kinetics of the cascade improved, and moving forward we used the 3:2:1 ratio in spin coat prep solutions for NG-EZ and EZ chips.

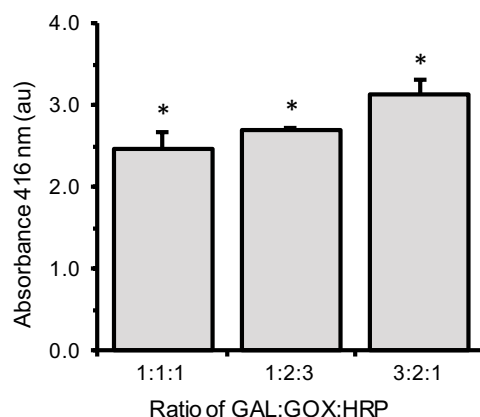


Figure IV-5. Relative absorbance measurements of 2,3-diaminophenazine at 416 nm after 30 min incubations in three different enzyme ratio concentrations (equivalent to 5  $\mu$ m) in free solution. Error bars are standard deviation (n=3), and asterisk (\*) denotes significance ( $p < 0.05$ ) between all sets as determined via ANOVA single factor analysis.

### Enzyme immobilization with nanogels

It has been described that nanoparticles improve sensitivity of colorimetric biosensor designs by covalent attachment, adsorption and encapsulation.<sup>40</sup> For example, gold-modified nanoparticles have been used for detection of selective polynucleotides that generate a colorimetric detection dependent on polymeric network spacing.<sup>41</sup> Enzyme cascade reactions also benefit from well-defined spatial arrangements so that bio sensing co-factors interact with target enzymes. Maynard and coworkers demonstrated this in the aforementioned immobilized 3-D arrangement of spatially separated and encapsulated enzymes within unique compartments of a single hydrogel structure which lead to a retained enzyme cascade activity.<sup>14</sup> However it requires multiple synthetic and EBL fabrication steps. Our thought was to employ a one-pot process with three unique enzyme-

encapsulated nanogels to spatially separate and orient the immobilization of enzymes on a surface for implementation towards reusable biosensing. As proof of concept, we independently loaded  $\beta$ -galactosidase, glucose oxidase and horseradish peroxidase into poly(glycidol) nanogels using a developed one-pot method, and resultant average loading was determined to be 20.7 wt% (83 %

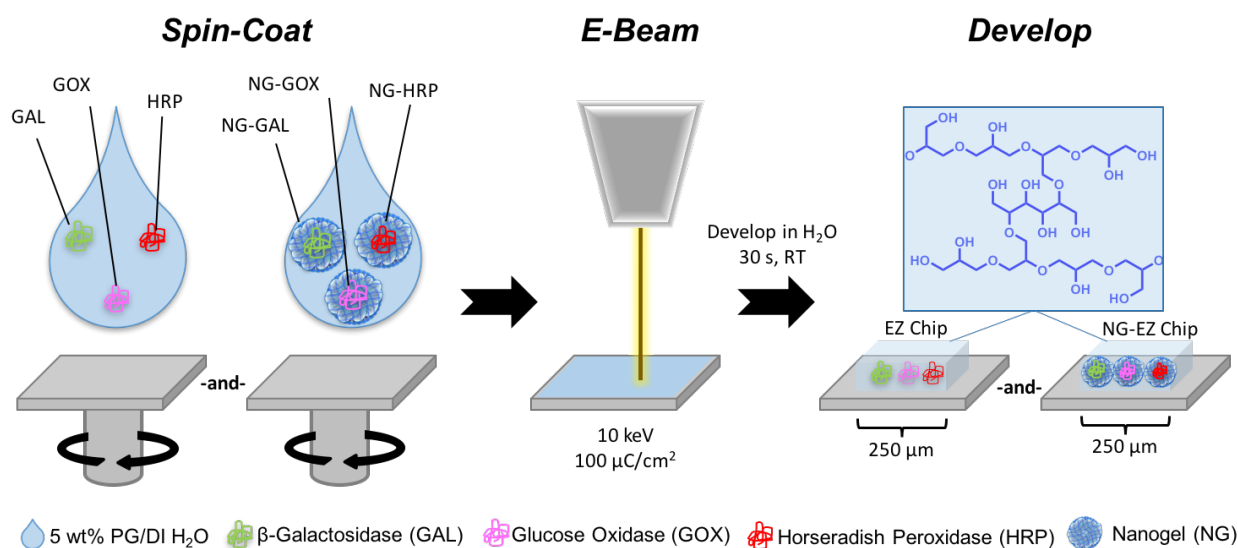


Figure IV-6. Devices were fabricated from spin-coating nanogels (NG) loaded with enzyme (NG-EZ) or free enzyme (EZ) within an aqueous solution of 5% semi-branched poly(glycidol) onto piranha-cleaned silicon chips. Electron beam lithography (EBL) was employed to cross-link poly(glycidol) in user-defined 250  $\mu\text{m}$  square patterns. Following EBL, chips were developed in water to wash away non-crosslinked polymer material to yield 3-D hydrogel structures of immobilized enzymes.

efficient) which agrees with previous work with nanogels.<sup>27</sup> The nanogel-enzymes were spin coated as shown in Figure IV-6 at a ratio 3:2:1 equivalences to free enzyme because it was determined as the optimal ratio in free solution, as described above. As a negative control, we built and tested immobilized enzyme cascade chips without nanogels to examine if there was any difference in activity. All chips were crosslinked similarly by EBL at 100  $\mu\text{C}/\text{cm}^2$  (10 keV), and the non-crosslinked material was easily removed by developing in water. The enzyme cascade activity was

assayed by adding 3 mM lactose with 5 mM o-phenylenediamine on top of the finished chip and measuring the colorimetric signal at 416 nm by UV-vis spectroscopy. Production of 2,3-diaminophenazine was measured in all samples after 2 h incubation at room temperature. All test measurements were blanked with solutions of 5 mM o-phenylenediamine and 3 mM lactose without enzyme. One major advantage of enzyme immobilization is the reusability feature.<sup>42-45</sup> To investigate reusability in our platform, we washed away the chips three times with H<sub>2</sub>O and re-applied the lactose/o-phenylenediamine mixture to measure the chip response 10 times over the

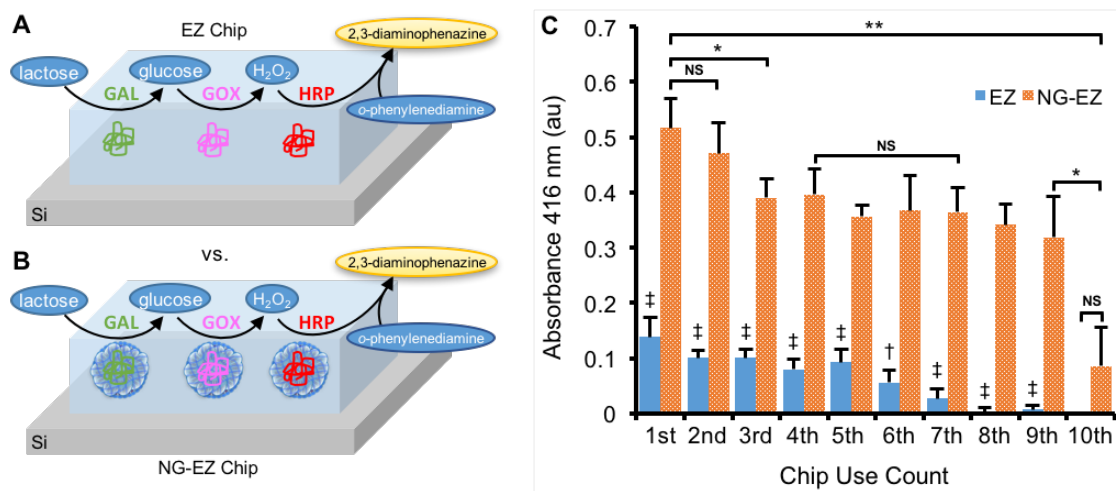


Figure IV-7. A) Schematic of lactose detection via enzyme cascade free enzyme device (EZ Chip) and B) enzyme-nanogel device (NG-EZ Chip). C) Results of enzyme cascade bioactivities after each use of chip are plotted as relative absorbance measurements of 2,3-diaminophenazine at 416 nm after each EZ and NG-EZ use count. Counts 1-6 were completed over a three-day time-period, while 7-10 were after 30 days in storage at 4 °C. Error bars indicate standard deviation of triplicate experiments. No statistical significance (NS) was found between NG-EZ data counts 1<sup>st</sup> through 2<sup>nd</sup>, 3<sup>rd</sup> through 7<sup>th</sup> and the 10<sup>th</sup> count (NG-EZ vs. EZ). Asterisks indicate statistical significance; a single asterisk (\*) at p-value < 0.05 and a double asterisk (\*\*) at p-value < 0.01 between NG-EZ data as determined via student's two-tailed t-test assuming equal variance. The daggers indicate statistical significance between EZ and NG-EZ data sets; a single dagger (†) denotes p < 0.05 and double dagger (‡) denotes p < 0.001.



course of 1 month. The results in Figure IV-7 indicate that the nanogel-enzyme chips continued to produce a colorimetric output after 9 uses and after 30 days with no significant change in signal from counts 3 through 7. In contrast, the chips without nanogel incorporation produced 5-fold lower signal intensity and exhibited failure (no response) after 7 uses. In all counts (with exception for the 6<sup>th</sup> and 10<sup>th</sup>), the relative EZ chip signal was significantly lower ( $p < 0.001$ ) signal than the NG-EZ chip. It is well-known that entrapment of enzyme can improve mechanical stability and minimize enzyme leaching.<sup>46</sup> In our experiments, it was observed that the nanogels help regulate the spatial orientation of the enzyme cascade such that a more optimal enzyme cascade reaction can be realized for reusable applications.

### Conclusion

In conclusion, semi-branched poly(glycidol) was investigated for the immobilization of a three-enzyme cascade of  $\beta$ -galactosidase (GAL), glucose oxygenase (GOX), and horseradish peroxidase (HRP) with and without polyglycidol nanogel pre-encapsulation for biorecognition of lactose. After incubation with o-phenylenediamine and lactose, the developed nanogel-enzyme microstructures resulted in a significantly ( $p < 0.001$ ) higher signal output and exhibited bioactivity after 9 uses and 30 days. The demonstrated bioactivity suggests that nanogel-mediated spatial orientation can be achieved with a single EBL fabrication step and without harsh synthetic chemical modifications.

## Experimental

### Materials

Poly(glycidol allylglycidyl ether) (pGLY/AGE, 20% AGE) was synthesized as previously reported.<sup>27</sup> Silicon wafers (4", 55 chips/wafer, 10mm x 10mm diced) were purchased from Ted Pella, Inc. (Redding, CA). Glucose oxidase from *Aspergillus niger* (GOX, 281 U/mg) was purchased from MP Biomedicals, LLC (Solon, OH).  $\beta$ -galactosidase from *Aspergillus oryzae* (GAL, 12.1 U/mg), peroxidase from horseradish (HRP, 179 U/mg), lactose, o-phenylenediamine (OPD), cholesterol, poly(ethylene glycol) dithiol (PEG dithiol, M<sub>n</sub> 1000 gmol<sup>-1</sup>), allyl glycidyl ether (AGE), tin(II)triflate (Sn(OTf)<sub>2</sub>) and glycidol (GLY) were purchased from Sigma Aldrich, USA. GLY was purified *via* Kugelrohr distillation before use. L- $\alpha$ -phosphatidylcholine (Egg-PC) was purchased from Avanti Polar Lipids (Alabaster, AL). 2,2-Azobis(2-methyl-N-(2-hydroxyethyl)propionamide (VA-086, 98%) was purchased from Wako Chemicals USA, Inc. and used without further purification. Phosphate buffered saline (PBS, 1X, pH 7.4) was obtained from Gibco by Life Technologies. Dialysis tubing SnakeSkin® (molecular weight cutoff (MWCO): 10 kDa and 1 kDa, 16 mm dry I.D) were purchased from Spectrum Laboratories, Inc. (Rancho Dominguez, CA). All other solvents or reagents were purchased from Sigma Aldrich unless mentioned otherwise and used as received.

### Characterization

Film thickness of spin-coated silicon chips were characterized using a JA Woollam M-2000VI Spectroscopic Ellipsometer. Bright field microscopy was used to verify electron beam patterning after development. <sup>1</sup>H and <sup>13</sup>C NMR spectra of poly(glycidol allylglycidyl ether), poly(GLY/AGE) were obtained from a Bruker AV400 Fourier transform spectrometer with deuterated methanol as

solvent. Gel permeation chromatography-size exclusion chromatography (GPC-SEC) of polymers was performed in DMF (with 1 mg/mL LiBr) at 45°C with a flow rate of 1.0 mL/min (Waters 1525 binary HPLC pump); columns: 7.8 x 300 mm; Styragel HR 5 DMF, Styragel HR 4E, and Styragel HR 3: molecular weight range 50,000 to 4x10<sup>6</sup>, 50 to 100,000, and 500 to 30,000 g/mol. GPC detection was accomplished using a Waters 2414 refractive index detector at 410 nm. Molecular weights ( $M_n$  and  $M_w$ ) and polydispersity were determined from PEG standards provided by Varian. The average size and size distribution (polydispersity index, PDI) of nanogels were analyzed *via* dynamic light scattering (DLS) on a Malvern Zetasizer Nano ZS apparatus with Malvern Instruments DTS software (v.6.0d1) (Malvern Instruments, UK). The mean hydrodynamic diameter ( $d_h$ ) was computed from the average intensity of 15 measurements of scattered light using Malvern software based on Brownian motion and the Stokes-Einstein equation. Enzyme loading was quantified using the microplate procedure of the Pierce® BCA Protein Assay Kit (Pierce Biotechnology, Rockford, IL) and a Synergy HT Microtiter Plate reader (BIO-TEK) at 562 nm. Enzyme cascade absorbance response was measured at 416 nm.

### **Synthesis of semi-branched poly(glycidol) homopolymer**

Synthesis of poly(glycidol) (pGLY) was performed *via* cationic ring-opening polymerization as previously reported in our group with minor changes.<sup>47-48</sup> Briefly, isoamyl alcohol (72.7  $\mu$ L, 0.67 mmol, 0.00035 eq) and Tin(II)triflate (7.9 mg, 19  $\mu$ mol, 1 eq) were allowed to stir in a sealed, flame-dried, N<sub>2</sub>-purged 25-mL round bottom flask at 0 °C for 30 minutes. Then, distilled GLY (3.25 mL, 49 mmol) was slowly added dropwise *via* syringe over the course of 45 minutes. The flask was stirred for 16 h or until stir bar was completely impeded to yield a translucent viscous product. The product was purified by dissolving first in 3 mL methanol and precipitating dropwise

over a 1L solution of vigorously stirring ethyl acetate at room temperature. The polymer was allowed to settle to the bottom so ethyl acetate could be easily decanted to yield a clear viscous product. The resulting pGLY was transferred to a 6 DRAM using methanol and dried *in vacuo* to remove all organics. Yield 3.41 g (85%), GPC  $M_n = 2828$  Da using PEG standards,  $M_w/M_n = 1.57$ .  $^1\text{H-NMR}$  (400 MHz, MeOD)  $\delta$  : 3.31-3.94 (6H), 0.91-0.92 (6H). Inverse-gated  $^{13}\text{C-NMR}$  (150 MHz, MeOD)  $\delta$  : 83.12, 81.34, 79.78, 73.88, 72.15, 70.59, 64.31, 63.20, 62.51, 61.21, 42.58, 39.54, 26.14, 26.03, 25.74, 22.99.

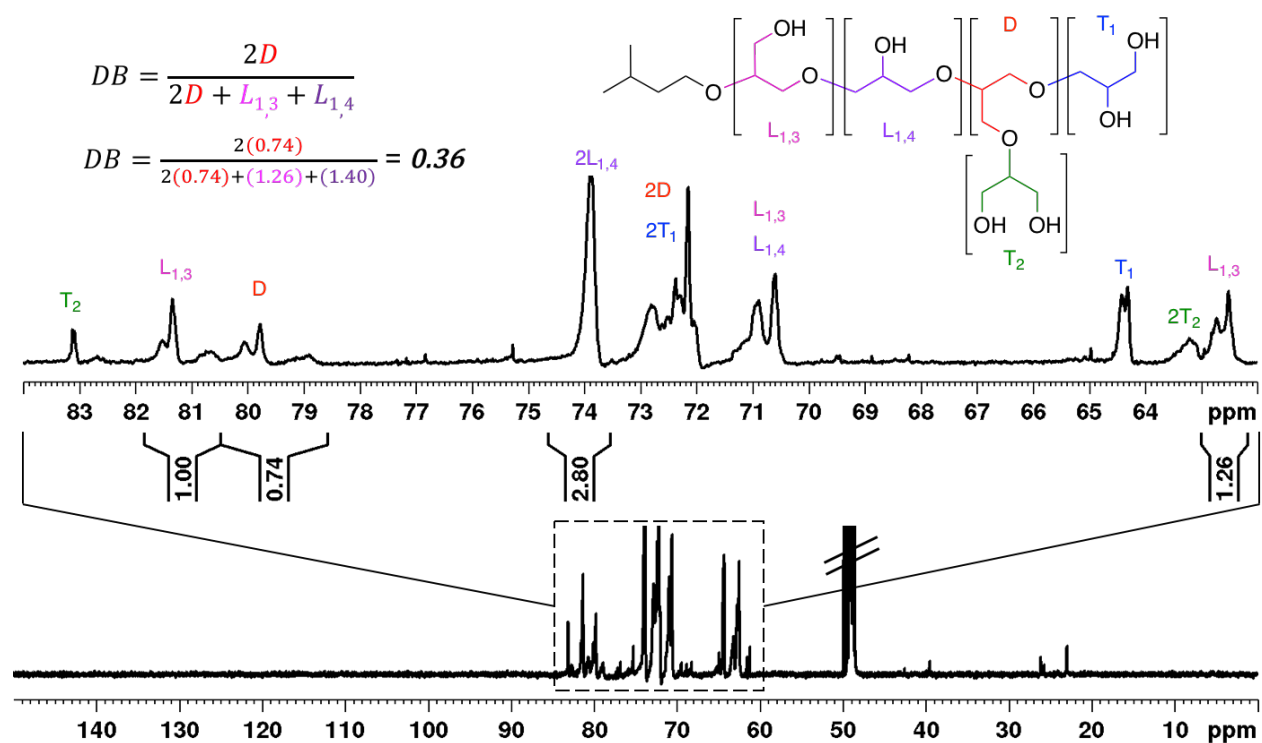


Figure IV-8. Full labeled inverse-gated  $^{13}\text{C-NMR}$  (600 MHz) spectrum of semi-branched polyglycidol homopolymer in deuterated methanol with inset (top) of 62-84 ppm region. Relaxation time ( $D_i$ ) was 10 sec, and number of scans (NS) was 1024. Degree of branching was calculated as 0.36 (semi-branched) based on relative integration values of dendritic units (D) compared with linear backbone units ( $L_{1,3}$ ,  $L_{1,4}$ ) as described in the literature.<sup>49 50 51 52</sup>

**Synthesis of enzyme-loaded nanogels** Synthesis of nanogels (NG) from semi-branched poly(glycidol allylglycidyl) ether (pGLY-AGE, 20% AGE)) was adapted from our previously reported one-pot method with minor changes.<sup>27</sup> Briefly, a solution of chloroform (1 mL) with egg-PC (100 mg, 0.13 mmol, 5 eq) and cholesterol (10 mg, 13  $\mu$ mol, 1 mol eq) was prepared in a 6 DRAM vial and vortexed well. Chloroform was then evaporated *via* nitrogen stream, and lipid mix was dried *in vacuo* overnight to yield a thin off-white film in the vial. A solution of pGLY/AGE polymer (90 mg, 0.20 mmol, 8 eq), 1 kDa PEG dithiol (102 mg, 0.10 mmol, 4 eq), VA-086 (29 mg, 0.10 mmol, 4 eq) with 25 wt% by mass of either  $\beta$ -galactosidase (0.21  $\mu$ mol, 0.01 eq), glucose oxidase (1.25  $\mu$ mol, 0.05 eq), or horseradish peroxidase (2.36  $\mu$ mol, 0.1 eq) were combined with 2 mL DI H<sub>2</sub>O before adding directly to the vial of dry phospholipids. The aqueous solution containing the pre-nanogel components was used to hydrate the film through 5 alternating cycles of 30 s vortexing followed by 1 min rest at room temperature to allow for complete formation of multilamellar vesicles swelled with pre-gel components. The pre-nanogel vesicles were then extruded through 0.8, 0.2 and 0.1  $\mu$ m polycarbonate membranes (Whatman, Piscataway, NJ, USA) 5 times each using an Avanti® Mini-Extruder (Avanti Polar Lipids, Inc., Alabaster, AL) to produce vesicles in the 100-200 nm dimension.<sup>53,54,55</sup> The resulting MLVs were diluted 3-fold to prevent macro scale gelation, purified by dialysis with 10 kDa MWCO Snakeskin tubing in DI water for 3 hours, transferred to a 6 DRAM vial, and irradiated under long UV light (365 nm, 6W) for 10 min. Small effervesces confirmed crosslinking.<sup>27</sup> Dry NG-enzyme yield was 50-87% after lyophilizing and stored at 0°C until use. Resulting enzyme load was measured five times at 562 nm following the microplate procedure of the Pierce® BCA Protein Assay Kit (Pierce Biotechnology, Rockford, IL). Enzyme weight percent of each nanogel-enzyme species was determined from standard curves

(0.001-1.0 mg/mL) of each enzyme (GAL, GOX, and HRP), and loading efficiencies were calculated according to the following equation:

$$\frac{\text{Enzyme Wt\%}_{\text{Measured}}}{\text{Enzyme Wt\%}_{\text{Feed}}} \times 100 = \text{Loading Efficiency (\%)}$$

### **Optimization of free enzyme cascade in solution**

To determine the optimal enzyme ratio for cascade reactions, 3 mL solutions of GAL, GOX and HRP in ratios of 1:1:1, 1:2:3, and 3:2:1 (equivalent to 5  $\mu$ M) were prepared in DI water at RT. Addition of o-phenylenediamine (5 mM) with lactose (3 mM) resulted in the evolution of yellow 2,3-diaminophenazine after 30 min, which was measured in 1 mL aliquots *via* UV-vis in a 24-well plate BioTek plate reader at 416 nm.

### **Coating of Si chips**

Silicon chips were cleaned by a gentle stream of methanol for 5 seconds, dried, then immersed in freshly prepared piranha solution (3:1 H<sub>2</sub>SO<sub>4</sub>/30%H<sub>2</sub>O<sub>2</sub>. *Caution! Piranha solution is a strong oxidizing agent and can react violently with organic matter.*) for 20 min maintained at 75 °C. Chips were subsequently rinsed 5 times with 200 mL DI water until the pH was neutral by litmus paper, and chips were dried under a stream of air for 20 min. Next, the cleaned chips were immediately spin coated (500 r.p.m., 5 s; 1000 r.p.m., 5 s; 2000 r.p.m., 5 s; 3000 r.p.m. for 10 s) using a Laurell WS400B Spin Coater (Laurell Technologies Corporation, North Wales, PA) with 50  $\mu$ L spin coat solutions. Poly(glycidol) (pGLY) solution consisted of 5 wt% semi-branched poly(glycidol) in DI H<sub>2</sub>O. The free enzyme solution (for negative control) was prepared with free GAL, GOX, and HRP at 15, 10, and 5  $\mu$ M, respectively in pGLY solution. The nanogel-enzyme spin coat solution (NG-

EZ) was prepared with the same equivalencies as free EZ, based on measured nanogel enzyme loading. All spin coat solutions were prepared in 5 wt% poly-GLY/DI H<sub>2</sub>O. Chips were dried overnight, and dry film thickness was characterized by ellipsometry as described in the characterization section.

### **Electron beam lithography**

Patterns for electron beam lithography were designed and fabricated using a Raith eLiNE (Software Version 5.0) instrument. Square dose test patterns were written in a linear range of 1-400  $\mu\text{C}/\text{cm}^2$  operating at 10 keV acceleration voltage. Enzyme cascade device squares were patterned in 250 x 250  $\mu\text{m}$  dimensions at 100  $\mu\text{C}/\text{cm}^2$ , beam current 150-180 pA with a sub-10 nm beam diameter, and 7-8 mm/s beam write speeds. Typical write time was ~11 minutes. Immediately after EBL, all chips were submerged in 5 mL DI H<sub>2</sub>O for 30 s, followed by drying under gentle stream of air. After development, the minimum irradiation dose needed for crosslinking poly(glycidol) was determined by visual inspection with an inverted bright-field microscope.

### **Assay of enzyme activity**

The immobilized enzyme cascade activity was assayed for each chip by adding 100  $\mu\text{L}$  solutions of lactose (3 mM) with o-phenylenediamine (5 mM) in DI H<sub>2</sub>O to freshly prepared chip surfaces at room temperature and measuring the absorbance of 2,3-diaminophenazine at 416 nm after incubation of 2 h using a Biotek plate reader. Testing of re-usability was conducted by washing chips with 1 mL H<sub>2</sub>O three times followed by re-incubation with lactose and o-phenylenediamine

at the same conditions as above. All tests were performed in triplicate and blanked with control poly(glycidol)-surfaces without enzyme.

### **Atomic force microscopy**

Characterization by AFM of generated patterns were performed on a Bruker Dimension Icon® Atomic Force Microscope in peak force soft tapping mode equipped with Nanoscope version 9.1 software. The scan size was 20 µm with a scan rate of 1.0 Hz, 64 samples per line and a peak force set point of 6.38 mV.

### **Statistics**

All data analysis and statistics were completed with the Data Analysis Tool of Microsoft Excel 2016 for Mac.

### **References**

1. Sassolas, A.; Blum, L. J.; Leca-Bouvier, B. D., Immobilization strategies to develop enzymatic biosensors. *Biotechnology Advances* **2012**, *30* (3), 489-511.
2. Lee, G. A.; Paul, M. A.; Empie, M., Enzyme Immobilization Technology for Specialty Chemical Production. *Journal of the American Oil Chemists Society* **1987**, *64* (5), 653-653.
3. Hagiwara, T.; Hirata, H.; Uchiyama, S., Poly(p-maleimidostyrene) coated cross-linked polystyrene beads as novel ultrasonic irradiation resistant enzyme immobilization materials - Applications for biosensors and bioreactors. *Reactive & Functional Polymers* **2008**, *68* (7), 1132-1136.



4. Huang, X. L.; Walsh, M. K.; Swaisgood, H. E., Simultaneous isolation and immobilization of streptavidin-beta-galactosidase: Some kinetic characteristics of the immobilized enzyme and regeneration of bioreactors. *Enzyme and Microbial Technology* **1996**, *19* (5), 378-383.
5. Kuchler, A.; Yoshimoto, M.; Luginbuhl, S.; Mavelli, F.; Walde, P., Enzymatic reactions in confined environments. *Nature Nanotechnology* **2016**, *11* (5), 409-20.
6. Kim, J.; Grate, J. W.; Wang, P., Nanostructures for enzyme stabilization. *Chemical Engineering Science* **2006**, *61* (3), 1017-1026.
7. Lee, K. B.; Lim, J. H.; Mirkin, C. A., Protein nanostructures formed via direct-write dip-pen nanolithography. *Journal of the American Chemical Society* **2003**, *125* (19), 5588-9.
8. Xing, C.; Zheng, Z.; Zhang, B.; Tang, J., Nanoscale patterning of multicomponent proteins by bias-assisted atomic force microscopy nanolithography. *Chemphyschem* **2011**, *12* (7), 1262-5.
9. Schnauber, P.; Schmidt, R.; Kaganskiy, A.; Heuser, T.; Gschrey, M.; Rodt, S.; Reitzenstein, S., Using low-contrast negative-tone PMMA at cryogenic temperatures for 3D electron beam lithography. *Nanotechnology* **2016**, *27* (19), 195301.
10. Lau, U. Y.; Saxer, S. S.; Lee, J.; Bat, E.; Maynard, H. D., Direct Write Protein Patterns for Multiplexed Cytokine Detection from Live Cells Using Electron Beam Lithography. *ACS Nano* **2016**, *10* (1), 723-9.
11. Zhang, J.; Cao, K.; Wang, X. S.; Cui, B., Metal-carbonyl organometallic polymers, PFpP, as resists for high-resolution positive and negative electron beam lithography. *Chemical Communications* **2015**, *51* (99), 17592-5.
12. Rundqvist, J.; Hoh, J. H.; Haviland, D. B., Directed immobilization of protein-coated nanospheres to nanometer-scale patterns fabricated by electron beam lithography of poly(ethylene glycol) self-assembled monolayers. *Langmuir* **2006**, *22* (11), 5100-7.

13. Kolodziej, C. M.; Maynard, H. D., Electron-Beam Lithography for Patterning Biomolecules at the Micron and Nanometer Scale. *Chemistry of Materials* **2012**, *24* (5), 774-780.
14. Mancini, R. J.; Paluck, S. J.; Bat, E.; Maynard, H. D., Encapsulated Hydrogels by E-beam Lithography and Their Use in Enzyme Cascade Reactions. *Langmuir* **2016**, *32* (16), 4043-4051.
15. Bae, M.; Divan, R.; Suthar, K. J.; Mancini, D. C.; Gemeinhart, R. A., Fabrication of Poly(ethylene glycol) Hydrogel Structures for Pharmaceutical Applications using Electron beam and Optical Lithography. *Journal of Vacuum Science & Technology B, Nanotechnology and Microelectronics: Materials, Processing, Measurement, and Phenomena* **2010**, *28* (6), C6P24-C6P29.
16. Wang, Y.; Firlar, E.; Dai, X. G.; Libera, M., Poly(ethylene glycol) as a biointeractive electron-beam resist. *Journal of Polymer Science Part B-Polymer Physics* **2013**, *51* (21), 1543-1554.
17. Dagar, K.; Pundir, C. S., An improved amperometric L-lactate biosensor based on covalent immobilization of microbial lactate oxidase onto carboxylated multiwalled carbon nanotubes/copper nanoparticles/polyaniline modified pencil graphite electrode. *Enzyme and Microbial Technology* **2017**, *96*, 177-186.
18. Krsko, P.; Kaplan, J. B.; Libera, M., Spatially controlled bacterial adhesion using surface-patterned poly(ethylene glycol) hydrogels. *Acta Biomaterialia* **2009**, *5* (2), 589-96.
19. Zhang, M. L.; Huang, J. Z.; Cui, W. W.; Pang, W.; Zhang, H.; Zhang, D. H.; Duan, X. X., Kinetic studies of microfabricated biosensors using local adsorption strategy. *Biosensors and Bioelectronics* **2015**, *74*, 8-15.

20. Bollella, P.; Schulz, C.; Favero, G.; Mazzei, F.; Ludwig, R.; Gorton, L.; Antiochia, R., Green Synthesis and Characterization of Gold and Silver Nanoparticles and their Application for Development of a Third Generation Lactose Biosensor. *Electroanalysis* **2017**, *29* (1), 77-86.
21. Bhakta, S. A.; Evans, E.; Benavidez, T. E.; Garcia, C. D., Protein adsorption onto nanomaterials for the development of biosensors and analytical devices: A review. *Analytica Chimica Acta* **2015**, *872*, 7-25.
22. Singh, S.; Solanki, P. R.; Pandey, M. K.; Malhotra, B. D., Covalent immobilization of cholesterol esterase and cholesterol oxidase on polyaniline films for application to cholesterol biosensor. *Analytica Chimica Acta* **2006**, *568* (1-2), 126-32.
23. Al-Lolage, F. A.; Meneghello, M.; Ma, S.; Ludwig, R.; Bartlett, P. N., A Flexible Method for the Stable, Covalent Immobilization of Enzymes at Electrode Surfaces. *ChemElectroChem* **2017**, *4* (6), 1528-1534.
24. Mohiuddin, M.; Arbain, D.; Islam, A. K.; Ahmad, M. S.; Ahmad, M. N., Alpha-Glucosidase Enzyme Biosensor for the Electrochemical Measurement of Antidiabetic Potential of Medicinal Plants. *Nanoscale Research Letters* **2016**, *11* (1), 95.
25. Calabria, D.; Caliceti, C.; Zangheri, M.; Mirasoli, M.; Simoni, P.; Roda, A., Smartphone-based enzymatic biosensor for oral fluid L-lactate detection in one minute using confined multilayer paper reflectometry. *Biosensors and Bioelectronics* **2017**, *94*, 124-130.
26. Bat, E.; Lee, J.; Lau, U. Y.; Maynard, H. D., Trehalose glycopolymer resists allow direct writing of protein patterns by electron-beam lithography. *Nature Communications* **2015**, *6*, 6654.
27. Lockhart, J. N.; Beezer, D. B.; Stevens, D. M.; Spears, B. R.; Harth, E., One-pot polyglycidol nanogels via liposome master templates for dual drug delivery. *Journal of Controlled Release* **2016**, *244*, Part B, 366-374.

28. Datta, S.; Christena, L. R.; Rajaram, Y. R., Enzyme immobilization: an overview on techniques and support materials. *3 Biotech* **2013**, *3* (1), 1-9.
29. Gosecki, M.; Gadzinowski, M.; Gosecka, M.; Basinska, T.; Slomkowski, S., Polyglycidol, Its Derivatives, and Polyglycidol-Containing Copolymers—Synthesis and Medical Applications. *Polymers* **2016**, *8* (6), 227.
30. Kim, S.; Marelli, B.; Brenckle, M. A.; Mitropoulos, A. N.; Gil, E. S.; Tsioris, K.; Tao, H.; Kaplan, D. L.; Omenetto, F. G., All-water-based electron-beam lithography using silk as a resist. *Nature Nanotechnology* **2014**, *9* (4), 306-10.
31. Haryanto; Singh, D.; Huh, P. H.; Kim, S. C., Hyperbranched poly(glycidol)/poly(ethylene oxide) crosslinked hydrogel for tissue engineering scaffold using e-beams. *Journal of Biomedical Materials Research Part A* **2016**, *104* (1), 48-56.
32. Celler, G. K.; Barr, D. L.; Rosamilia, J. M., Etching of silicon by the RCA Standard Clean 1. *Electrochemical and Solid State Letters* **2000**, *3* (1), 47-49.
33. de Vos, W. M.; Cattoz, B.; Avery, M. P.; Cosgrove, T.; Prescott, S. W., Adsorption and Surfactant-Mediated Desorption of Poly(vinylpyrrolidone) on Plasma- and Piranha-Cleaned Silica Surfaces. *Langmuir* **2014**, *30* (28), 8425-8431.
34. Arai, F.; Ng, C.; Maruyama, H.; Ichikawa, A.; El-Shimy, H.; Fukuda, T., On chip single-cell separation and immobilization using optical tweezers and thermosensitive hydrogel. *Lab on a Chip* **2005**, *5* (12), 1399-1403.
35. Zhu, Z.; Frey, O.; Ottoz, D. S.; Rudolf, F.; Hierlemann, A., Microfluidic single-cell cultivation chip with controllable immobilization and selective release of yeast cells. *Lab on a Chip* **2012**, *12* (5), 906-915.

36. Moore, E.; Delalat, B.; Vasani, R.; Thissen, H.; Voelcker, N. H., Patterning and Biofunctionalization of Antifouling Hyperbranched Polyglycerol Coatings. *Biomacromolecules* **2014**, *15* (7), 2735-2743.
37. Gao, Z.; Hou, L.; Xu, M.; Tang, D., Enhanced colorimetric immunoassay accompanying with enzyme cascade amplification strategy for ultrasensitive detection of low-abundance protein. *Scientific Reports* **2014**, *4*, 3966.
38. Mize, P. D.; Hoke, R. A.; Linn, C. P.; Reardon, J. E.; Schulte, T. H., Dual-enzyme cascade-an amplified method for the detection of alkaline phosphatase. *Analytical Biochemistry* **1989**, *179* (2), 229-35.
39. Fornera, S.; Yazawa, K.; Walde, P., Spectrophotometric quantification of lactose in solution with a peroxidase-based enzymatic cascade reaction system. *Analytical and Bioanalytical Chemistry* **2011**, *401* (7), 2307-2310.
40. Lei, J. P.; Ju, H. X., Signal amplification using functional nanomaterials for biosensing. *Chemical Society Reviews* **2012**, *41* (6), 2122-2134.
41. Elghanian, R.; Storhoff, J. J.; Mucic, R. C.; Letsinger, R. L.; Mirkin, C. A., Selective colorimetric detection of polynucleotides based on the distance-dependent optical properties of gold nanoparticles. *Science* **1997**, *277* (5329), 1078-1081.
42. Cao, Y.; Wen, L. Y.; Svec, F.; Tan, T. W.; Lv, Y. Q., Magnetic AuNP@Fe<sub>3</sub>O<sub>4</sub> nanoparticles as reusable carriers for reversible enzyme immobilization. *Chemical Engineering Journal* **2016**, *286*, 272-281.
43. Feng, Q.; Zhao, Y.; Wei, A. F.; Li, C. L.; Wei, Q. F.; Fong, H., Immobilization of Catalase on Electrospun PVA/PA6-Cu(II) Nanofibrous Membrane for the Development of Efficient and

Reusable Enzyme Membrane Reactor. *Environmental Science & Technology* **2014**, *48* (17), 10390-10397.

44. Lv, Y. Q.; Lin, Z. X.; Tan, T. W.; Svec, F., Preparation of Reusable Bioreactors Using Reversible Immobilization of Enzyme on Monolithic Porous Polymer Support With Attached Gold Nanoparticles. *Biotechnology and Bioengineering* **2014**, *111* (1), 50-58.

45. Long, J.; Hutcheon, G. A.; Cooper, A. I., Combinatorial discovery of reusable noncovalent supports for enzyme immobilization and nonaqueous catalysis. *Journal of Combinatorial Chemistry* **2007**, *9* (3), 399-406.

46. Mohamad, N. R.; Marzuki, N. H. C.; Buang, N. A.; Huyop, F.; Wahab, R. A., An overview of technologies for immobilization of enzymes and surface analysis techniques for immobilized enzymes. *Biotechnology & Biotechnological Equipment* **2015**, *29* (2), 205-220.

47. Spears, B. R.; Waksal, J.; McQuade, C.; Lanier, L.; Harth, E., Controlled branching of polyglycidol and formation of protein-glycidol bioconjugates via a graft-from approach with "PEG-like" arms. *Chemical Communications* **2013**, *49* (24), 2394-6.

48. Beezer, D. B.; Harth, E., Post-polymerization modification of branched polyglycidol with N-Hydroxy phthalimide to give ratio-controlled amino-oxy functionalized species. *Journal of Polymer Science Part A: Polymer Chemistry* **2016**, *54* (17), 2820-2825.

49. Spears, B. R.; Marin, M. A.; Montenegro-Burke, J. R.; Evans, B. C.; McLean, J.; Harth, E., Aqueous Epoxide Ring-Opening Polymerization (AEROP): Green Synthesis of Polyglycidol with Ultralow Branching. *Macromolecules* **2016**, *49* (6), 2022-2027.

50. Spears, B. R.; Waksal, J.; McQuade, C.; Lanier, L.; Harth, E., Controlled branching of polyglycidol and formation of protein-glycidol bioconjugates via a graft-from approach with "PEG-like" arms. *Chem Commun (Camb)* **2013**, *49* (24), 2394-6.

51. Schull, C.; Gieshoff, T.; Frey, H., One-step synthesis of multi-alkyne functional hyperbranched polyglycerols by copolymerization of glycidyl propargyl ether and glycidol. *Polymer Chemistry* **2013**, *4* (17), 4730-4736.
52. Wilms, D.; Stiriba, S. E.; Frey, H., Hyperbranched Polyglycerols: From the Controlled Synthesis of Biocompatible Polyether Polyols to Multipurpose Applications. *Accounts of Chemical Research* **2010**, *43* (1), 129-141.
53. An, S. Y.; Bui, M.-P. N.; Nam, Y. J.; Han, K. N.; Li, C. A.; Choo, J.; Lee, E. K.; Katoh, S.; Kumada, Y.; Seong, G. H., Preparation of monodisperse and size-controlled poly(ethylene glycol) hydrogel nanoparticles using liposome templates. *Journal of Colloid and Interface Science* **2009**, *331* (1), 98-103.
54. Vemuri, S.; Rhodes, C. T., Preparation and characterization of liposomes as therapeutic delivery systems: a review. *Pharmaceutica Acta Helveticae* **1995**, *70* (2), 95-111.
55. Kant Shashi, K. S., Prashar Bharat, A Complete Review On: Liposomes. *International Research Journal of Pharmacy* **2012**, *3* (7), 10.

## CHAPTER V

### POLYGLYCIDOL COATING ON ULTRA-HIGH MOLECULAR WEIGHT POLYETHYLENE FOR REDUCED BIOFILM GROWTH

#### Introduction

The development of novel polymeric biomaterials for reducing bacterial adhesion and biofouling is a pressing concern.<sup>1,3</sup> Out of 1 million total hip and knee replacement surgeries every year in the United States, over 59,000 cases fail due to bacterial infection from biofilm growth and require revision surgeries within the first 10 years.<sup>4</sup> Ultra-high molecular weight polyethylene (UHMWPE) is strong, inert, stable and the most commonly used polymer for artificial hip and knee replacements.<sup>5</sup> However, its strong hydrophobic surface chemistry leaves it susceptible for bacterial adhesion and biofilm formation, which is known to be the first conditioning step for infections.<sup>6</sup> The vast majority of recent advances in biomaterial technology involve techniques that alter the surface chemistry from hydrophobic to hydrophilic with polymer coating techniques such as layer-by-layer (LBL) deposition or self-assembled monolayers (SAM), which use van der Waals secondary or electrostatic forces.<sup>7</sup> It has been more recently shown that a covalent bond however is more ideal to impart both structural stability and effective hydrophilicity to a biomedical implant surface.<sup>8</sup> Aside from the most prominent hydrophilic polymers like PEG or zwitterionic coatings, it has been recently realized that poly(glycidol) has potential to achieve bioinertness with more advanced functionality. Poly(glycidols) (PG) are comparable in structure to poly(ethylene glycol) (PEG) but offer tremendous advantages in terms of increased thermal stability, oxidative stability and can form a hydrophilic barrier to biological adsorption.<sup>9</sup> Poly(glycidol) structural branching



can be easily tuned by synthetic reaction temperature<sup>10</sup> and copolymerized with pendant alkene groups<sup>11</sup> to remain hydrophilic even at 20% allyl incorporation. Due to the chemical inertness of polyolefin, harsh activation methods such as UV-irradiation or plasma treatments are often required to modify the surface.<sup>12,13</sup> Haag and coworkers put forth an elegant “graft-to” approach using dendritic poly(glycidols) that were post-modified with amines in three synthetic steps, followed by grafting to plasma-brominated polypropylene.<sup>14</sup> In light of demonstrating effective protein resistance, the highly branched structures may limit surface coverage due to steric hindrance. Bucio and coworkers demonstrated that gamma-ray induced grafting of poly[2-(dimethylamino) ethyl methacrylate] (PDMAEMA) onto polyethylene (PE) films could be achieved by first exposing polyethylene to ionizing radiation, followed by exposure to high concentrations of monomer in solution.<sup>15</sup> Inspired by both Haag and Bucio, we sought to achieve an effective anti-biofilm coating with fewer processing steps using a “graft-from” approach with irradiated PE and our unique semi-branched poly(glycidols) to coat the most commonly utilized biomaterial for hip-and-knee implants, ultra-high-molecular weight polyethylene (UHMWPE).<sup>16</sup> Characterization of the resulting coatings along with their capabilities to resist bacterial biofilm growth were investigated.

## Results and Discussion

### **Radiation grafting and characterization**

The “graft-from” method was initiated by trapped radicals throughout a radiated surface of the polyethylene by a mechanism described in Figure V-1. Briefly, the ionizing radiation from Cesium-137 decays to generate gamma rays that cause homolytic cleavages of C-H bonds on polyethylene (PE). This generates carbon and hydrogen radicals that undergo chain transfer to

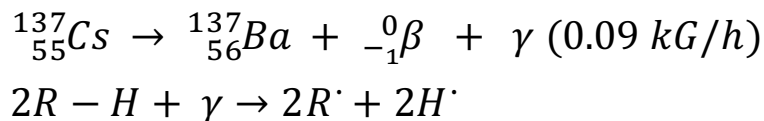


Figure V-1. General graft mechanism proceeds by radical generation from cesium-137 decay leading to ionizing gamma radiation at 0.09 kilograys per hour (kG/h) of absorbed dose that homolytically cleaves R-H bonds to create radicals. The radicals then undergo chain transfer between polymers and cause crosslinking grafts of poly(glycidol) to polyethylene to form coating.

poly(glycidol) during exposure. Finally, the radical PE and PG undergo radical association producing PE-PG, PG-PG and hydrogen gas. This process occurs multiple times on the surface leaving a crosslinked poly(glycidol) coating attached to the polyethylene surface. We hypothesized that the copolymer poly(glycidol allyl glycidyl) ether (20% allyl) would graft more effectively on the surface due to increased reactivity of pendant alkene groups compared to poly(glycidol) homopolymer. Our hypothesis was tested by conducting a time-dependent study of pre-irradiated chips exposed to equivalent concentrations of each polymer in solution and analyzing the surface results by scanning electron microscopy (SEM) at 5, 7 and 15 day time points after thorough washing to remove non-grafted material. Figure V-2 shows images of the surface of PE chips

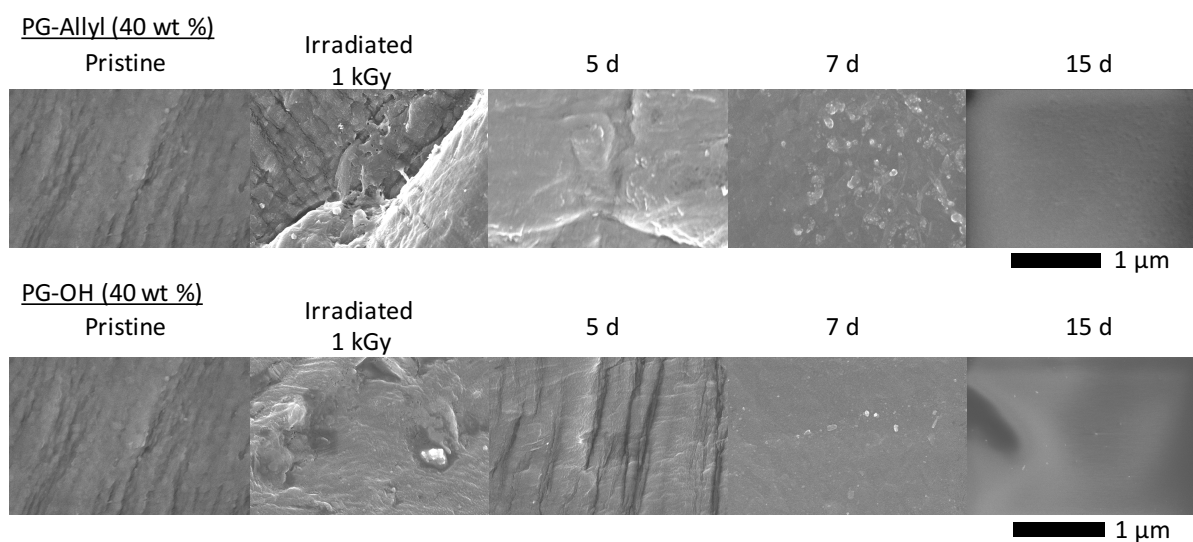


Figure V-2. SEM images at 5, 7 and 15 days graft time.

before and after exposure to the polymer graft solution, and one can see the gradual decrease of observed crevasses, particularly after 15 d, due to the coating formation. One may also note the slightly darker and denser image associated with the PG-Allyl coating compared with the PG-OH after 15 d exemplified by Figure V-3, which we attribute to the increased reactivity of the pendant allyl groups. This evidence was corroborated by grafting pre-irradiated PE with a fluorescent N-

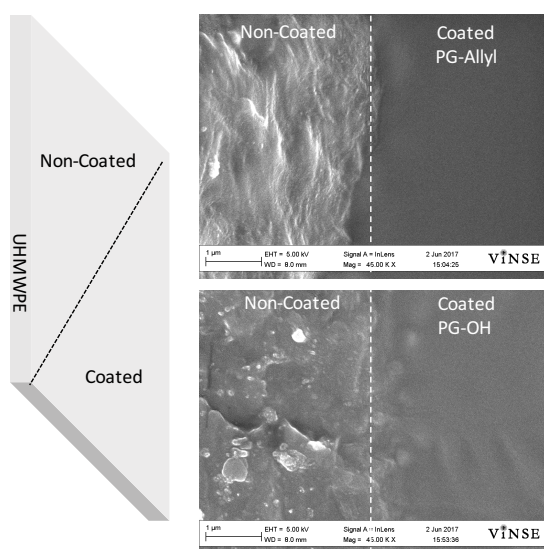


Figure V-3. SEM imaging was performed at the dotted line shown above between coating and non-coating sides of the chip. Notice the more thorough coating coverage in the PG-Allyl chip compared to the PG-OH.

hydroxysuccinimide (NHS) ester dye conjugated to PG-Allyl in solution compared to a solution of simple dye mixed with PG-OH and control solution of dye alone (negative control) at equivalent dye concentrations for 15 days. The grafting was followed by careful washing to remove non-grafted materials. The fluorescent imaging results in Figure V-5D indicate presence of dye, and more homogeneous coating was observed in the grafted PG-Allyl compared to PG-OH. We attribute this difference to the greater reactivity provided by the allyl groups.

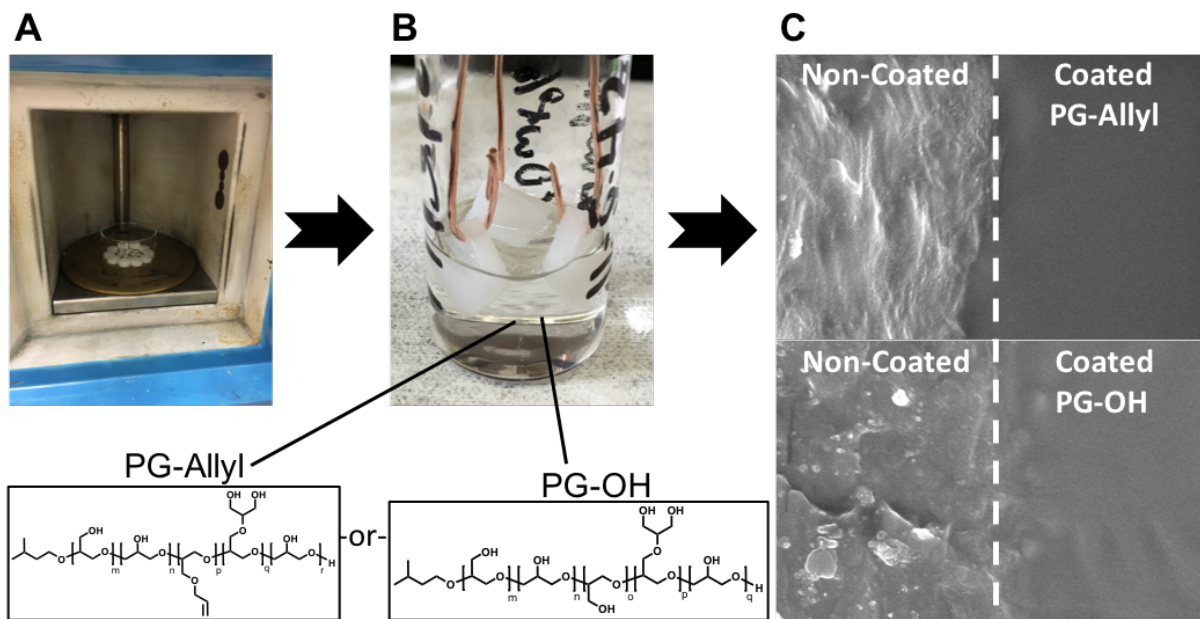


Figure V-4. General procedure for pre-irradiation grafting of Polyglycidols to UHMWPE. A) Sample of UHMWPE were exposed to Cesium-137 source to initiate trapped radicals in the plastic. B) We then use the trapped radicals within UHMWPE to graft poly(glycidol) homopolymer (PG-OH) or poly(glycidol allylglycidyl ether) (PG-Allyl) to the surface for 15 d. C) Upon developing the samples through exhaustive washings in water to remove the non-crosslinked polymer and thorough drying, we characterized the surface coatings by scanning electron microscopy.

Evidence of poly(glycidol) coating on UHMWPE was characterized initially by Fourier transform infrared-attenuated total reflectance spectroscopy (FTIR-ATR) as shown in Figure V-4B, and the resulting spectra showed strong presence of PG-OH and PG-Allyl coatings characterized by the broad hydroxyl peak at  $3400\text{ cm}^{-1}$  and ethylene peaks at  $2915$  and  $2848\text{ cm}^{-1}$ . However, we could not distinguish a clear characteristic peak that would differentiate the PG-Allyl coating from the PG-OH, so we employed x-ray photoelectron spectroscopy (XPS) to obtain a more detailed view of the atoms present on the surface of our UHMWPE chips. In Figure V-5C, both PG-Allyl and PG-OH coating samples showed elevated presence of hydroxyl groups compared to a control UHMWPE surface which confirmed a coating was present. Additionally, the PG-Allyl coated sample showed 36%  $-\text{CH}_2-$  character while the PG-OH coating showed only

25%. This difference can be attributed to the higher presence of ethylene groups on the PG-Allyl polymer structure compared with the PG-OH.

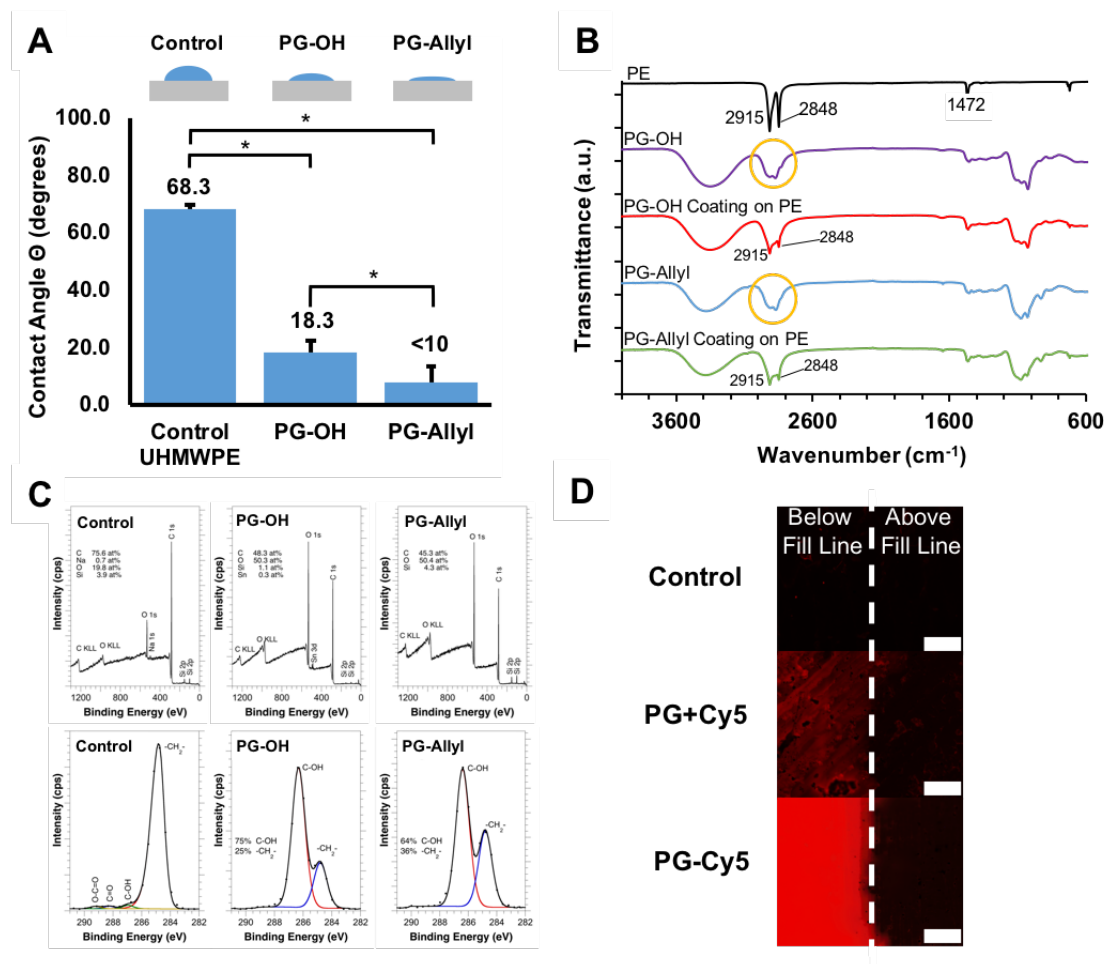


Figure V-5. A) Contact angle  $\Theta$  (degrees) versus test sample group for control non-coating (UHMWPE), poly(glycidol) (PG-OH) coating and poly(glycidol allylglycidyl ether) (PG-Allyl). A significant reduction in contact angle was observed in the PG-Allyl coating compared to the PG-OH which can be attributed to the more effective coating. Data represent mean  $\pm$  SD (n=3) with significance ( $p < 0.05$ ) indicated by asterisk. B) FTIR-ATR data confirms presence of polyglycidol coated on the polyethylene, particularly in the samples circled which show the strong broad hydroxyl peak at 3400 cm<sup>-1</sup> from polyglycidol along with the sharp ethylene peaks from polyethylene at 2915 and 2848 cm<sup>-1</sup>. C) Top row of plots indicate XPS full spectral results for control UHMWPE, poly(glycidol) and poly(glycidol allylglycidyl ether) chip samples. The bottom row represents zoomed in spectral data between 282-291 eV for each of the same sample types. D) Fluorescent imaging was performed at the fill line after washing the non-grafted material away. No detectable signal was observed in the control (top), while some dye molecules were entrapped within the PG-OH coating (middle), and a substantial fluorescence was observed in the PG-Allyl-Dye coating (bottom).

An important feature of the PG-OH and PG-Allyl polymer coatings include the hydrophilic characteristic they can impart on an implantable substrate. We employed contact-angle goniometry to quantify the wettability of the coated surfaces by measuring the angle created at the liquid-vapor interface when a water droplet is deposited onto the surface. The results for UHMWPE, PG-OH coating, and PG-Allyl coating groups were 18.3 and <10, respectively, as shown by Figure V-5A. The results from measuring contact angle ( $\Theta$ , degrees) on PG-Allyl coating came to < 10 degrees, which was below the detection limit, compared to PG-OH coatings that measured 18.3 degrees. While the non-coated surface data suggests significant ( $p < 0.05$ ) increase in hydrophilicity from both treatment groups, the PG-Allyl coating created a surface that was more hydrophilic than the PG-OH treatment. Despite a lesser percentage of hydroxyl groups, the PG-allyl chips possessed a more complete coating which can be attributed to its increased reactivity during the graft step.

### **Biofilm in vitro assay**

The ability for *S. aureus* cells to adhere and proliferate on medical implants has been a major challenge in the biomedical field. *S. aureus* cells are able to tolerate high doses of antibiotics and the ability to inhibit infection on implanted devices has yet to be solved.<sup>17</sup> Infections can be potentially avoided by inhibiting adherence of bacteria on the surface in the first place, thus eliminating the possibility for an infection to persist on the implant and spread to the surrounding area (See Figure V-6A). As proof of principle, samples of polymer-coated and non-coated UHMWPE chips were inoculated with  $10^5$  CFUs/cm<sup>2</sup> UAMS-1 strain *S. aureus* cells in solution and incubated at 37°C for 24 and 48 hours in a 24-well plate to assess the ability for poly(glycidol) coating to inhibit *S. aureus* cell adherence and growth. After the incubation period, any adherent cells were separated from the surface and counted. The results suggest that chips that were coated

with PG-Allyl inhibit any and all cells from adhering to the surface during the 24- and 48-hour incubations (see Figure V-6B). Similarly, the bacterial growth on PG-OH samples exhibited significant ( $p < 0.05$ ) reduction of bacteria growth compared to the significantly-infected non-coated UHMWPE control (see Figure V-6B). *S. aureus* colonization of non-coated control samples exceeded  $10^6$  CFU/cm<sup>2</sup> after 48 h which suggests these implant surfaces would be prone to chronic

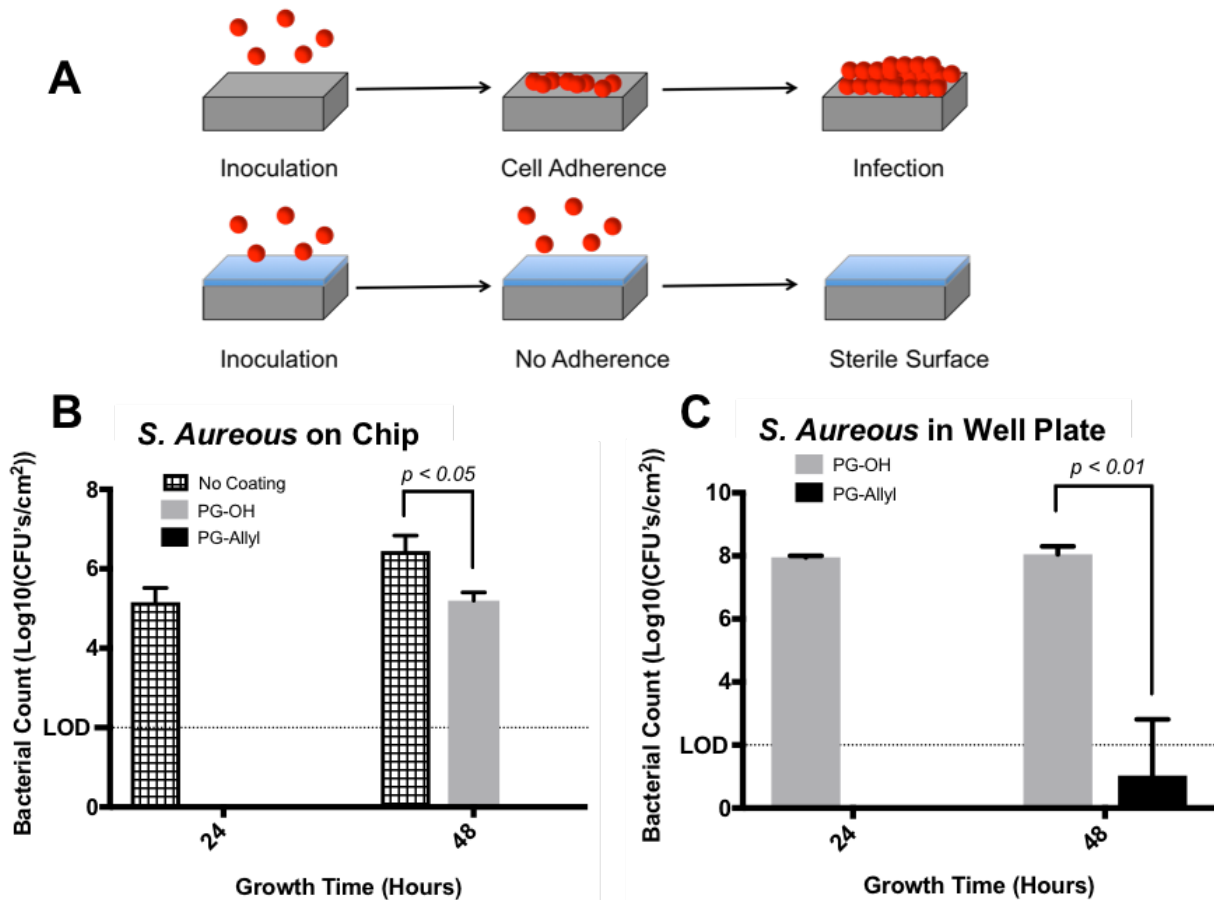


Figure V-6. A.) *S. aureus* cells are the most prominent biofilm-forming bacteria that are found to adhere and proliferate on UHMWPE medical implant surfaces and create an infection. Our coating has been shown to inhibit adherence, thus eliminating the ability for bacterial cells to form an infection. B.) This plot indicates adherent *S. aureus* bacterial counts from the surface of coated and non-coated test samples after 24 and 48 h incubation periods. The dotted line indicates the limit of detection (LOD) at  $2 \log_{10}(\text{CFU's/cm}^2)$ . C.) Plot shows the adherent *S. aureus* cells that remained in surrounding well plate of test samples after 24 and 48 h incubation. Interestingly the PG-Allyl wells exhibited less bacterial growth than PG-OH wells and will be a focus of future experiments. All data represent  $\pm$  mean SD ( $n=3$ ).

infection as supported by the literature<sup>18,19</sup>. It is important to point out that we continued the bacterial incubation period to 48 h when previous groups who studied anti-biofilm coatings stopped at 90 min or 24 h before counting cells as can be found in reports by Puértolas and coworkers<sup>18</sup> and Haag and coworkers<sup>14</sup>, respectively. We wanted to ensure enough time for a biofilm to develop on UHMWPE, which is why our experiments went 48 h. To the best of our knowledge, the PG-allyl demonstrated to be one of the best performing anti-adherence coatings for *S. aureus* cells in recent literature. Additionally, we analyzed the 24-well plate surfaces which were used to incubate *S. aureus* with the coated PG-Allyl and PG-OH samples to predict how the coatings would affect colonization of bacteria in surrounding areas. As shown in Figure V-6C, the quantified cell counts of *S. aureus* cells in well surfaces that were surrounding PG-Allyl coated samples indicate a significantly decreased adherence to the well-plate surface when compared to wells that incubated PG-OH samples. Figure V-6C shows the PG-Allyl coating exhibited an interesting proximity effect by reduction of bacteria colonization in the well-plate that will be a focus of future experiments. It is important to note that PG-Allyl and PG-OH have previously demonstrated strong biocompatibility by Harth and coworkers<sup>11</sup> and Brooks and coworkers<sup>20</sup>, respectively, among others. The proof-of-concept *in vitro* experiments suggest that the PG-Allyl coating on the surface of an implantable material demonstrated a promising potential to inhibit adherence and colonization of biofilm-forming bacteria that often develop into persistent infections.

## Conclusion

In conclusion, we presented a simple pre-irradiation graft-from method for coating the most commonly used material for hip-and-knee implants, UHMWPE, with semi-branched poly(glycidols) in efforts to reduce infectious biofilm growth. Both PG-Allyl and PG-OH surface



coatings were characterized by FTIR, XPS, SEM and fluorescent microscopy and tested against the most prominent biofilm-forming bacteria, *S. aureus*. Coated samples either inhibited or delayed *S. aureus* cell colonization of a UHMWPE chips after 24 and 48 hours of incubation. The PG-Allyl coating led to 3 log reduction in colonization of *S. aureus* cells compared to the highly infected non-coated UHMWPE control sample when incubated for 24 and 48 hours, indicating a strong potential for preventing infection in biomaterials that contain UHMWPE.

## Experimental

### Materials

Semi-branched poly(glycidol) (GPC  $M_n = 2828$  Da,  $M_w/M_n = 1.57$  using PEG standards) and poly(glycidol allylglycidyl ether) (pGLY/AGE, 20% AGE, GPC  $M_n = 3218$  Da,  $M_w/M_n = 1.42$  using PEG standards) were synthesized as previously reported.<sup>11, 21</sup> Allyl glycidyl ether (AGE), tin(II)triflate (Sn(OTf)<sub>2</sub>) and glycidol (GLY) were purchased from Sigma Aldrich, USA. GLY was purified *via* Kugelrohr distillation before use. L- $\alpha$ -phosphatidylcholine (Egg-PC) was purchased from Avanti Polar Lipids (Alabaster, AL). 2,2-Azobis(2-methyl-*N*-(2-hydroxyethyl)propionamide (VA-086, 98%) was purchased from Wako Chemicals USA, Inc. and used without further purification. Dialysis tubing SnakeSkin® (molecular weight cutoff (MWCO): 1 kDa, 16 mm dry I.D) were purchased from Spectrum Laboratories, Inc. (Rancho Dominguez, CA). A sheet of ultra high molecular weight polyethylene (UHMWPE, ~3000 kDa, opaque white, standard tolerance, ASTM D4020, 0.125" thickness, 12" width, 12" length) was purchased from Amazon, Inc (Amazon.com) and machined into 1 x 1 cm squares with 16-gauge holes strategically placed in the corner of squares by the Vanderbilt Machine Shop. Sulfo-Cyanine5 NHS Ester (Cy5) dye was purchased from Lumiprobe Corporation (Hallandale Beach, FL). Unless mentioned otherwise, all

other solvents or reagents were purchased from Sigma Aldrich and used as received. Milli-Q water was used in these experiments and ultra-purified by a Modulab Water Systems USA with 0.2  $\mu\text{m}$  filter with minimum resistivity of 18.2  $\text{M}\Omega\text{cm}$  at 25  $^{\circ}\text{C}$ .

## **Instrumentation**

The UHMWPE sample chips were irradiated using a Mark I 68A Cs-137 Irradiator, manufactured by JL Shepherd and Associates (San Fernando, CA). X-ray photoelectron spectroscopy data was acquired with a Physical Electronics (PHI) XPS 5000 Versaprobe. Samples were sputter-coated with 1-2 nm of gold before scanning electron microscope (SEM) images were acquired on a Zeiss Merlin Scanning Electron Microscope operating at 10 keV and 8 mm working distance. Fourier transform infrared spectroscopy-attenuated total reflectance (FTIR-ATR) was performed using a Nicolet™ iS™ 5 FT-IR Spectrometer with an iD5 ATR Accessory equipped with OMNIC™ FTIR Software (Thermo Scientific, USA). Samples were pressed against the diamond tip, and resulting spectra represent the average over 32 scans. Epi-fluorescent images of Cy5 dye coatings were collected on a Nikon AZ100 Upright Wide Field Microscope equipped with NIS-Elements Software with a 5x objective and Cy5 filter at 3.0x zoom (0.72  $\mu\text{m}/\text{pixel}$ ).

## **Pre-irradiation grafting of polyglycidol to UHMWPE**

The UHMWPE chips were cleaned by rinsing both sides first with methanol (5 s), then acetone (5 s) and dried under vacuum before submitting to the Cs-137 irradiator. Samples were then exposed to irradiation for 15.5 hrs (1 kGy of absorbed irradiation) and quickly transferred to polymer graft solutions while unused chips were stored under Argon until later use. Solutions of 40 wt % poly(glycidol) and 40 wt % poly(glycidol allylglycidyl ether) in methanol were prepared in 6

DRAM vials and bubbled with Argon for 20 min before submerging the pre-irradiated chips, outfitted with copper wire hooks to stabilize, into the vial solutions. A razor was used to score a line at the solution-air interface as an indicator in order to locate the resulting coating edge later *via* SEM (See Figure V-3). The 6DRAMS were sealed with parafilm, and the samples incubated at room temperature for up to 15 days. Following incubation, samples were thoroughly rinsed in milli-Q water for 5 minutes to ensure any non-grafted material was removed before characterization. After washing, the coated chips were dried under gentle stream of nitrogen for at least 3 hours before drying overnight in ambient conditions.

### **Fluorescent dye conjugation**

The synthesis proceeded in 5 steps. First, the poly(glycidol allylglycidyl) ether (PG-CC, 20 % allyl) shown in Figure V-7. Compound **1** was prepared as previously reported.<sup>11</sup> Product **1** was converted to partial epoxide functionality using 1.2 equivalents of purified meta-chloroperoxybenzoic acid (mcpba) in methanol (MeOH, 0.4 M), stirred at 1100 rpm for 48 h at room temperature in a sealed, flame-dried, N<sub>2</sub>-purged 6-DRAM vial. The product **2** was dialyzed in 1 kDa MWCO tubing for 24 h against 500 mL methanol (changed six times), and dried *in vacuo* overnight (dry yield = 85%, 9% allyl, 11% epoxide by H<sup>1</sup>-NMR calculated ratio). The partial epoxide functional groups in **2** were converted to an *N*-Boc-ethylenediamine group with 1.4 equivalents of *N*-Boc-ethylenediamine, 0.1 equivalents of sodium bicarbonate in 0.04 M MeOH stirred at 800 rpm in a flame-dried, N<sub>2</sub>-purged 25-mL round bottom flask heated at 50 °C for 16 h. The product **3** was purified by dialysis in 1 kDa MWCO tubing against 500 mL MeOH for 3 days (changed twice daily) and dried *in vacuo* overnight (dry yield = 84%, 7% allyl, 6.4% *N*-Boc by H<sup>1</sup>-NMR calculated ratio). Just before dye conjugation, the BOC group was deprotected with 569

equivalents of trifluoroacetic acid (TFA) mixed in 50 % (v/v) MeOH (0.02 M) stirring at 800 rpm at 25 °C for 24 h in a 6DRAM vial open to the air. The resulting product **4** was diluted 5x in MeOH and dried by rotovap four times to remove all TFA. Product **4** was further purified by passing through a glass pipet column made with 20 mg Sephadex® G-25 (Sigma) in MeOH. Product **4** was collected in a 6DRAM vial, dried overnight, and characterized by dry weight (dry yield = 87%, 7% allyl, 6.4% amine, 3 amines/polymer as determined by NMR). In the final step, Cy5 Dye (6.5 µmol) was added to product **4** (11 µmol, 3 amines per polymer) in a 0.5 DRAM vial with a flea stir with 284 µL d<sub>6</sub>-DMSO (1 % trimethylamine) stirred for 16 h at room temperature in dark. Dry yield = 75 %, 15 mg. <sup>1</sup>H-NMR (400 MHz, d<sub>6</sub>-DMSO) δ: 10.51 (1H), 9.05 (1H), 8.38 (1H), 7.81 (1H), 7.65 (1H), 7.30 (1H), 6.55 (1H), 6.30 (1H), 5.92 (1H), 5.29 (2H), 4.11 (2H), 4.07 (4H), 3.08-3.94 (33H), 0.98 (6H) ppm. See Figure V-8 for full NMR labeled product.

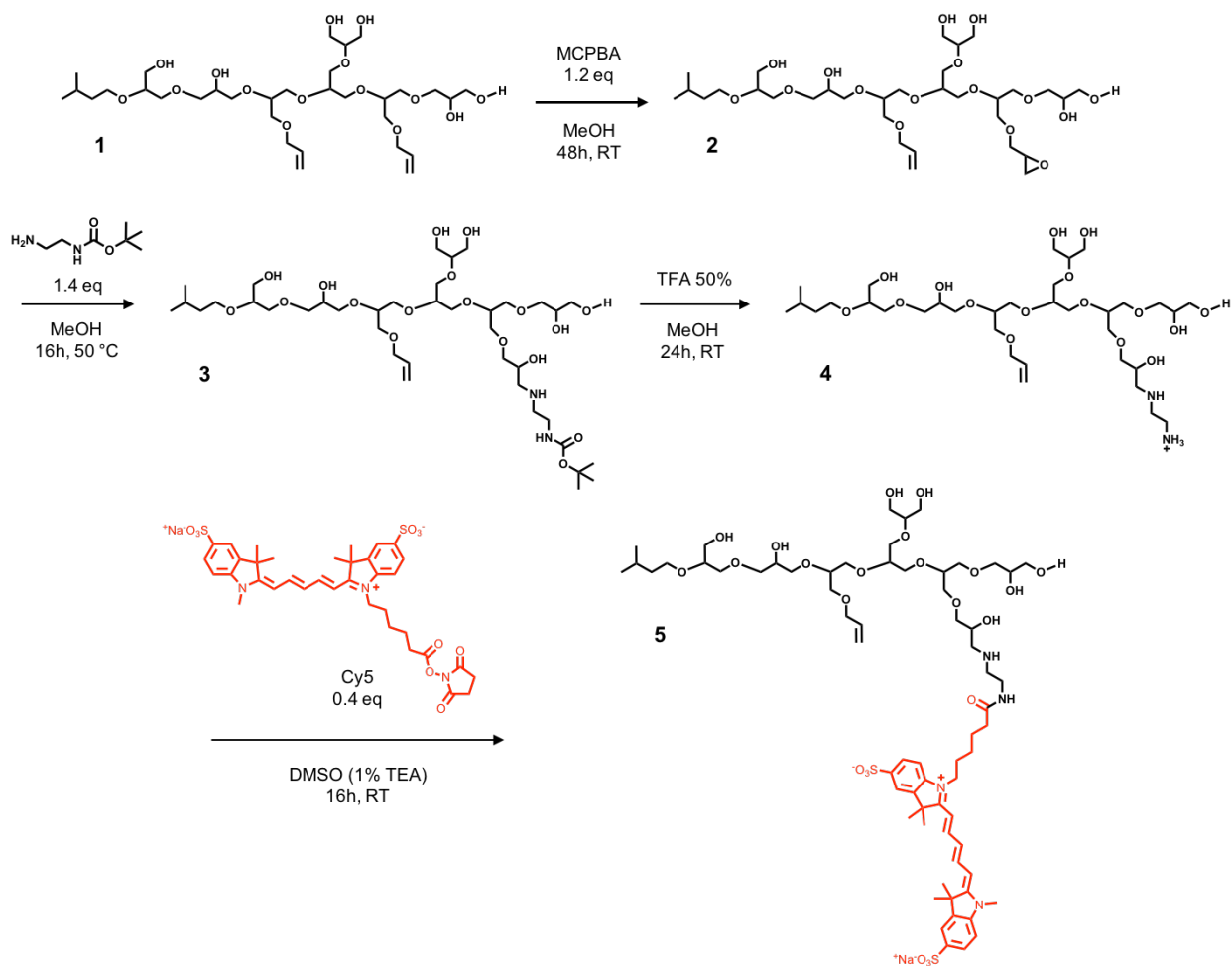


Figure V-7. Synthesis scheme of poly(glycidol)-Cy5 Dye conjugate. Full proton NMR characterization of the PG-Cy5 Dye conjugate can be found in Figure V-8.

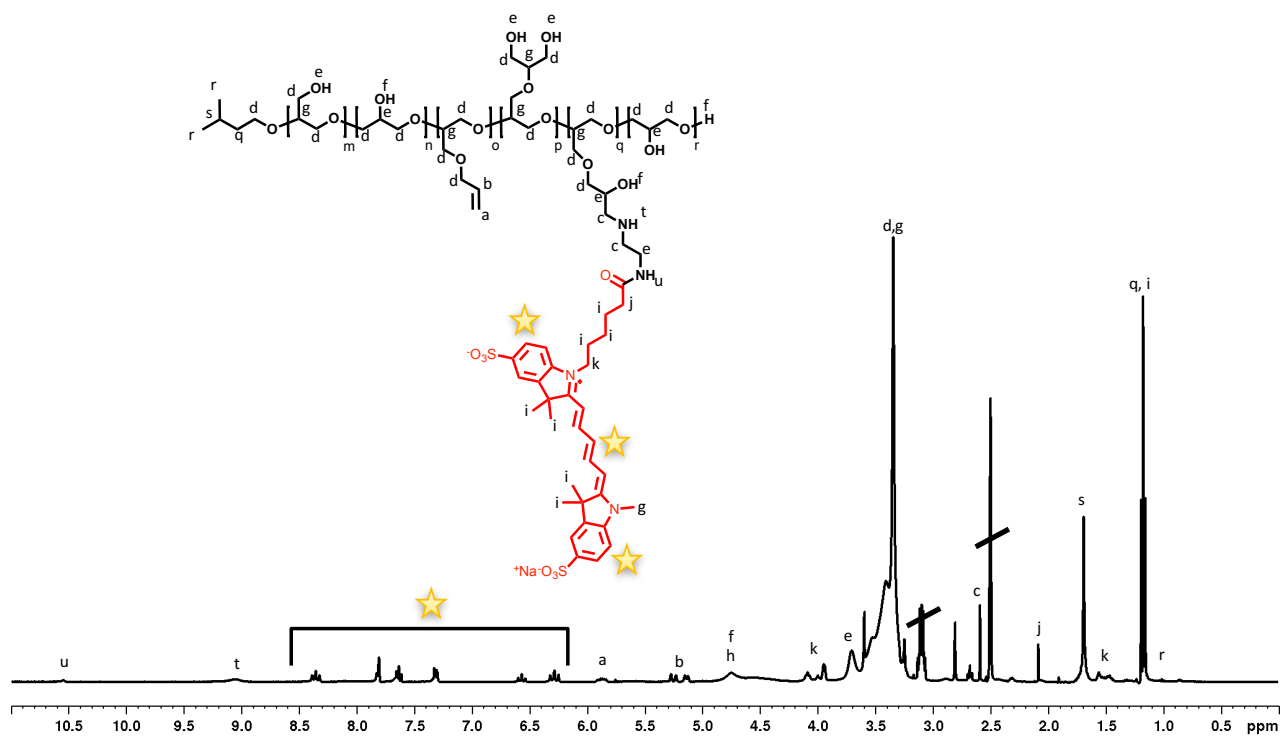


Figure V-8. Labeled  $^1\text{H}$ -NMR (400 MHz,  $d_6$ -DMSO) spectrum of poly(glycidol)-Cy5 conjugate.

### Fluorescent dye coating

UHMWPE was machined into rectangular cubes (1 x 0.3 x 0.3 cm) with holes on one end and thoroughly cleaned with methanol and acetone. Following cleaning, samples were dried and irradiated to 1 kGy (15.5 h) using a Cs-137 irradiator. Immediately after irradiation, samples were oriented using common sewing thread inside 0.5-DRAM vials with 200  $\mu\text{L}$  solutions of free Cy5 dye (1.5 mg, the control) in MeOH, Cy5 dye (1.5 mg) with roughly 400 mg of polyglycidol (unfunctionalized, 40 wt%) in MeOH, or 15 mg of polyglycidol-Cy5 conjugated (10 % functionalized, effectively 1.5 mg of dye) with 385 mg of polyglycidol (unfunctionalized, 40 wt% total polymer) in MeOH. Graft solutions were bubbled with Argon for 20 min before submerging UHMWPE samples. Samples were allowed to graft for 15 d. Following graft, samples were thoroughly washed

for 5 min in milli-Q water to remove unattached dye or polymer material. Samples were allowed to dry overnight in the dark and imaged on a Nikon AZ100 upright wide-field microscope as described in the instrumentation section.

### **Contact angle measurement**

The contact angle measurements were conducted using a Rame-Hart manual contact angle goniometer with a microliter syringe. A 5  $\mu\text{L}$  droplet of DI water was added to 1  $\text{cm}^2$  chips of untreated UHMWPE, semibranched poly(glycidol) film, or semibranched poly(glycidol allylglycidyl ether) film on UHMWPE surfaces, and the angle ( $\Theta$ ) was measured between the solid surface and liquid-air interface of the static droplet. Measurements were performed in triplicate.

### **X-ray photoelectron spectroscopy (XPS)**

XPS analyses were performed using an Ulvac-PHI Versaprobe 5000. The three samples were mounted onto one large sample holder using stainless steel masks. The mounted samples were pumped in the intro chamber over a weekend to minimize outgassing of any remaining water or other volatile species in the analysis chamber. Monochromatic Al  $K\alpha$  x-rays (1486 eV), a 100  $\mu\text{m}$  diameter x-ray spot rastered over a 600  $\mu\text{m}$  by 400  $\mu\text{m}$  area, and a takeoff angle of 45 degrees off sample normal were used in each acquisition. Pass energies of 187.7 eV and 23.5 eV were used for the survey and high-resolution acquisitions, respectively. Charge neutralization was accomplished using 1.1 eV electrons and 10 eV  $\text{Ar}^+$  ions. Binding energies were calibrated to  $-\text{CH}_2$ - type bonding in the carbon 1s spectrum of 284.8 eV. Relative atomic concentrations were calculated using peak areas and PHI handbook sensitivity factors.<sup>22</sup>

### **Bacterial strain and reagents**

*Staphylococcus aureus* strain UAMS-1 was used for the biofilm assay due to its elevated ability to form biofilms.<sup>23</sup> Bacterial cell cultures were grown in 5 mL Tryptic Soy Broth (TSB) overnight shaking at 180 rpm. Bacterial cells were quantified by optical density at 600 nm (OD<sub>600</sub>).

### ***S. aureus* in vitro adherence assay**

Standard assay procedures were performed as described previously.<sup>24</sup> To ensure sterility, samples were submerged in 70% EtOH for 2 seconds and placed in sterile PBS prior to inoculation. Samples were placed in 24-well plates with 1 mL of TSB containing 10<sup>6</sup> CFUs/mL *S. aureus* and incubated at 37°C for 24 and 48 hours. Plates were rotated on an orbital shaker at 80 RPM to encourage mixing and allow for adherence. Following incubation, samples were extracted from bacterial solution and washed 3 times with sterile PBS to ensure that any cells that were not adhered to the surface were removed. Sonication of samples was performed for 5 minutes in a fresh 24 well plate containing 1 mL of sterile PBS for each sample to separate adhered cells from the surface of the sample. Similarly, surfaces of the 24-well plates that were used during incubation were also washed 3 times with sterile PBS and sonicated for 5 minutes using 1 mL of sterile PBS. Sonicated media was then serial diluted and plated on Tryptic Soy Agar (TSA) plates to quantify CFUs per surface area of sample substrate.

### **Statistics**

Data analysis and statistics were performed with the Data Analysis Tool from Microsoft Excel 2016 for Mac. A student one-tailed t-test was performed using two-sample unequal variance parameters. In all cases, a p-value < 0.05 was considered significant.



## References

1. Katsikogianni, M.; Missirlis, Y. F., Concise review of mechanisms of bacterial adhesion to biomaterials and of techniques used in estimating bacteria-material interactions. *European Cells & Materials* **2004**, *8*, 37-57.
2. Extremina, C. I.; da Fonseca, A. F.; Granja, P. L.; Fonseca, A. P., Anti-adhesion and antiproliferative cellulose triacetate membrane for prevention of biomaterial-centred infections associated with *Staphylococcus epidermidis*. *International Journal of Antimicrobial Agents* **2010**, *35* (2), 164-168.
3. Gristina, A.; Sherk, H. H., Biomaterial-centered infection - Microbial adhesion versus tissue integration - (Reprinted from *Science*, vol. 237, pg. 1588-1595, 1987). *Clinical Orthopaedics and Related Research* **2004**, (427), 4-12.
4. Song, Z.; Borgwardt, L.; Hoiby, N.; Wu, H.; Sorensen, T. S.; Borgwardt, A., Prosthesis infections after orthopedic joint replacement: the possible role of bacterial biofilms. *Orthopedic Reviews* **2013**, *5* (2), 65-71.
5. Vu, N. B.; Truong, N. H.; Dang, L. T.; Phi, L. T.; Ho, N. T. T.; Pham, T. N.; Phan, T. P.; Pham, P. V., In vitro and in vivo biocompatibility of Ti-6Al-4V titanium alloy and UHMWPE polymer for total hip replacement. *Biomedical Research and Therapy* **2016**, *3* (3), 567-577.
6. Wei, Q.; Becherer, T.; Angioletti-Uberti, S.; Dzubiella, J.; Wischke, C.; Neffe, A. T.; Lendlein, A.; Ballauff, M.; Haag, R., Protein interactions with polymer coatings and biomaterials. *Angewandte Chemie. International Ed. In English* **2014**, *53* (31), 8004-31.
7. Banerjee, I.; Pangule, R. C.; Kane, R. S., Antifouling Coatings: Recent Developments in the Design of Surfaces That Prevent Fouling by Proteins, Bacteria, and Marine Organisms. *Advanced Materials* **2011**, *23* (6), 690-718.

8. Ngo, B. K. D.; Grunlan, M. A., Protein Resistant Polymeric Biomaterials. *Acs Macro Letters* **2017**, *6* (9), 992-1000.
9. Siegers, C.; Biesalski, M.; Haag, R., Self-assembled monolayers of dendritic polyglycerol derivatives on gold that resist the adsorption of proteins. *Chemistry-A European Journal* **2004**, *10* (11), 2831-2838.
10. Spears, B. R.; Waksal, J.; McQuade, C.; Lanier, L.; Harth, E., Controlled branching of polyglycidol and formation of protein-glycidol bioconjugates via a graft-from approach with "PEG-like" arms. *Chemical Communications* **2013**, *49* (24), 2394-6.
11. Lockhart, J. N.; Beezer, D. B.; Stevens, D. M.; Spears, B. R.; Harth, E., One-pot polyglycidol nanogels via liposome master templates for dual drug delivery. *Journal of Controlled Release* **2016**, *244*, Part B, 366-374.
12. Deng, J. P.; Wang, L. F.; Liu, L. Y.; Yang, W. T., Developments and new applications of UV-induced surface graft polymerizations. *Progress in Polymer Science* **2009**, *34* (2), 156-193.
13. Farag, Z. R.; Friedrich, J. F.; Kruger, S., Adhesion promotion of thick fire-retardant melamine polymer dip-coatings at polyolefin surfaces by using plasma polymers. *Journal of Adhesion Science and Technology* **2014**, *28* (21), 2113-2132.
14. Lukowiak, M. C.; Wettmarshausen, S.; Hidde, G.; Landsberger, P.; Boenke, V.; Rodenacker, K.; Braun, U.; Friedrich, J. F.; Gorbushina, A. A.; Haag, R., Polyglycerol coated polypropylene surfaces for protein and bacteria resistance. *Polymer Chemistry* **2015**, *6* (8), 1350-1359.
15. Melendez-Ortiz, H. I.; Peralta, R. D.; Bucio, E.; Zerrweck-Maldonado, L., Preparation of Stimuli-Responsive Nanogels of Poly [2-(dimethylamino) Ethyl Methacrylate] by Heterophase

and Microemulsion Polymerization Using Gamma Radiation. *Polymer Engineering and Science* **2014**, *54* (7), 1625-1631.

16. Jaganathan, S. K.; Balaji, A.; Vellayappan, M. V.; Subramanian, A. P.; John, A. A.; Asokan, M. K.; Supriyanto, E., Review: Radiation-induced surface modification of polymers for biomaterial application. *Journal of Materials Science* **2015**, *50* (5), 2007-2018.

17. Davey, M. E.; O'Toole G, A., Microbial biofilms: from ecology to molecular genetics. *Microbiology and Molecular Biology Reviews* **2000**, *64* (4), 847-67.

18. Gomez-Barrena, E.; Esteban, J.; Molina-Manso, D.; Adames, H.; Martinez-Morlanes, M. J.; Terriza, A.; Yubero, F.; Puertolas, J. A., Bacterial adherence on UHMWPE with vitamin E: an in vitro study. *Journal of Materials Science: Materials in Medicine* **2011**, *22* (7), 1701-6.

19. Del Pozo, J. L.; Patel, R., Clinical practice. Infection associated with prosthetic joints. *New England Journal of Medicine* **2009**, *361* (8), 787-94.

20. Kainthan, R. K.; Janzen, J.; Levin, E.; Devine, D. V.; Brooks, D. E., Biocompatibility testing of branched and linear polyglycidol. *Biomacromolecules* **2006**, *7* (3), 703-9.

21. Spears, B. R.; Marin, M. A.; Montenegro-Burke, J. R.; Evans, B. C.; McLean, J.; Harth, E., Aqueous Epoxide Ring-Opening Polymerization (AEROP): Green Synthesis of Polyglycidol with Ultralow Branching. *Macromolecules* **2016**, *49* (6), 2022-2027.

22. John F. Moulder, W. F. S., Peter E. Sobol, Kenneth D. Bomben, *Handbook of X-Ray Photoelectron Spectroscopy*. Physical Electronics USA, Inc: Chanhassen, Minnesota, 1995.

23. Blevins, J. S.; Beenken, K. E.; Elasri, M. O.; Hurlburt, B. K.; Smeltzer, M. S., Strain-dependent differences in the regulatory roles of sarA and agr in *Staphylococcus aureus*. *Infection and Immunity* **2002**, *70* (2), 470-480.

24. Amorena, B.; Gracia, E.; Monzon, M.; Leiva, J.; Oteiza, C.; Perez, M.; Alabart, J. L.; Hernandez-Yago, J., Antibiotic susceptibility assay for *Staphylococcus aureus* in biofilms developed in vitro. *Journal of Antimicrobial Chemotherapy* **1999**, *44* (1), 43-55.

## CHAPTER VI

### FUTURE DIRECTIONS

The formulation strategy for encapsulating tamoxifen (TAM) and quercetin (QT) into a single dosage form with nanosponges demonstrated a great potential for how the nanosponges can further enhance therapeutic efficacy of anti-cancer treatments, which was re-enforced by the cytotoxicity studies and *in vitro* metabolism work. As a future opportunity for advancing this nanoformulation development, multiple dose kinetics and *in vivo* distribution studies can be performed to better understand the advantages of our combined formulation over any individual free drug regimen. One can envision an expanded mouse model study where mice with breast cancer are treated with the nanosponge-TAM-QT formulations, the mouse tumor volumes are tracked over time, and one can compare the outcomes to mice treated with free drug combinations. It is anticipated that the nanosponge carriers will improve uptake of anti-cancer drugs into the tumor vasculature via the enhanced permeation and retention effect, and offer greater improvement of the health condition of mice with breast cancer.

Opportunities to advance the synthesis and development of nanogels exist as well. In this work, precise size-controlled nanogels were developed using liposome templates which were optimized using a one-pot method. The one-pot method afforded the most controlled release kinetics and showed the highest biocompatibility of all our prepared nanocarriers. While the one-pot nanogels serve as a promising strategy for dual nano-delivery of small hydrophobic and large biologicals drugs for combined immunotherapy and chemotherapy applications, future studies can be envisioned where one can tailor the allyl-functional percentage in the polyglycidol structure

before utilization in the one-pot procedure to probe the ability for drug releases to be controlled from the allyl group composition. Additionally, one could study the influence of different incorporated lipids and measure the impact on release kinetics or cell viability. One step further, a mouse *in vivo* study could be employed with nanogel formulations to measure the anti-cancer effects.

In the biosensor work, semi-branched poly(glycidol) was investigated for the immobilization of a three-enzyme cascade of  $\beta$ -galactosidase (GAL), glucose oxygenase (GOX), and horseradish peroxidase (HRP) with and without polyglycidol nanogel pre-encapsulation for biorecognition of lactose. The demonstrated bioactivity suggests that nanogel-mediated spatial orientation can be achieved with a single EBL fabrication step without harsh synthetic chemical modifications. Through these investigations, we encapsulated each enzyme into individual nanogels. Taking this one step further, one could potentially attempt to combine all three enzymes into one nanocarrier and evaluate its activity in detecting lactose compared to the separately synthesized entities. Additionally, one could test polyglycidol further as an electron beam resist by modifying the pitch distances in dot patterns to find the maximum distance required to form well-defined individual spikes as shown in Figure IV-4.

Lastly, the polyglycidol surface coating for anti-biofilm applications has opportunities for further development. In this dissertation, a simple pre-irradiation graft-from method for coating the most commonly used material for hip-and-knee implants, UHMWPE, with semi-branched poly(glycidols) was described. To improve the 15-d graft time, one could optimize the irradiation step by trying surface plasma treatments or a Cobalt-60 irradiator, which offers higher dosing of radiation in a shorter period of time. This would likely shorten the graft time period as well. Additionally, one could engineer a polyglycidol coating on other relevant biomedical implant

materials like titanium and evaluate the biofilm reduction potential to broaden the scope of applications for this polymer coating.

## APPENDIX A

### REFERENCES OF ADAPTATION FOR CHAPTERS

- Chapter II. Lockhart, J. N.; Stevens, D. M.; Beezer, D. B.; Kravitz, A.; Harth, E., Dual drug delivery of tamoxifen and quercetin: Regulated metabolism for anticancer treatment with nanosponges. *Journal of Controlled Release* **2015**, 220, 751-757.
- Chapter III. Lockhart, J. N.; Beezer, D. B.; Stevens, D. M.; Spears, B. R.; Harth, E., One-pot polyglycidol nanogels via liposome master templates for dual drug delivery. *Journal of Controlled Release* **2016**, 244, Part B, 366-374.
- Chapter IV. Lockhart, J. N.; Hmelo, A.B.; Harth, E., Electron beam patterning of semi-branched polyglycidol nanogels for immobilization of enzyme cascade reaction. *Manuscript Submitted to Polymer Chemistry* **2017**.
- Chapter V. Lockhart, J. N.; Spoonmore, T. J.; McCurdy, M. W.; Rogers, B. R.; Guelcher, S.A.; Harth, E., Polyglycidol coating on ultra high molecular weight polyethylene for reduced biofilm growth. *Manuscript Submitted to ACS Applied Materials and Interfaces* **2017**.



## APPENDIX B

### CURRICULUM VITAE

# Jacob N. Lockhart

6820 Highway 70 S, Unit 307, Nashville, TN 37221

C: 317-709-7909 || E: [jacob.n.lockhart@gmail.com](mailto:jacob.n.lockhart@gmail.com) || [www.linkedin.com/in/jacoblockhart](http://www.linkedin.com/in/jacoblockhart)

## EXECUTIVE SUMMARY

Vanderbilt PhD, Exxon and Eli Lilly trained, innovative leader and problem solver. A unique blend of 3 years of commercial R&D experience covering Oil & Gas, Pharmaceuticals, and 4 years of Academic R&D with 5 years of management experience. Seeking technical role or technical management role with product development, business management or marketing growth opportunities where knowledge of polymer chemistry, nanotechnology and material science adds value to your organization. Highlights include:

- Industrial experience
- Strong business acumen with deep chemistry expertise
- Proven track record of managing others and advancing multiple projects independently
- 1<sup>st</sup> Place, Management Consulting Challenge, Owens School, Vanderbilt University, 2017

## EDUCATION

Vanderbilt University, Nashville, TN December 2017 (*expected*)

- PhD Chemistry, Thesis title: “Synthesis of Nanomaterials and Macromolecular Architectures for Dual Drug Delivery Systems, Biosensors, and Antimicrobial Films”
- Advised by renowned Professor of Chemistry, Material Science and Engineering, Dr. Harth
- Certificate, Management and Business Principles for Scientists

Vanderbilt University, Nashville, TN May 2010

- BA Chemistry (*cum laude*)
- Dean’s List Honors, 2006—2010

## PROFESSIONAL EXPERIENCE

**PhD Research Scientist, INVISTA, Koch Industries**, Camden, SC January 2018 (projected start)

- Performance Solutions Business: design, approval and execution of experimental programs
- Product and process improvement, new technology commercialization
- Partner with cross-functional teams involving technology, sales, and marketing

**Products Technology Cooperative, ExxonMobil Corporation**, Paulsboro, NJ June—December 2015

- Developed new test for Mobil 1 proof-of-performance and formulated motor oils
- Utilized DOE, statistics, and root cause analysis
- Presented to cross-business teams including marketing, operations, and product deployment
- Delivered site-wide oral progress report, a poster and multiple written reports

**Graduate Research Assistant, Vanderbilt University**, Nashville, TN (*current*) 2013—Current

- Developed and characterized polymeric nanomaterials for multi-drug delivery, biosensor and anti-biofilm coating applications
- Utilized cationic ring-opening polymerization, nano-fabrication, DLS, TEM, SEM, AFM
- Supervised 300+ undergraduates in various laboratory settings

**Bioanalytical Chemist, Eli Lilly & Company**, Indianapolis, IN (2 years) 2011—2013

- Developed new efficient quantification methods for *in vitro* safety of drug candidates
- Maintained HPLC Mass spectrometers AB Sciex 4000 and 5500, Analyst software
- Reduced service calls to vendors by 20%, decreased equipment maintenance by 8%

## TECHNICAL SKILLS

- Expertise in ChemDraw, Topspin, and MS Office
- Intermediate in Raith eLine Nanofabrication suite
- Minor experience in JMP, MATLAB, Javascript

## HONORS AND AWARDS

- Winner, Graduate Travel Award, Polymer Division, 254<sup>th</sup> Meeting of the American Chemical Society, Washington DC, 2017
- 1<sup>st</sup> Place, Management Consulting Challenge, Vanderbilt University 2017
- Outstanding Poster Award, Polymer Division, 252<sup>nd</sup> Meeting of the American Chemical Society, Philadelphia, PA, 2016
- Cook Fellowship Award, Outstanding Undergraduate, Department of Chemistry, Vanderbilt University, 2009
- Dean's List Honors 5 times, 2006—2010

## PUBLICATIONS

1. Lockhart, J. N.; Spoonmore, T. J.; McCurdy, M. W.; Rogers, B. R.; Guelcher, S.A.; Harth, E., Polyglycidol coating on ultra high molecular weight polyethylene for reduced biofilm growth. *Manuscript Submitted* **2017**.
2. Lockhart, J. N.; Hmelo, A.B.; Harth, E., Electron beam patterning of semi-branched polyglycidol nanogels for immobilization of enzyme cascade reaction. *Manuscript Submitted* **2017**.
3. Lockhart, J. N.; Beezer, D. B.; Stevens, D. M.; Spears, B. R.; Harth, E., One-pot polyglycidol nanogels via liposome master templates for dual drug delivery. *Journal of Controlled Release* **2016**, *244, Part B*, 366-374.
4. Lockhart, J. N.; Stevens, D. M.; Beezer, D. B.; Kravitz, A.; Harth, E., Dual drug delivery of tamoxifen and quercetin: Regulated metabolism for anticancer treatment with nanosponges. *Journal of Controlled Release* **2015**, *220*, 751-757.

## SELECT POSTER PRESENTATIONS

- 254<sup>th</sup> National Meeting of the American Chemical Society, Washington, D.C., August 2017. "Electron Beam Patterning of Polyglycidol Nanogels For Immobilized Enzyme Cascade Reaction."

- 252<sup>nd</sup> National Meeting of the American Chemical Society, Philadelphia, PA, August 2016. “Dual drug delivery: Generation of nanosponges and precise nanohydrogels via liposome master templates.”
- ExxonMobil Early Career Technical Networking Poster Event, Clinton, NJ, November 2015.

#### **AFFILIATIONS**

- American Chemical Society (ACS)
- ACS Division of Polymer Science and Engineering (PMSE)
- ACS Division of Polymer Chemistry (POLY)
- Alpha Epsilon Delta (AED) Honors Society

#### **LEADERSHIP/VOLUNTEER EXPERIENCE**

- Committee Chair, The Chemistry Forum, Vanderbilt University, 2017
- Group Leader, Vanderbilt Students Volunteering for Science Outreach, 2015
- Vice President and Cofounder, American Red Cross at Vanderbilt, 2011